2

LBL-31592

Lawrence Berkeley Laboratory
UNIVERSITY OF CALIFORNIA

Nuclear Magnetic Resonance Studies of the Regulation of the Pentose Phosphate Pathway

N.R. Bolo
(Ph.D. Thesis)

November 1991

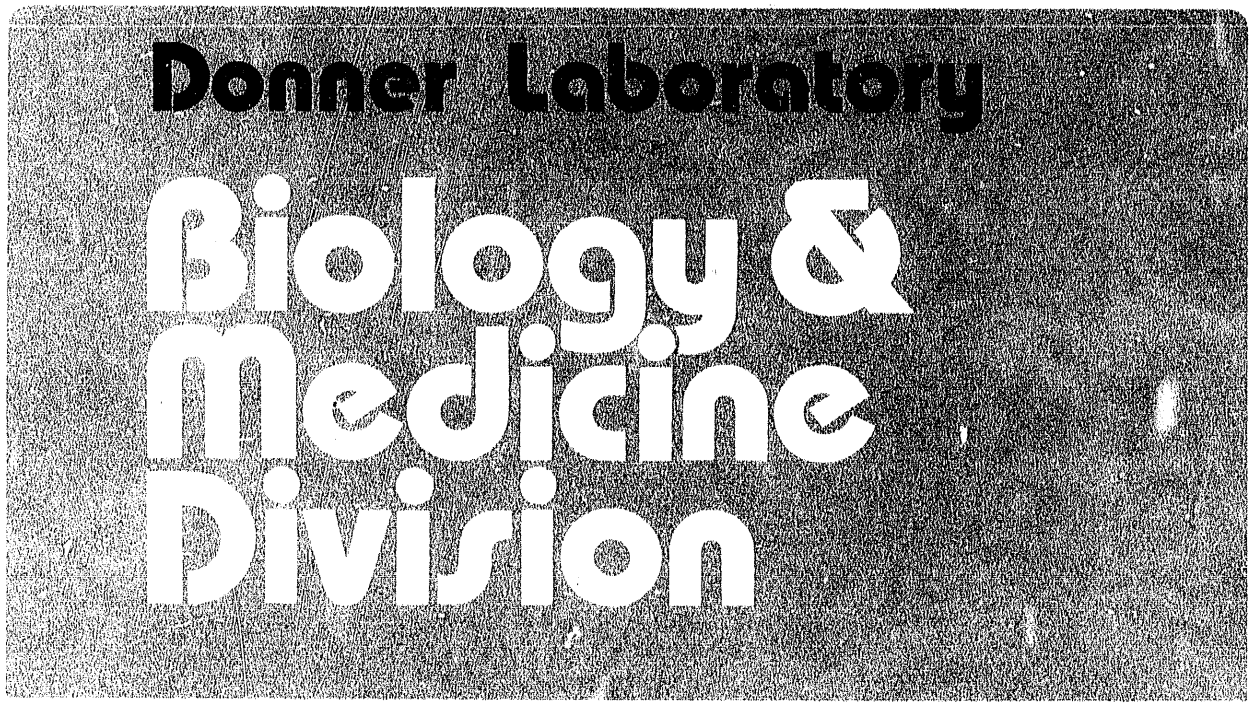

Prepared for the U.S. Department of Energy under Contract Number DE-AC03-76SF00098

LBL--31592

DE92 010257

Nuclear Magnetic Resonance Studies of the Regulation of the Pentose Phosphate Pathway

Nicolas Robin Bolo
Ph.D. Thesis

Graduate Group in Biophysics
University of California

and

Research Medicine & Radiation Biophysics Division
Lawrence Berkeley Laboratory
University of California
Berkeley, CA 94720

November 1991

This work was supported in part by the National Institutes of Health under Grant No. HL07367 and by the Director, Office of Energy Research, Office of Health and Environmental Research, Medical Applications and Biophysical Research Division, of the U.S. Department of Energy under Contract No. DE-AC03-76SF00098.

Nuclear Magnetic Resonance Studies of the Regulation of the Pentose Phosphate Pathway

by

Nicolas Robin Bolo

Nuclear Magnetic Resonance Studies of the Regulation of the Pentose Phosphate Pathway

By

Nicolas Robin Bolo

Abstract

The goal of this work is to investigate the potential for and limitations of *in vivo* nuclear magnetic resonance (NMR) spectroscopy for quantitation of glucose flux through the pentose phosphate pathway (shunt). Interest in the shunt is motivated by the possibility that its activity may be greatly increased in cancer and in the pathological states of cardiac and cerebral ischemia. The ability to dynamically monitor flux through the pentose shunt can give new knowledge about metabolism in pathological states.

Methods developed in this research use ^{13}C NMR spectroscopy to monitor shunt activity by determination of the ratios of [^{13}C-4] to [^{13}C-5]-glutamate, [^{13}C-3] to [^{13}C-2]-alanine or [^{13}C-3] to [^{13}C-2]-lactate produced when [^{13}C-2]-glucose is infused. The principal operational relation for the fractional shunt activity under aerobic conditions is $3r_G/(2+3r_G)$, where r_G is the ratio of the ^{13}C enrichment at C4 to that at C5 of glutamate. These methods provide measures of the effect of oxidative stresses on shunt activity in systems ranging from cell free enzyme-substrate preparations to cell suspensions and whole animals.

In anaerobic cell free preparations, the fraction of glucose flux through the shunt was monitored with a time resolution of 3 minutes. Oxidized glutathione (GSSG 1.5 mM) was shown to increase flux by a factor of 3 from its control value. In aerobic yeast cells, GSSG (1.5 mM) increased flux by a factor of 3, and t-butyl-hydroperoxide (TBHP, 1-10 mM) by a factor of 1.6. A shunt flux of 25±4% was measured from brain extracts from the anesthetized rat infused with [^{13}C-2]-glucose.

This work predicts the potential for *in vivo* human studies of pentose phosphate pathway activity based on the mathematical simulation of the ^{13}C fractional enrichments of C4 and C5-glutamate as a function of shunt activity and on the signal-to-noise ratio acquired in ^{13}C NMR human studies from the current literature. A signal-to-noise of 5, sufficient to infer 5% glucose flux through the shunt, is estimated to be acquired from the NMR signals of [^{13}C-4] and [^{13}C-5]-glutamate in the human brain at a field strength of 4 Tesla, in a localized volume of 6x6x6 cm with an acquisition time of 30 minutes, if a total [^{13}C-2]-glucose dose of about 33 grams (471 mg/(kg body-weight)) is infused over a total period of 90 minutes and 82% plasma [^{13}C-2]-glucose fractional enrichment is obtained.

To Andrea, my dearest.

Acknowledgements

I particularly wish to thank Dr. Thomas F. Budinger for his counsel, encouragement and funding for this work. Special thanks to Dr. Thomas L. James and Dr. George A. Brooks for their helpful discussions and suggestions. I wish to warmly thank Dr. John R. Baker and Dr. Sam T-S.Wong who were always there when I needed them, and Dr. Mark S. Roos and all the people in the Research Medicine group who created a pleasant and stimulating environment for research over the years. Thanks to Dr. Robert K. Mortimer for providing the yeast cell strains.

Contents

Chapter 1.

Introduction.

We hypothesize that using nuclear magnetic resonance (NMR) spectroscopy it is possible to measure the fractional flux of glucose through the pentose phosphate pathway (pentose shunt) in the brain under aerobic conditions *in vivo*. In this study we develop and evaluate NMR methods for measuring the flux of glucose through the pentose shunt in anaerobic and aerobic tissues. The NMR based methods are used in this study to investigate the effects of oxidative stresses on regulation of glucose utilization *via* the pentose shunt in systems ranging from cell free enzyme-substrate preparations to cell suspensions and whole animals. The cellular regulation of the flux of glucose through the shunt is dependent on the redox state of the NADPH/NADP couple. The utilization of glucose *via* the pentose shunt provides the cell with reducing power in the form of NADPH and with ribose-5-phosphate for the biosynthesis of nucleotides. A major function of the shunt is to provide NADPH for maintaining sulfhydryl groups reduced (1), thus assuring protection against oxidative damage. Thus we expect variations in pentose shunt activity to be reflective of applied oxidative stress in the brain and the heart. The mathematical model developed in this study is used to predict the potentials for and limitations of the methods

applied to *in vivo* human studies of the brain. Based on these results inferences can be drawn regarding the ability to monitor the pentose shunt in other organs as well as cancerous tissue.

1.1. Motivation.

The pentose phosphate pathway in the brain.

The brain, with its continuous electrical and biochemical activity involved in neurotransmission, depends mainly on glucose supplied from the blood for its energetic needs (2). Although glycolysis is the main pathway for glucose utilization in the brain, the alternate pentose phosphate pathway o. pentose shunt must have important specific functions to fulfill since blockage of the pentose shunt leads to neurological disorders and brain cell damage (3) & (4). In brain tissue, the pentose shunt provides ribose-5-phosphate for synthesis of nucleotides and NADPH for reductive biosyntheses (such as lipid biosynthesis in myelin formation). In neurons, NADPH is important in the catecholamine-linked metabolism (1) and plays the role of a protector against oxidative damage or intoxication that would occur during the normal process of monoamine neural transmission. In this case, the reductive potential provided by NADPH is involved in maintaining sulfhydryl groups such as glutathione in the reduced state. Glutathione in turn scavenges peroxides produced either in the normal functioning of the brain or under pathological conditions. It would then appear that regulation of activity between the two pathways, glycolysis and the pentose shunt, enables the brain to maintain a high energetic level while assuring cell protection against oxidative stress.

Oxidative stress in the brain.

The use of oxygen in the cell's energetic reactions enables higher energy production than that produced under anaerobic conditions. Only 2 ATP molecules are produced for

one glucose molecule degraded to lactate anaerobically, whereas 36 are produced when glucose is completely oxidized to CO_2 aerobically (5). But oxygen metabolism comes at the cost of potential toxicity in the form of the highly reactive species superoxide radical, singlet oxygen, hydroxyl radical and peroxides. If unquenched by some protective system these species react with membrane lipids, with proteins, or nucleic acids, altering macromolecular structure and hindering function. The origins of these toxic free radicals are from both normal and pathological processes.

In the monoamine neuroanatomical pathways of the brain, monoamine neurotransmitters (norepinephrine, epinephrine, dopamine and serotonin) released in the synaptic cleft are taken up by the neuron and nearby glia after interaction with the post-synaptic receptor (see figure 1). The neurotransmitter is further inactivated through degradation by monoamine oxidase. Monoamine oxidase in the mitochondrial membrane uses molecular oxygen to oxidize the monoamine producing an aldehyde and hydrogen peroxide (HOOH). Glutathione peroxidase metabolizes the peroxide using reduced glutathione which is then regenerated by glutathione reductase which uses NADPH. The constant production of peroxide in the normal operation of neurotransmission constitutes the basis for the hypothesized importance of the pentose shunt in neurons (1) & (6).

The processes occurring during and after transient ischemia are numerous and complex. Various mechanisms have been implicated in ischemic damage including acidification due to increased lactate, toxic levels of aspartate and glutamate, and changes in calcium concentration. It has been suggested that the lesions observed following hypoxic hypoxia, *status epilepticus*, hypoglycemia and ischemia, are most likely due to oxidative reactions e.g. lipid peroxidation of membranes that have been structurally damaged by a primary defect in energy metabolism (2). In fact, in some cases it has been possible to single out free radical production as being implicated in injury to brain tissue after transient ischemia (7) & (8).

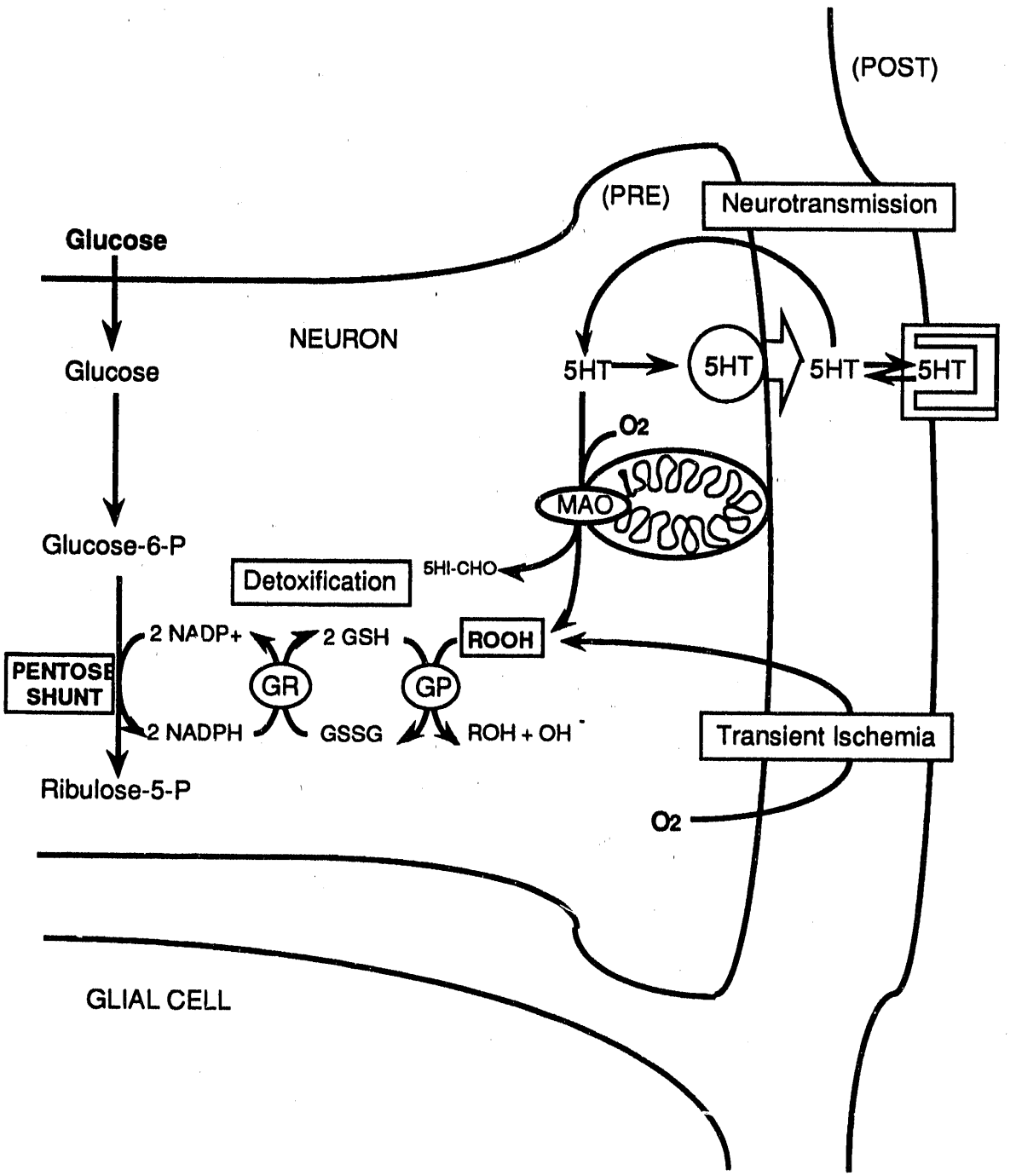

Figure 1. Protection against peroxides in the brain. In monoamine neurotransmission (for example 5-hydroxytryptamine: 5-HT), after release of the neurotransmitter from the presynaptic neuron (PRE) in the synaptic cleft and interaction with the receptor in the post synaptic neuron (POST), uptake and degradation of 5-HT by monoamine oxidase (MAO) will result in the production of hydrogen peroxide (R=H). Transient ischemia produces free radicals resulting in peroxides ROOH. ROOH are scavenged by the glutathione-peroxidase (GP) -reductase (GR) system. Reduced glutathione (GSH) is regenerated from its oxidized form (GSSG) by NADPH which is generated by pentose shunt activity.

Since the pentose shunt is linked to protection against deleterious effects of free radicals it is possible that pentose shunt activity may be increased in transient ischemia (see figure 1).

Systems protecting against oxidative damage in the brain.

The brain is subjected to a particularly high risk from peroxides and free radicals due to the importance of its content in polyunsaturated lipids, and protective systems are expected to be equally important. The cellular antioxidant enzyme systems present in measurable amounts in the brain include superoxide dismutase, which reacts with the superoxide radical to produce hydrogen peroxide, and the other enzymes catalase and glutathione peroxidase-reductase which scavenge the peroxides. The main fraction of glutathione peroxidase-reductase activity is located in the cytosol (9). The concentrations of these enzymes are small relative to other tissue types. For example in the rat brain glutathione peroxidase activity is about 70 nmol GSH oxidized/minute/mg protein (10) & (11). The activity is reported to be 2 to 9 (11) & (12) times higher in the heart and 5 to 20 (11) & (12) times higher in the liver. In the human brain, activity is reported to be from 30 to 56 nmol GSH oxidized/minute/mg protein depending on the cerebral localization (9). Efficient protection via glutathione peroxidase in the brain is dependent on rapid regeneration of of the reduced species and this is dependent on a rapid regulation of NADPH production via the pentose shunt.

1.2. Non-NMR approaches to measurement of the pentose phosphate pathway.

Our objective is to present a method for measurement of the pentose phosphate pathway activity under aerobic conditions in the brain *in vivo*. The techniques which have historically built up our present knowledge of the pentose pathway fall short of this objective. Foremost this is because the *in vivo* condition is not fulfilled. Chemical assays

in vitro of the individual enzyme activities provide us with valuable information about individual properties of the constituent enzymes of the pathway, but regulation of the pathway must be understood under the physiological conditions in the cells and organisms in which they occur. The use of radioactively labeled substrates in perfused tissue preparations or injected in the live animal in part respond to this condition. The first formulations of the pathway relied on incubation of radioactively labeled substrates in tissue preparations and indeed our present formulation of the shunt is based on these studies, but analysis of the radiotracer's fate involves the degradation of the tissue (except in the case of CO_2 analysis) during which metabolic changes may occur. Furthermore the localization of the tracer in the metabolic intermediate can only be determined by isolation and degradation of the compound. Dynamic studies imply sacrificing organisms at each time point, and subjecting the tissues to extraction procedures. Positron emission tomography (PET) permits radioactive tracer studies to be done dynamically *in vivo*, but as in the previous case the position of the label in the metabolic intermediate is not obtained unless the tissue is extracted and analyzed chemically for each species. Therefore, in fact, dynamic detection of the tracer in PET studies does not yield any information on the chemical state of the tracer.

1.3. NMR approach to measurement of the pentose phosphate pathway.

The technique of nuclear magnetic resonance spectroscopy permits detection of nuclei possessing magnetic spin in intermediate metabolites *in vivo* and yields information on their physico-chemical state. As opposed to radioactive tracer techniques, information on label position is obtained because the resonant frequency of a given spin is determined by its molecular environment. For these reasons it is theoretically possible to follow variations in time of metabolic pools, or metabolic transformations undergone by a tracer

molecule. Practical limitations to such measurements depend on the specific case under study. One limitation that applies in all cases is the sensitivity of the NMR technique. In order to be detected, the concentration of the metabolic pool of interest must be sufficiently large. Conversely, the volume of detection must be sufficiently small for it to be of biological significance. We estimate the lower concentration limit for ^1H NMR detection of small metabolites in the human brain with a signal to noise ratio (SNR) of 5 from a ^1H NMR study from the current literature (13). In that study, the peak arising from creatine and phosphosphocreatine was detected in humans *in vivo* with a signal to noise ratio (SNR) of 95 using localized proton spectroscopy at 2.1 Tesla in a detection volume of 14 ml with an acquisition time of 4 minutes (13). The concentration of creatine plus phosphosphocreatine in the brain was assumed to be 10.5 mM (14). From these observations, and assuming a linear relationship between concentration and SNR, and volume and SNR, we estimate that a proton species at a concentration of about 0.9 mM in a volume of 8 ml with 4 minutes of acquisition time at a field strength of 2.1 Tesla would yield a SNR of 5.

With this limitation in mind we will approach the problem of measurement of pentose shunt activity by applying two strategies concerning the physiological parameters of interest. These physiological strategies involve:

- Targeting the metabolic pools of largest size in the organ. A spin label goes through alternative metabolic pathways before arriving in a target metabolite (glutamate) which has a large pool size in the tissue. The position of the spin label in the target metabolite yields information on which pathway has been taken by the label. The method we develop based on this strategy is called the glutamate fractional enrichment method.
- Increasing the pool size of a specific intermediate of the pathway using a specific metabolic blocker. The method we develop based on this strategy is called the aminonicotinamide method.

The metabolic hypotheses will be tested on biological systems which may be studied at high static magnetic fields.

Chapter 2.

Models for measurement of flux through the pentose phosphate pathway.

2.1. Radioactive tracer studies.

The pentose phosphate pathway is shown in its classical formulation (15) in figure 2.1. The oxidative branch of the pentose shunt produces reduced NADPH and ribose-5-phosphate (R5P) by oxidation of glucose-6-phosphate (G6P). The first reaction of the shunt (oxidation of glucose-6-phosphate by glucose-6-phosphate dehydrogenase) is irreversible and rate limiting under physiological conditions. In the non-oxidative branch of the shunt, the reversible action of transketolase and transaldolase enzymes produces fructose-6-phosphate (F6P) and glyceraldyhyde-3-phosphate (G3P) from R5P. Under physiological conditions where more NADPH than R5P is required and gluconeogenesis reactions are limited, G6P flows through the shunt to produce F6P and G3P which are then metabolized to pyruvate by the reactions of the glycolysis branch. Existence of these pathways is based on chemical inference and radiotracer studies. Another formulation

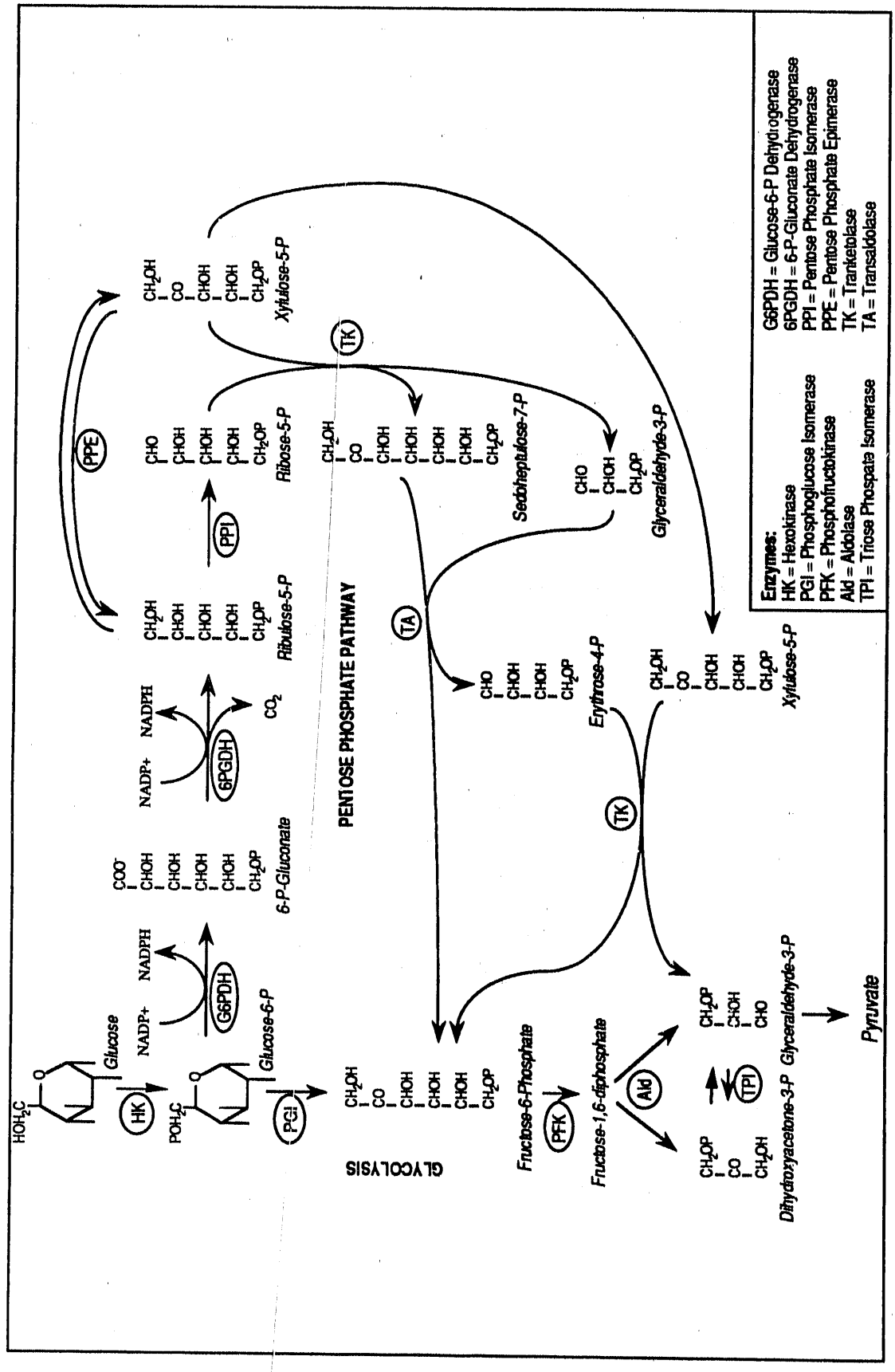

Figure 2.1. Classical formulation of the Pentose Phosphate Pathway

called the L-type pathway has been proposed by Williams (16). The L-type was proposed to account for results of radioactive tracer studies in liver whence its name (L for liver) as opposed to the F-type (F for fat tissue) which is the name given to the classical formulation of the pathway. A review by the same author (17) presents results in accord with the L-type pathway, but none of these was in brain tissue. Other reviews suggest that the majority of radiotracer studies are in accord with the classical formulation (18), and there is to this date a controversy concerning the operation of the pathway in the liver. More recently, a comparison of NMR data in red blood cells to computer simulations of the L-type and F-type pathways showed that the results were more consistent with the F-type than with the L-type formulation (19). The model we use in the development of our method is the classical formulation of the pathway and our data are also consistent with this formulation.

2.2. Models for the anaerobic fractional enrichment of the lactate pool.

The following two methods for measurement of glucose flux through the pentose shunt rely on the NMR detection of the lactate pool produced after ^{13}C labeled glucose is given as a substrate to the cell system. The two labeled glucose substrate species considered are [^{13}C-1]-glucose and [^{13}C-2]-glucose. The accumulation of a lactate pool results from consumption of glucose in cell systems under anaerobic conditions. The cessation of this accumulation accompanied by the inhibition of glucose consumption with the onset of respiration is called the Pasteur effect and is described in general biochemistry textbooks (5). Lactate pools may also occur in tissues under aerobic conditions , when rates of lactate production and removal differ (20). We will see that the C1 of glucose is lost to CO_2 in the pentose shunt and the C2 is conserved. This implies that [^{13}C-1]-

glucose can be used for determination of the relative fluxes only by observation of labeling patterns in lactate, whereas [^{13}C-2]-glucose can be used by observation of either lactate or glutamate labeling patterns. Therefore [^{13}C-1]-glucose can be used for determination of the relative fluxes in the aerobic case only if rates of lactate production and removal differ. The use of [^{13}C-2]-glucose in the aerobic case by observation of glutamate labeling patterns is developed in the next section (2.3).

The glucose substrate flows to lactate by alternative pathways: direct glycolysis or pentose shunt. The fraction of glucose that has been consumed through either pathway is called the relative flux. It is possible to obtain information on the relative fluxes because the labeling pattern of the lactate produced from glucose consumption depends on the initial position of label in the substrate and on the pathway that was taken. The final lactate pool therefore contains lactate molecules with different ^{13}C labeling patterns, each different type being called a lactate species. (The different lactate species are lactate isotope isomers or isotopomers and this notion is developed further in the next section). The relative amounts of the different lactate species in the lactate pool are related to the relative fluxes, and the models described here yield the mathematical equations of that relationship. The relative amounts of lactate species are obtained experimentally in the NMR spectrum, and the relative fluxes are therefore calculated from the experimental data with the model's equations. The relative amounts may be defined in different ways depending on what information is most easily extracted from the NMR spectrum. The fractional enrichment defines the amount of species labeled in a given position relative to all species (including unlabeled species) whereas the relative enrichment defines the amount of label in a given position relative to amount of label in other positions. It is not always possible to obtain the fractional enrichment from the NMR data and therefore in the following development, expressions are given for the flux both as a function of fractional enrichments and of relative enrichments.

2.2.1. Use of [^{13}C-1]-glucose as a precursor.

This model was first used to measure relative flux of glucose via the pentose shunt in anaerobic preparations of rabbit lens (21). In this method, the substrate provided to the cell system is glucose labeled in the C1 position ([^{13}C-1]-glucose). The method is based on the loss of the label in the C1 position when [^{13}C-1]-6-phosphogluconate ([^{13}C-1]-6PG) is oxidized to ribulose 5-phosphate in the second oxidative step of the pathway. The model is shown in figure 2.2.

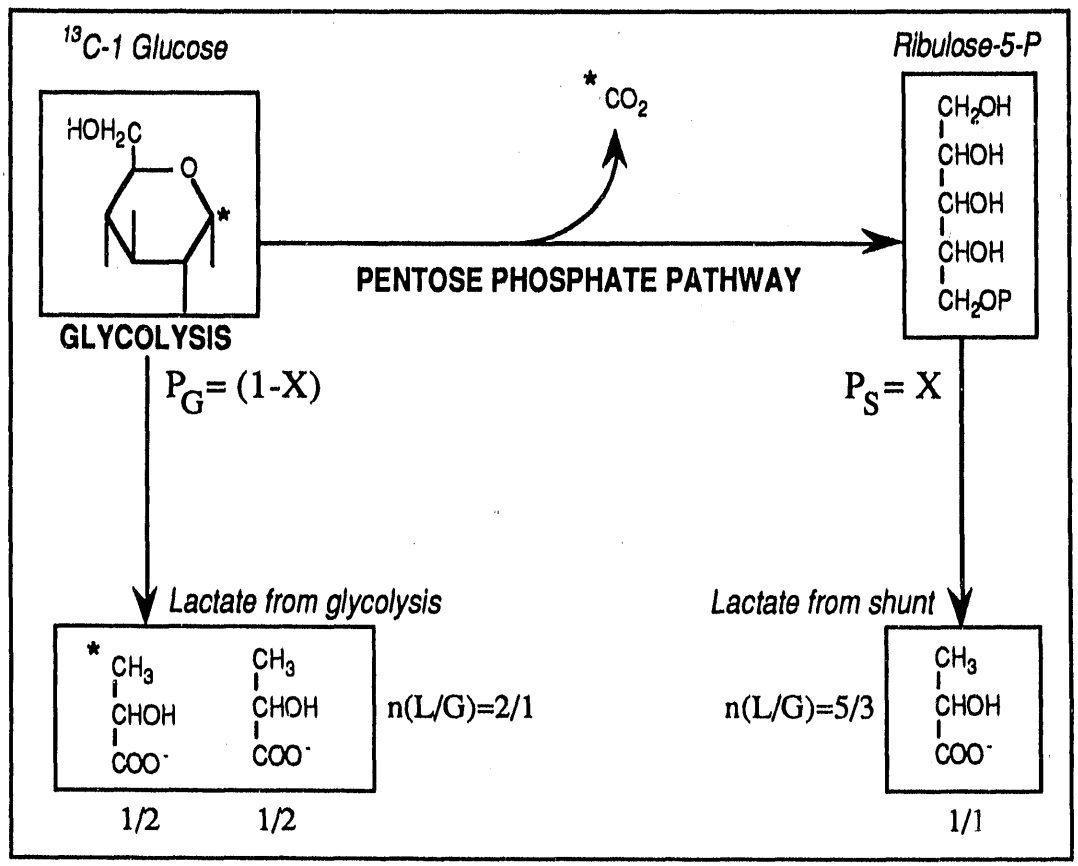

Figure 2.2. Model for the anaerobic fractional enrichment of lactate using initial [^{13}C-1]-glucose. P_S=X is the fraction of glucose flux through the pentose shunt and P_G is the fraction of glucose flux through direct glycolysis ($P_G + P_S = 1$). n(L/G) is the number of lactate molecules produced per glucose molecule consumed in either case. The number indicated at the bottom of each species is the fraction of that species in the pool produced by either glycolysis or shunt.

For each glucose molecule that goes through direct glycolysis to lactate there are one [^{13}C-3]-lactate molecule and one unlabeled [^{12}C-3]-lactate molecule produced. However for every three glucose molecules going through the shunt five unlabeled lactate molecules are produced. The fraction X of glucose that that has been through the shunt is expressed as a function of the ratio r of labeled to unlabeled lactate.

The following assumptions are applied in the model (21). The label entering the lactate pool does so via either the direct glycolysis pathway or via the pentose shunt and not via any other pathway. Therefore from glucose to lactate, there are only two branches. There are no unlabeled endogenous lactate precursors; the only lactate precursor is the labeled glucose supplied by the experimenter. There is no recycling of pentose shunt products. The fractional enrichment of the glucose substrate is 100%. We may note here that it is not necessary to assume steady state.

Although the "no unlabeled endogenous lactate precursors" assumption should be valid in brain tissue in which glycogen stores are low and glucose from the blood is the main energy source, it is not valid in skeletal muscle where glycolytic flux from glycogen can be 4 times greater than from glucose. A method of correction of the NMR pentose shunt measurement for endogenous carbon sources that uses both [^{13}C-1]-glucose and [^{13}C-6]-glucose has been proposed (22). We show in the next section (2.2.2) that by using [^{13}C-2]-glucose and observing relative ^{13}C enrichment of lactate carbons, the measurement can be made independently of endogenous carbon sources.

The following defines the notations to be used in the the present and subsequent models and develops the relationship between X and r.

Fractional fluxes.

Assuming that the observed lactate comes from glucose which is consumed only through either direct glycolysis or pentose shunt pathways, the fractional fluxes P_G for direct glycolysis, P_S for the shunt are defined so that their sum equals 1:

$$P_G + P_S = 1$$

Calling $P_S = X$, we have $P_G = 1\text{-}X$ as shown in figure 2.2.

Labeling of lactate produced.

According to the model, consumption of glucose labelled in the C1 position will lead to a label only in the C3 position of lactate after glycolysis. Let's call [glucose] the amount of glucose consumed, [[^{13}C-3]-lactate] and [[^{12}C]-lactate] respectively the amounts of labeled and unlabeled lactate produced. The amount of a given species of lactate is obtained by summing the amounts produced from each pathway. [[^{13}C-3]-lactate] is produced only from direct glycolysis and is proportional to the fractional flux through glycolysis P_G, the number of molecules of lactate produced per molecule glucose consumed through glycolysis (n(L/G)=2/1 for glycolysis in figure 2.2), and the fraction of labeled lactate produced from glycolysis (fraction = 1/2). [[^{12}C]-lactate] is produced from glycolysis and from the shunt. The amount of [[^{12}C]-lactate] produced from the shunt is proportional to the fractional flux through the shunt P_S, the number of molecules of lactate produced per molecule glucose consumed through the shunt (n(L/G)=5/3 for the shunt in figure 2.2), and the fraction of unlabeled lactate produced from the shunt (fraction = 1/1). Therefore we have:

$$[[^{13}\text{C-3}]\text{lactate}] = P_G\,[\text{glucose}] = (1\text{-}X)\,[\text{glucose}] \qquad (2.1)$$

(one labeled lactate for each glucose via glycolysis)

$$[[^{12}\text{C}]\text{lactate}] = P_G[\text{glucose}] + (5/3)P_S[\text{glucose}] = (1\text{-}X)[\text{glucose}] + (5/3)X[\text{glucose}] \qquad (2.2)$$

(one unlabeled lactate for each glucose through glycolysis)

(five unlabeled lactate for three glucose through the shunt)

And the total amount of lactate produced is therefore:

$$[\text{lactate}] = [[^{13}\text{C-3}]\text{lactate}] + [[^{12}\text{C}]\text{lactate}] = [\text{glucose}]\ (\ 2P_G\ +\ (5/3)P_S\ )$$

$$[\text{lactate}] = [\text{glucose}]\frac{6-X}{3} \tag{2.3}$$

The ratio r of labeled to unlabeled lactate is:

$$r = \frac{[[^{13}\text{C}-3]\text{lactate}]}{[[^{12}\text{C}-3]\text{lactate}]} = \frac{P_G}{P_G + \tfrac{5}{3}P_S} = \frac{3(1-X)}{3+2X} \tag{2.4}$$

Which yields X as a function of r:

$$X = \frac{3(1-r)}{3+2r} \tag{2.5}$$

The ratio r is obtained experimentally from the proton NMR spectrum and then used to calculate the fraction X of glucose flux through the shunt. Labeled lactate peaks appear in the proton spectrum as ^{13}C satellites symmetrically placed on each side of the unlabeled lactate peak because of the 128 Hz scalar coupling between the ^{13}C and ^{1}H in the C3 position. Expression 2.5 may also be derived by using fractional enrichments which are defined in the following.

Fractional enrichments.

The fractional enrichment F_{Li} of lactate in the Ci position is defined as the ratio of the amount of lactate species labeled in Ci to the total amount of lactate :

$$F_{Li} = \frac{[[^{13}\text{C}-i]\text{lactate}]}{[\text{lactate}]} \tag{2.6}$$

In this case the only lactate species present after glucose consumption are the unlabeled and C3 labeled species Therefore if we call F_{L0} the fraction of unlabeled lactate, we have:

$$F_{L0} + F_{L3} = 1$$

Inserting the expressions for amounts of lactate species produced (equations 2.1 to 2.3) in the definition of F_{Li} , we obtain the following expressions for the fractional enrichments:

$$F_{L0} = \frac{[[^{12}C-3]\text{lactate}]}{[\text{lactate}]} = \frac{P_G + \frac{5}{3}P_S}{2P_G + \frac{5}{3}P_S} = \frac{3+2X}{6-X} \qquad (2.7)$$

$$F_{L3} = \frac{[[^{13}C-3]\text{lactate}]}{[\text{lactate}]} = \frac{P_G}{2P_G + \frac{5}{3}P_S} = \frac{3(1-X)}{6-X} \qquad (2.8)$$

The ratio r may be expressed as a function of F_{L0} and F_{L3}:

$$r = \frac{F_{L3}}{F_{L0}} = \frac{3(1-X)}{3+2X} \qquad (2.9)$$

which is equivalent to equation 2.4.

Likewise, expressions 2.7 and 2.8 may be used to express the flux simply as a function of the fractional enrichments:

$$X = \frac{3(2F_{L0}-1)}{2+F_{L0}} \qquad (2.10)$$

$$X = \frac{3(1-2F_{L3})}{3-F_{L3}} \qquad (2.11)$$

2.2.2. Use of [^{13}C-2]-glucose as a precursor.

In this method, the substrate provided to the cell system is glucose labeled in the C2 position ([^{13}C-2]-glucose). We base this model on the classical formulation of the non-oxidative steps of the pathway which is shown in figure 2.3.

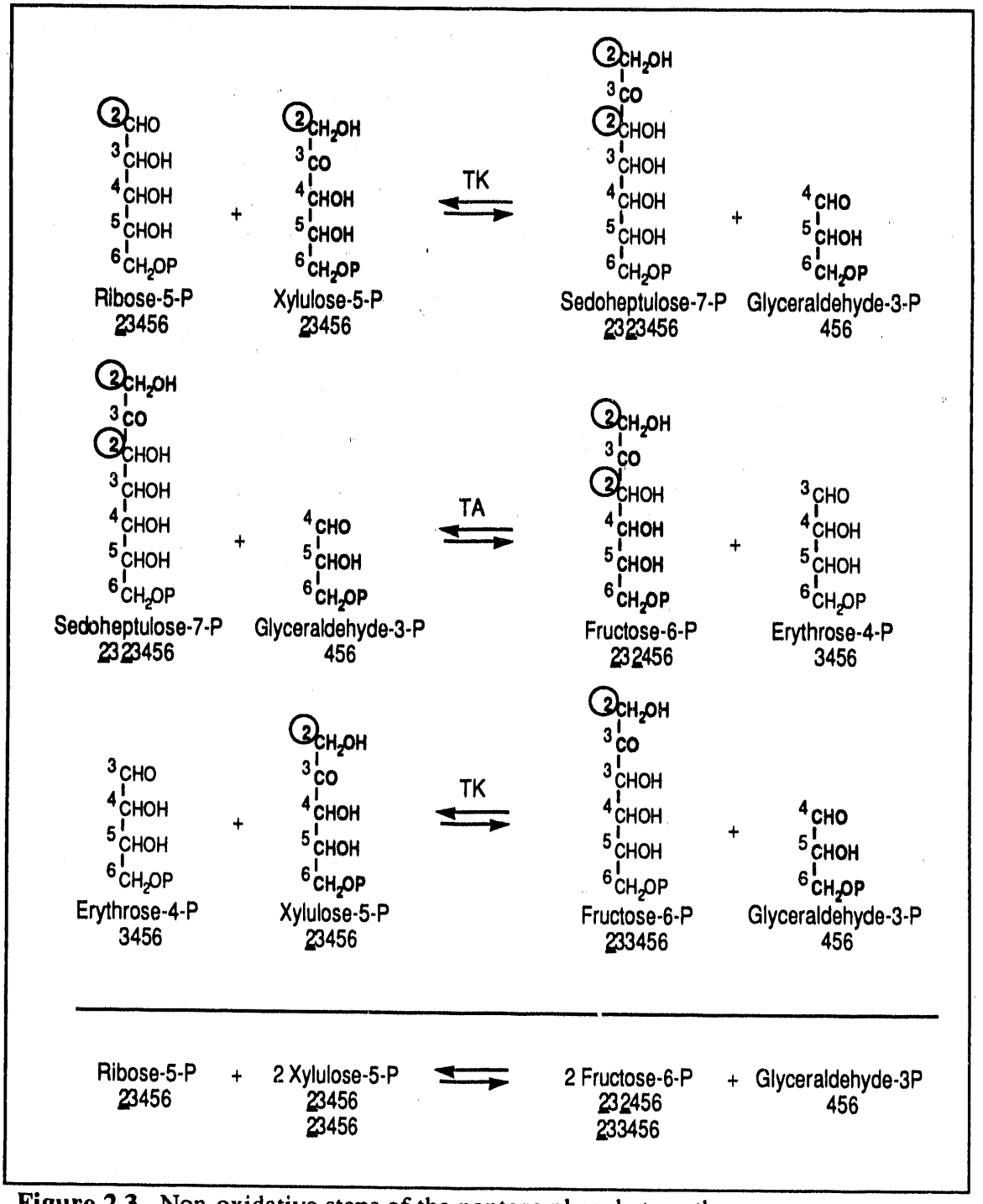

Figure 2.3. Non-oxidative steps of the pentose phosphate pathway.
The carbons of each molecule are assigned numbers which correspond to the numbers given to the initial substrate glucose carbons by starting with 1 in the aldehyde position. A ^{13}C label placed in position 2 of glucose is indicated by a circle around 2 in the molecule and an underlined 2 in the name.

Figure 2.3 shows the scrambling of labels re-entering the glycolytic route in the form of F6P and GA3P. The glucose carbons are numbered starting from 1 in the aldehyde position. The C1 is lost to carbon dioxide in the 6-phosphogluconate dehydrogenase (6PGDH) step. In this figure the initial C2 label from glucose is circled to highlight the fate of the ^{13}C isotope placed there. The model for the method based on measurement of [C-3]-lactate fractional enrichment is shown in figure 2.4. There are two advantages conferred by taking a label in the C2 position instead of the C1 position because of the fact that the C2 label is not lost to CO_2 with passage of the glucose molecule through the steps of the shunt.

Firstly, the characteristic positioning of the ^{13}C label in lactate due to passage through the shunt allows us to develop expressions for relative shunt flux as a function of relative ^{13}C enrichments of the lactate carbon positions i.e. not having to take into account the amount of ^{12}C incorporated into a particular lactate carbon position. Since ^{12}C incorporated into lactate positions may come from endogenous unlabeled sources such as glycogen stores, by using only the relative amounts of ^{13}C incorporated into lactate positions we free ourselves from the assumption of "no endogenous unlabeled lactate precursors". When only relative amounts of ^{13}C incorporated into lactate positions are used then the amount of unlabeled lactate positions produced doesn't matter . The assumption needed to replace the "no endogenous unlabeled lactate precursors" assumption is that the only source of labeled lactate is the labeled precursor. Concurrently, this assumes we neglect the 1.1% natural abundance of ^{13}C. The expressions of relative shunt flux based on relative enrichments are applicable to tissues which have large endogenous carbon sources such as muscle tissue where glycolytic flux from glycogen can be 4 times greater than from glucose.

Secondly, under aerobic conditions the ^{13}C label from [^{13}C-2]-glucose is able to incorporate into glutamate after glucose has passed through the shunt. This enables us to develop expressions of relative shunt flux based on glutamate relative ^{13}C enrichments in the aerobic case.

In the following, expressions for the relative shunt flux as a function of labeled and unlabeled positions or only of labeled positions of lactate are developed, so we restate here the same assumptions that were applied in the previous model, noting that the "no unlabeled endogenous lactate precursors" assumption is not necessary when relative amounts are used:

The label entering the lactate pool does so via either the direct glycolysis pathway or via the pentose shunt and not via any other pathway. Therefore from glucose to lactate, there are only two branches. There are no unlabeled endogenous lactate precursors, the only lactate precursor is the labeled glucose supplied by the experimenter. There is no recycling of pentose shunt products. The fractional enrichment of the glucose substrate is 100%.

The model in figure 2.4 shows that once [^{13}C-2]-glucose has been consumed, there are 4 possible labeling patterns for lactate: [^{12}C-1,2,3]-lactate (unlabeled lactate), [^{13}C-2]-lactate, [^{13}C-3]-lactate and [^{13}C-1,3]-lactate. First we develop the flux through the shunt as a function of the amount of C3 labeled relative to C2 labeled species, then of C3 labeled relative to C3 unlabeled species. Then for completeness the flux is given as functions of the fractional enrichments in positions 2 and 3 of lactate.

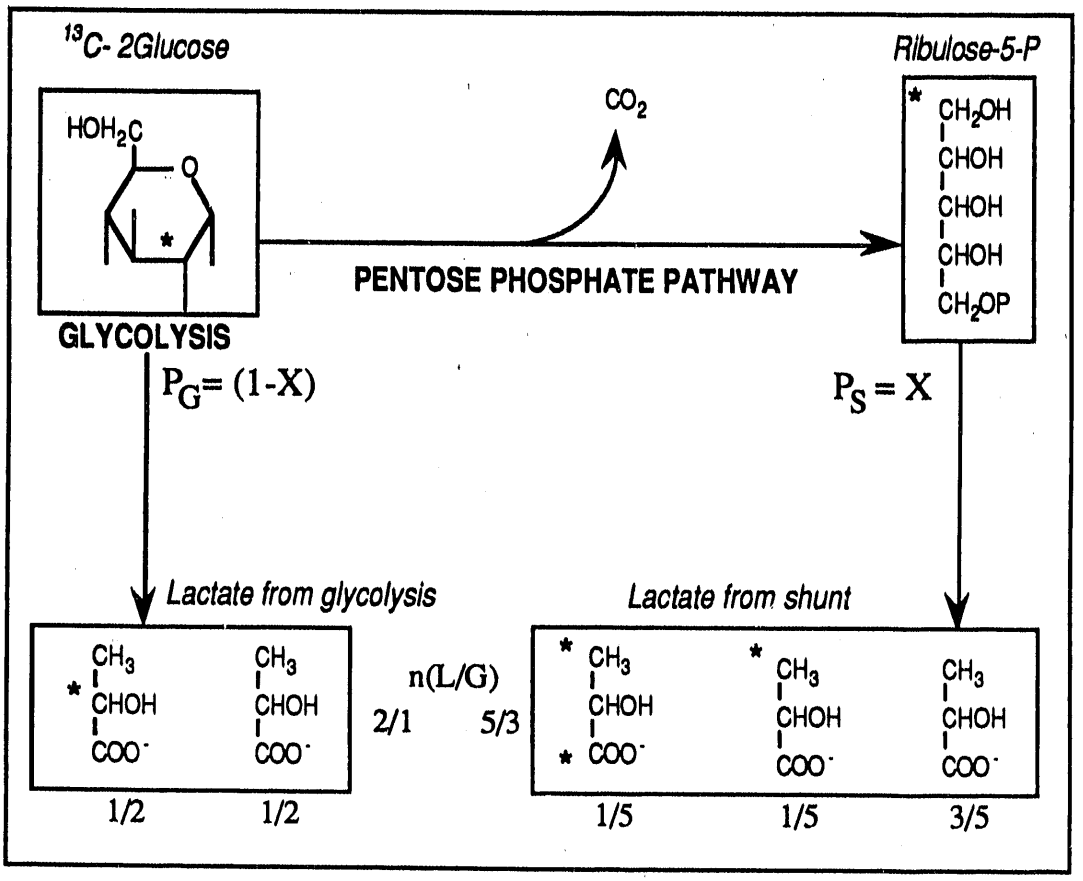

Figure 2.4. Model for the anaerobic fractional enrichment of lactate using initial [^{13}C-2]-glucose. P_S=X is the fraction of glucose flux through the pentose shunt and P_G is the fraction of glucose flux through direct glycolysis ($P_G + P_S = 1$). n(L/G) is the number of lactate molecules produced per glucose molecule consumed in either case. The number indicated at the bottom of each species is the fraction of that species in the pool produced by either glycolysis or shunt.

The expression for the fraction X of glucose that has gone through the shunt is obtained by applying conservation of label in the lactate pool. In this case we consider the amount of label in the C2 and C3 positions of lactate.

When one glucose molecule is consumed through the pathway of direct glycolysis the result is the formation of one [^{13}C-2]-lactate molecule and one unlabeled lactate molecule. On the other hand for every three glucose molecules that have gone through the shunt, the shuffling of label results in the formation of two [^{13}C-3]-lactate molecules and three unlabeled lactate molecules. The fractional fluxes P_G and P_S are defined as in the

previous model. The amounts of labeled lactate species formed expressed as a function of the glucose consumed [glucose] are therefore given by:

$$[[^{13}C-2]\text{lactate}] = P_G\,[\text{glucose}] = (1-X)[\text{glucose}] \qquad (2.12)$$

(one [^{13}C-2]lactate for each glucose via glycolysis)

$$[[^{13}C-3]\text{lactate}] = (\tfrac{2}{3})P_S[\text{glucose}] = \frac{2X}{3}[\text{glucose}] \qquad (2.13)$$

(two [^{13}C-2]lactate for each three glucose via shunt)

$$[[^{12}C-3]\text{lactate}] = 2P_G[\text{glucose}] + P_S[\text{glucose}] = (2-X)[\text{glucose}] \qquad (2.14)$$

(two for each via glycolysis one for each glucose via shunt)

The [^{13}C-2]-lactate and [^{13}C-2]-glucose are observed in the carbon spectrum whereas [^{13}C-3]- and [^{12}C-3]-lactate are observed in the proton spectrum. The ratio r_1, fraction of the [^{13}C-3] to [^{13}C-2] lactate species is expressed as a function of the fractional fluxes P_G and $P_S = X$ of glucose:

$$r_1 = \frac{[[^{13}C-3]\text{lactate}]}{[[^{13}C-2]\text{lactate}]} = \frac{\tfrac{2}{3}P_S}{P_G} = \frac{2X}{3(1-X)} \qquad (2.15)$$

or as in the previous case the ratio r_2 of [^{13}C-3]- to [^{12}C-3]-lactate:

$$r_2 = \frac{[^{13}C-3]\text{lactate}}{[^{12}C-3]\text{lactate}} = \frac{\tfrac{2}{3}P_S}{2P_G + P_S} = \frac{2X}{6-3X} \qquad (2.16)$$

Or addition of equations 2.12 and 2.14 enable one to express X as a function of [^{13}C-2]-lactate, [^{12}C-3]-lactate and glucose consumed.

Three expressions evaluating the fraction X of glucose consumed via the pentose shunt as a function of observables from the NMR spectra are therefore given by:

$$X = \frac{3r_1}{2+3r_1} \tag{2.17}$$

$$X = \frac{6r_2}{2+3r_2} \tag{2.18}$$

$$X = \frac{[[^{12}C-3]\text{lactate}] - 2[[^{13}C-2]\text{lactate}]}{[\text{glucose}]} \tag{2.19}$$

Fractional enrichments.

Expressions for the fractional enrichments F_{Li} as a function of the fractional fluxes are given by the following. As mentioned earlier, figure 2.4 shows that once [^{13}C-2]-glucose has been consumed, there are 4 possible labeling patterns for lactate: [^{12}C-1,2,3]-lactate (unlabeled lactate), [^{13}C-2]-lactate, [^{13}C-3]-lactate and [^{13}C-1,3]-lactate. It is sufficient to consider the fractional enrichments in C2 and C3 positions, F_{L2} and F_{L3} and the fraction of unlabeled lactate F_{L0} to obtain equations similar to the previous ones relating flux to fractional enrichments.

The fractional enrichments are obtained by substituting equations 2.12 and 2.13 in the definitions and using the additional expressions for total lactate produced [lactate] and unlabeled lactate produced [[^{12}C-1,2,3]-lactate]:

$$[\text{lactate}] = (2P_G + \tfrac{5}{3}P_S)[\text{glucose}] = \frac{6-X}{3}[\text{glucose}] \tag{2.20}$$

$$[[^{12}C\text{-}1,2,3]\text{-lactate}] = [\text{glucose}]\,P_G + [\text{glucose}]\,P_S = [\text{glucose}] \tag{2.21}$$

This gives:

$$F_{L0} = \frac{P_G + P_S}{2P_G + \tfrac{5}{3}P_S} = \frac{3}{6-X} \tag{2.22}$$

$$F_{L2} = \frac{P_G}{2P_G + \tfrac{5}{3}P_S} = \frac{3(1-X)}{6-X} \tag{2.23}$$

$$F_{L3} = \frac{\tfrac{2}{3}P_S}{2P_G + \tfrac{5}{3}P_S} = \frac{2X}{6-X} \tag{2.24}$$

It is also possible to give expressions of X as a function of the fractional enrichments using the formulae above, assuming all of the lactate comes from consumption of [^{13}C-2]-glucose:

$$X = \frac{6F_{L0} - 3}{F_{L0}} \tag{2.25}$$

$$X = \frac{6F_{L2} - 3}{F_{L2} - 3} \tag{2.26}$$

$$X = \frac{6F_{L3}}{F_{L3} + 2} \tag{2.27}$$

2.3. Model for pentose shunt activity under aerobic conditions. The glutamate enrichment method.

In the following we develop expressions linking the relative enrichment of glutamate carbons with the fractional flux X of glucose through the shunt using the assumption that the relative enrichment of acetyl-CoA carbons reflects the relative enrichment of pyruvate carbons. The models we develop for measurement of flux of glucose through the pentose shunt based on the classical formulation of the shunt assume the distribution of labels in fructose 6 phosphate and glyceraldehyde-3-phosphate after passage of [^{13}C-2]-glucose through the shunt shown in figure 2.3. This labeling scheme is shown again in figure 2.5. where the entry of labeled pyruvate into the citrate cycle *via* pyruvate dehydrogenase (PDH) and transamination to glutamate is also shown. The labeling scheme of pyruvate is the same as that of lactate shown in figure 2.4 where the C1 of lactate corresponds to the C1 of pyruvate. In the following, expressions for the fractional enrichment of pyruvate as a function of the fractional flux X through the shunt are developed. The incorporation of label into glutamate from pyruvate will depend on the relative activities of PDH and pyruvate carboxylase (PC), the equilibration of α-

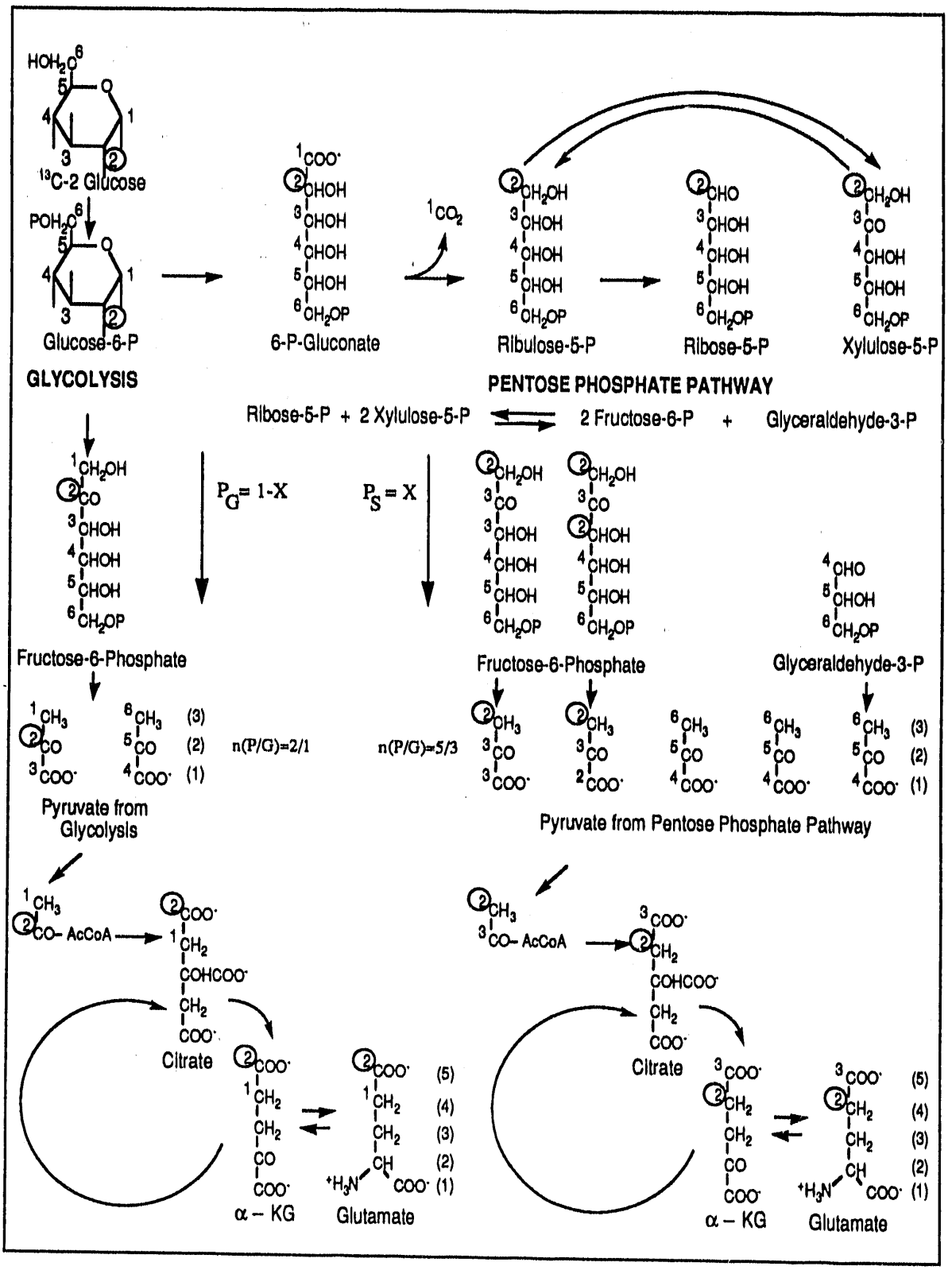

Figure 2.5. Model for the [C-4]-glutamate enrichment from [^{13}C-2]-glucose method. Numbers in parentheses at right of molecules are carbon positions, Pi are fractional fluxes, n(P/G) are number or pyruvate molecules produced per glucose molecule consumed. Carbon 2 of glucose is circled to indicate a label ^{13}C placed there.

ketoglutarate with glutamate via glutamate transaminase and the amount of cycling in the citrate cycle. Using a model for the citrate cycle that takes into account cycling and anaplerotic reactions, expressions for the fractional enrichment of acetyl-CoA species as a function of the fractional enrichment of glutamate species are developed. Relative enrichments of pyruvate carbons, acetyl-CoA carbons are defined, and the relative enrichment of glutamate carbons are given as a function of the glutamate fractional enrichments.

2.3.1. Fractional enrichment and relative enrichment of pyruvate.

Fractional enrichment of pyruvate.

The fractional enrichment of pyruvate as a function of the flux X of glucose via the shunt can be developed in the same manner as it was for lactate in the previous section. The following notation is used :

[pyruvate] = total pool of pyruvate

F_{P0} = fraction of unlabeled pyruvate = [[^{12}C-1,2,3]]pyruvate / [pyruvate]

F_{P2} = fraction of [^{13}C-2]-pyruvate = [[^{13}C-2]-pyruvate] / [pyruvate]

F_{P3} = fraction of [^{13}C-3]-pyruvate = [[^{13}C-3]-pyruvate] / [pyruvate]

where [^{13}C-3]-pyruvate refers to all pyruvate labeled in position C3 i.e. [^{13}C-3]- and [^{13}C-1,3]-pyruvate.

Applying the model in figure 2.5., pyruvate formed from the consumed glucose yields:

$$[\text{pyruvate}] = (2P_G + \tfrac{5}{3}P_S)[\text{glucose}] = \frac{6-X}{3}[\text{glucose}] \qquad (2.28)$$

$$[[^{12}C-1,2,3-\text{pyruvate}]] = (P_G + P_S)[\text{glucose}] = [\text{glucose}] \qquad (2.29)$$

$$[[^{13}C-2]\text{pyruvate}] = P_G[\text{glucose}] = (1-X)[\text{glucose}] \qquad (2.30)$$

$$[[^{13}C-3]\text{pyruvate}] = (\tfrac{2}{3})P_S[\text{glucose}] = \frac{2X}{3}[\text{glucose}] \qquad (2.31)$$

and if all the pyruvate present is formed only from glucose then the fractional enrichments would be:

$$F_{P0} = \frac{P_G + P_S}{2P_G + \frac{5}{3}P_S} = \frac{3}{6-X} \tag{2.32}$$

$$F_{P2} = \frac{P_G}{2P_G + \frac{5}{3}P_S} = \frac{3(1-X)}{6-X} \tag{2.33}$$

$$F_{P3} = \frac{\frac{2}{3}P_S}{2P_G + \frac{5}{3}P_S} = \frac{2X}{6-X} \tag{2.34}$$

Expression 2.28 gives the total amount of pyruvate if all pyruvate is formed from glucose. In an open cellular system, pyruvate is at the crossroads of metabolic pathways, and unlabeled pyruvate may be produced from unlabeled alanine, lactate or oxaloacetate pools present in the cell. If unlabeled pyruvate is produced from other undetermined sources, expression 2.28 and 2.29 need another term on their right hand side to take this into account and the expressions for the fractional enrichments also need correction. In this case the fractional flux of glucose via the pentose shunt cannot be determined from the fractional enrichments which will contain an unmeasurable term. However we can measure the relative enrichments which do not contain this term.

Definition of relative enrichments.

The relative enrichment R_{Pi} of position Ci of a given intermediate is defined as the ratio of the amount of label in position i over the sum of amount of label in all positions:

$$R_{Pi} = \frac{[[^{13}C-i]\text{pyruvate}]}{\sum_{j=3}^{j}[[^{13}C-j]\text{pyruvate}]} \tag{2.35}$$

Relative enrichments of pyruvate.

Under the assumption that the only source for labeled pyruvate is the labeled glucose, the relative enrichments do not rely on the total amount of pyruvate and may be expressed as a function of the fractional fluxes by substituting equations 2.30 and 2.31 into the definition (equation 2.35):

$$R_{P2} = \frac{[[^{13}C-2]\text{pyruvate}]}{[[^{13}C-2]\text{pyruvate}]+[[^{13}C-3]\text{pyruvate}]} = \frac{P_G}{P_G + \frac{2}{3}P_S} = \frac{3(1-X)}{3-X} \qquad (2.36)$$

$$R_{P3} = \frac{[[^{13}C-3]\text{pyruvate}]}{[[^{13}C-2]\text{pyruvate}]+[[^{13}C-3]\text{pyruvate}]} = \frac{\frac{2}{3}P_S}{P_G + \frac{2}{3}P_S} = \frac{2X}{3-X} \qquad (2.37)$$

Therefore the expressions for the flux as a function of the relative enrichments of pyruvate are:

$$X = \frac{3(R_{P2}-1)}{R_{P2}-3} \qquad (2.38)$$

$$X = \frac{3R_{P3}}{2+R_{P3}} \qquad (2.39)$$

Or X may be expressed as the ratio r_P of [^{13}C-3] to [^{13}C-2]-pyruvate:

$$r_P = \frac{R_{P3}}{R_{P2}} \qquad (2.40)$$

$$X = \frac{3r_P}{2+3r_P} \qquad (2.41)$$

This is identical to the expression for relative shunt flux from the ratio r_1 of C3 to C2 labeled lactate. The same result is obtained by expressing the relative enrichments as a function of the ratios of fractional enrichments, since the denominators of the fractional enrichments containing the undetermined term will eliminate in the ratio.

Relative enrichments of alanine.

Alanine is produced from pyruvate via transaminase and ^{13}C labeled alanine is observed in the NMR spectrum. Under the assumption that the only labeled alanine produced is from labeled pyruvate, the relative enrichments of alanine are equal to the relative enrichments of pyruvate:

$$R_{A2} = \frac{3(1-X)}{3-X} \tag{2.42}$$

$$R_{A3} = \frac{2X}{3-X} \tag{2.43}$$

From the above equations X may be expressed as the ratio r_A of [^{13}C-3] to [^{13}C-2]-alanine:

$$r_A = \frac{R_{A3}}{R_{A2}} \tag{2.44}$$

$$X = \frac{3r_A}{2+3r_A} \tag{2.45}$$

Relative enrichments of acetyl-CoA.

R_{Ci} are the relative enrichments of acetyl-CoA carbon positions. Under the assumption that labeled acetyl-CoA is produced only from labeled pyruvate *via* pyruvate dehydrogenase (see figure 2.5) then at steady state the relative enrichment of acetyl-CoA at position C1 (R_{C1}) is equal to the relative enrichment of pyruvate at position C2 (R_{P2}), and the relative enrichment of acetyl-CoA at position C2 (R_{C2}) is equal to the relative enrichment of pyruvate at position C3 (R_{P3}).

$$R_{C1} = \frac{3(1-X)}{3-X} \tag{2.46}$$

$$R_{C2} = \frac{2X}{3-X} \tag{2.47}$$

In the next section we link these expressions to the relative enrichments of glutamate.

2.3.2. Model taking into account cycling and anaplerotic reactions.

A mathematical model of the citrate cycle which allows evaluation of the fractional enrichment of molecules entering both the oxidative and anaplerotic pathways under steady state conditions was developed by Malloy et al. (23). Figure 2.6 shows the network of reactions of the citrate cycle and transamination reactions necessary to describe the model. Individual enzyme reactions of the cycle not shown in figure 2.6 are: aconitase, succinyl-CoA synthetase, succinate dehydrogenase and fumarase. When the cycle turns, the oxidative decarboxylations following the incorporation of the acetyl group via citrate synthase produce NADH for the electron transport chain which generates ATP for the cell. When citrate cycle intermediates are used for biosynthesis of amino acids or porphyrins, the intermediate pools must be replenished in order for the cycle to continue operating. The reactions resulting in the *de novo* synthesis of citrate cycle intermediates, excluding the citrate synthase reaction, are called the anaplerotic reactions. Anaplerosis includes the formation of oxaloacteate from pyruvate via pyruvate carboxylase or from aspartate via transaminase and results in the replacement of the intermediate's label by an unlabeled or differently labeled species. The model takes into account replacement of label by anaplerosis, cycling of label in the cycle and production of labeled glutamate from α-ketoglutarate via transaminase.

The strategy of the model is based on the analysis of the glutamate ^{13}C spectrum. ^{13}C coming from the labeled glucose provided to the cell system in the experiment is incorporated into glutamate. The various species of ^{13}C labeled glutamate are isotope isomers of unlabeled glutamate and are called glutamate isotopomers. There are 32 possible

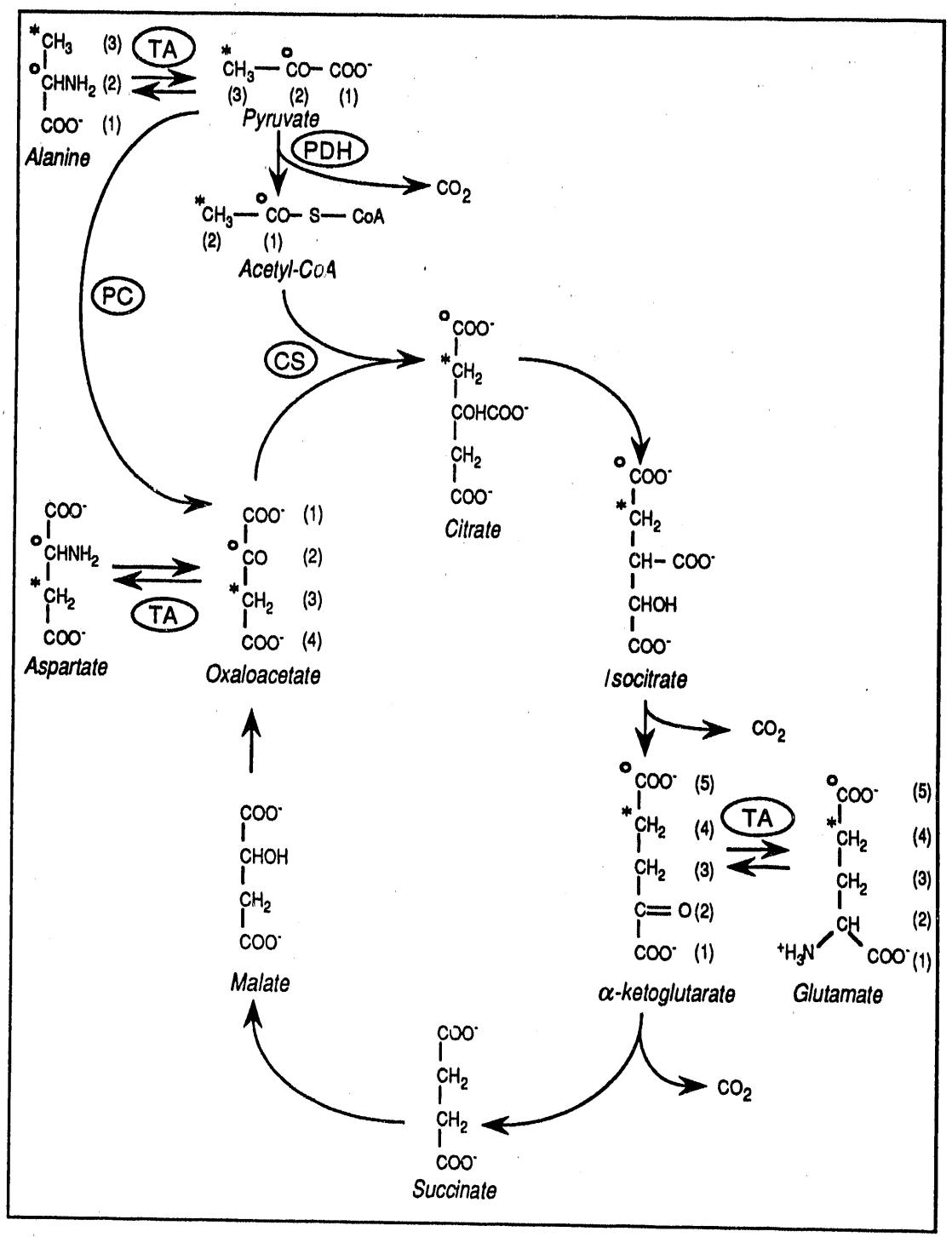

Figure 2.6. Simplified citrate cycle and transamination reactions.
Enzymes: PDH=pyruvate dehydrogenase, PC=pyruvate decarboxylase, CS=citrate synthase, TA = transaminase. The o and * follow the fate of a C-13 label placed at respectively C2 and C3 of pyruvate.

^{13}C isotopomers for glutamate resulting from the 2^5= 32 possible different combinations of the 5 labeled (or unlabeled) positions of glutamate. The appearance and relative intensities of the glutamate resonances in the NMR spectrum depend on the mixture of isotopomers present in solution. The model yields the fraction of each isotopomer (amount of isotopomer i relative to the total amount of glutamate) as a function of 7 metabolic parameters describing the citrate cycle at steady state. These parameters are:

F_{C0} = fraction of unlabeled acetyl-CoA

F_{C1} = fractional enrichment of [^{13}C-1]-acetyl-CoA

F_{C2} = fractional enrichment of [^{13}C-2]-acetyl-CoA

F_{C3} = fractional enrichment of [^{13}C-1,2]-acetyl-CoA (doubly labeled species)

y = flux of anaplerotic reactions relative to citrate synthase flux

F_{A0} = fraction of unlabeled anaplerotic substrate

F_{A1} = fractional enrichment of anaplerotic substrate that yields either [^{13}C-2] or [^{13}C-3]-oxaloacetate in the first span of the citrate cycle.

F_{A2} = fractional enrichment of anaplerotic substrate that yields [^{13}C-2,3]-oxaloacetate in the first span of the citrate cycle.

The model is developed with the following assumptions (23):

1. The citrate cycle is in steady state: the concentrations of the citrate cycle intermediates and their exchanging pools are constant, the fractional enrichment at each carbon of the substrates and citrate cycle intermediates is not changing, and the rate of disposal reactions equals the rate of anaplerotic reactions.

2. All ^{13}C entering oxaloacetate has been randomized between C1 and C4 and between C2 and C3.

3. The fraction of labeled CO_2 involved in carboxylation of pyruvate is negligible.

4. The relative concentration of glutamate isotopomers is identical to the relative concentrations of α-ketoglutarate isotopomers.

The general case developed includes all four possible labeling patterns in acetyl-CoA (unlabeled, singly labeled in C1 or C2 and doubly labeled) and three possible labeling patterns in the anaplerotic substrates. Development of the model to yield the concentration of each isotopomer of glutamate as a function of the metabolic variables defined above is done in the following manner.

The distribution of isotopomers is determined by the input-output method (24). Consider a given α-ketoglutarate isotopomer as the input molecule. After one turn of the cycle, the labeling pattern of the output α-ketoglutarate isotopomer depends firstly on whether the succinate formed has proceeded directly to oxaloacetate or has been replaced in an anaplerotic reaction, and secondly, on which acetyl isotopomer oxaloacetate has combined with. So the probability of obtaining a given output α-ketoglutarate isotopomer depends on the alternative pathways available to the input α-ketoglutarate isotopomer, and is a function of the metabolic parameters given above. Conservation of mass at steady state implies that the concentration of a given input α-ketoglutarate isotopomer must equal the sum of all isotopomer concentrations times the probability that each isotopomer will yield that isotopomer of interest after one turn of the cycle. This results in 32 equations in 32 unknowns which is solved to relate the relative concentration of each isotopomer to the metabolic variables (23).

Although the concentration of a single isotopomer cannot be measured from the ^{13}C spectrum, the relative concentration of the glutamate carbon groups can be directly measured , thereby relating the ^{13}C spectrum to physiological variables. For example in the ^{13}C NMR spectrum the peak for [C-4]-glutamate is due to the contribution at 36.10 ppm of all 16 isotopomers that have a ^{13}C label in position C4 : [^{13}C-4]-glutamate, [^{13}C-1,4]-glutamate, [^{13}C-2,4]-glutamate, [^{13}C-1,2,4]-glutamate, [^{13}C-3,4]-glutamate, [^{13}C-1,3,4]-glutamate, [^{13}C-2,3,4]-glutamate, [^{13}C-1,2,3,4]-glutamate, [^{13}C-4,5]-glutamate, [^{13}C-1,4,5]-glutamate, [^{13}C-2,4,5]-glutamate, [^{13}C-1,2,4,5]-glutamate, [^{13}C-3,4,5]-glutamate, [^{13}C-1,3,4,5]-glutamate, [^{13}C-2,3,4,5]-glutamate, [^{13}C-1,2,3,4,5]-glutamate.

These are shown below (where a star indicates ^{13}C label):

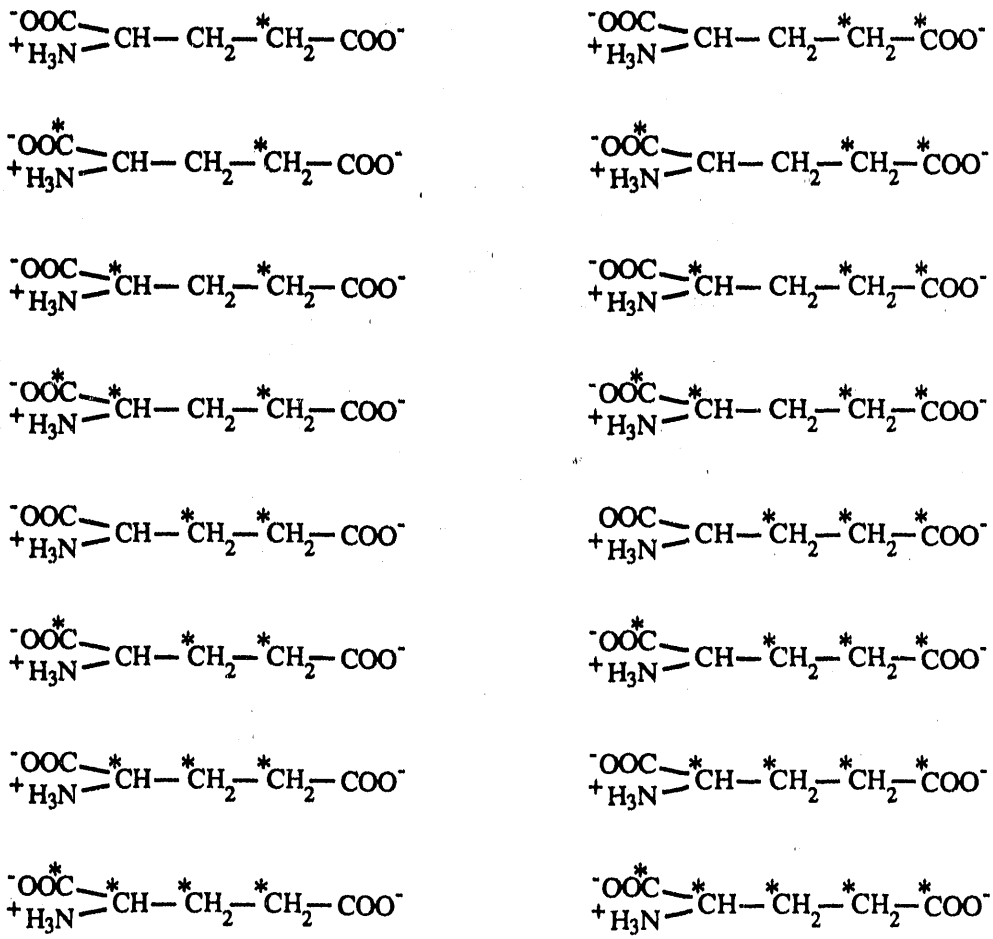

The first four isotopomers will contribute to the singlet peak at 36.10 ppm while the others which have a ^{13}C adjacent to C4 will contribute to multiplets centered at 36.10 ppm. The fractional enrichment of [C-4]-glutamate is therefore given by the sum of relative areas of the above 16 isotopomers. Before giving the expressions relating the fractional enrichment of each of the five carbons of glutamate to the physiological parameters, the following simplification is applied.

When [^{13}C-2]-glucose is the labeled substrate, the first four isotopomers are the predominant C4-labeled species. The glucose generated pyruvate pool supplying the acetyl-

CoA pool is approximately half unlabeled half singly labeled. This is explained by the equivalent production of labeled and unlabeled pyruvate via glycolysis and the production of 2/5 labeled to 3/5 unlabeled pyruvate via the shunt (see figure 2.5). This is supported by the experimental NMR spectrum: species labeled in adjacent positions should give rise to multiplets, and no multiplet structure was observed in the ^{13}C spectrum. Consequently the probability of having doubly labeled acetyl-CoA is negligible, and in the [^{13}C-2]-glucose substrate case one sets $F_{C3} = 0$. For the same reasons the probability of having doubly labeled anaplerotic substrate is negligible and F_{A2} is also set to 0. The fractional enrichments F_{Gi} after this simplification are given by:

$$F_{G1} = \frac{(1 - 2F_{C0} + F_{C0}^2 - F_{C1} + F_{C0}F_{C1} + 4y - 6F_{C0}y + 2F_{C0}^2y - 3F_{C1}y + 2F_{C0}F_{C1}y - 2F_{C2}y - F_{A0}F_{C2}y + 2F_{C0}F_{C2}y + 2F_{C1}F_{C2}y + 3y^2 - F_{A0}y^2 - 2F_{C0}y^2 - 2F_{C2}y^2)}{2(1+y)(1-F_{C0}-F_{C1}+y)(1+2y)} \quad (2.48)$$

$$F_{G2} = \frac{1 - F_{C0} - F_{C1} + y - F_{A0}y}{1+2y} \quad (2.49)$$

$$F_{G3} = \frac{1 - F_{C0} - F_{C1} + y - F_{A0}y}{1+2y} \quad (2.50)$$

$$F_{G4} = F_{C2} \quad (2.51)$$

$$F_{G5} = F_{C1} \quad (2.52)$$

One notes that with the simplification taken into account, the fractional enrichments in positions C4 (F_{G4}) and C5 (F_{G5}) of glutamate are determined by the two physiological parameters F_{C1} and F_{C2}.

The relative enrichments between C4 and C5 positions are defined as:

$$R'_{G4} = \frac{F_{G4}}{F_{G4} + F_{G5}} \quad (2.53)$$

$$R'_{G5} = \frac{F_{G5}}{F_{G4} + F_{G5}} \tag{2.54}$$

Substituting the F_{G4} and F_{G5} by the metabolic parameters F_{C1} and F_{C2} in equations 2.53 and 2.54 gives the relative enrichments between C4 and C5 expressed as relative enrichments of acetyl-CoA which in turn is expressed as a function of the fractional flux X of glucose via the shunt (equations 2.46 and 2.47):

$$R'_{G4} = \frac{F_{C2}}{F_{C1} + F_{C2}} = R_{C2} = \frac{2X}{3-X} \tag{2.55}$$

$$R'_{G5} = \frac{F_{G5}}{F_{G4} + F_{G5}} = R_{C1} = \frac{3(1-X)}{3-X} \tag{2.56}$$

From the above equations X may be expressed as the ratio r_G of [^{13}C-4] to [^{13}C-5]-glutamate:

$$r_G = \frac{R'_{G4}}{R'_{G5}} \tag{2.57}$$

$$X = \frac{3r_G}{2 + 3r_G} \tag{2.58}$$

Therefore the fractional flux of glucose via the pentose shunt may be expressed as a function of the ratio r_L of relative enrichments of C2 and C3 of lactate in the anaerobic case (equation 2.17) and of the ratio r_A of relative enrichments of C3 and C2 of alanine (equation 2.45) or of the ratio r_G of relative enrichments of C4 and C5 of glutamate in the aerobic case (equation 2.58). Information about the fractional enrichment of the anaplerotic substrates and the total flux of anaplerotic reactions relative to citrate synthase flux may be extracted from the relative enrichments of C1, C2 and C3 carbons of glutamate in the aerobic case.

The different proposed methods for calculating the relative flux of glucose through the pentose shunt are summarized in table 2.1.

Table 2.1. Table of fractional flux X of glucose through the pentose shunt related to ratio of relative and fractional enrichments of metabolic intermediates.

Intermediate	Glucose label	Ratio	Flux
Lactate	C1	$r = \frac{[[^{13}C-3]lac]}{[[^{12}C-3]lac]}$	$X = \frac{3(1-r)}{3+2r}$
		$F_{L0} = \frac{[[^{12}C-3]lac]}{[lac]}$	$X = \frac{3(2F_{L0}-1)}{2+F_{L0}}$
		$F_{L3} = \frac{[[^{13}C-3]lac]}{[lac]}$	$X = \frac{3(1-2F_{L3})}{3-F_{L3}}$
Lactate	C2	$r_1 = \frac{[[^{13}C-3]lac]}{[[^{13}C-2]lac]}$	$X = \frac{3r_1}{2+3r_1}$
		$r_2 = \frac{[[^{13}C-3]lac]}{[[^{12}C-3]lac]}$	$X = \frac{6r_2}{2+3r_2}$
			$X = \frac{[[^{12}C3]lac]-2[[^{13}C2]lac]}{[gluc]}$
		$F_{L0} = \frac{[[^{12}C-3]lac]}{[lac]}$	$X = \frac{6F_{L0}-3}{F_{L0}}$
		$F_{L2} = \frac{[[^{12}C-2]lac]}{[lac]}$	$X = \frac{6F_{L2}-3}{F_{L2}-3}$
		$F_{L3} = \frac{[[^{13}C-3]lac]}{[lac]}$	$X = \frac{6F_{L3}}{F_{L3}+2}$
Pyruvate	C2	$R_{P2} = \frac{[[^{13}C2]pyr]}{[[^{13}C2]pyr]+[[^{13}C3]pyr]}$	$X = \frac{3(R_{P2}-1)}{R_{P2}-3}$
		$R_{P3} = \frac{[[^{13}C3]pyr]}{[[^{13}C2]pyr]+[[^{13}C3]pyr]}$	$X = \frac{3R_{P3}}{2+R_{P3}}$
		$r_P = \frac{[[^{13}C-3]pyr]}{[[^{13}C-2]pyr]}$	$X = \frac{3r_P}{2+3r_P}$
Alanine	C2	$r_A = \frac{[[^{13}C-3]ala]}{[[^{13}C-2]ala]}$	$X = \frac{3r_A}{2+3r_A}$
Glutamate	C2	$r_G = \frac{[[^{13}C-4]glu]}{[[^{13}C-5]glu]}$	$X = \frac{3r_G}{2+3r_G}$

2.4. Model for the Aminonicotinamide method.

This model is based on the selective inhibition of 6-phosphogluconate dehydrogenase (6PGDH) by by 6-amino-NADP (6-ANADP) formed when tissue is incubated with 6-aminonicotinamide (6-AN)(3). The model is shown in figure 2.7. When

6-AN is administered to a cell system, 6-ANADP is synthesized by the action of endoplasmic glycohydrolase (25). The 6-amino analog of the coenzyme NADP is unable to act as a hydrogen acceptor and is a competitive inhibitor of NADP-dependent oxido-reduction enzymes (26). It has been shown to preferentially inhibit 6PGDH under physiological conditions in brain tissue, and lead to accumulation of the substrate 6-phosphogluconate (6PG) (3) & (27). From 2 to 8 hours after administration of 6-AN, the accumulation of 6PG has been shown to to be approximately linear with time. This can be accounted for with the simple model shown in figure 2.7.

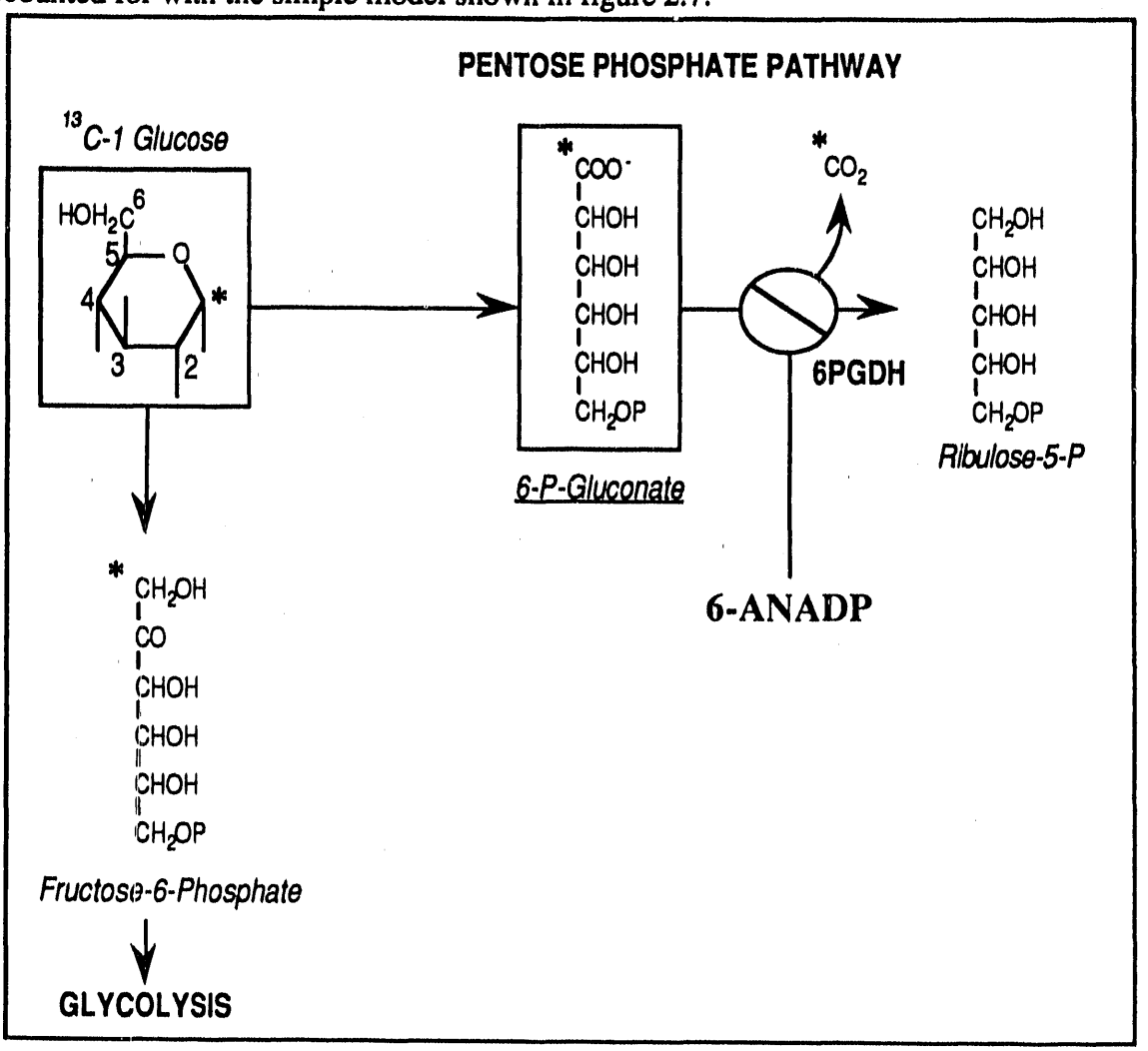

Figure 2.7. Model for the 6-aminonicotinamide blockage method. Injection of 6-aminonicotinamide (6-AN) leads to the production of 6-amino-NADP which is a specific inhibitor of 6-phosphogluconate dehydrogenase (6PGDH). After I.V. infusion with [^{13}C-1]-glucose, [^{13}C-1]-6-phosphogluconate accumulates in the tissue. * = ^{13}C label.

[^{13}C-1]-glucose injected I.V. is taken up by the tissue and flows through glycolysis and pentose shunt pathways. Glucose consumed *via* the shunt undergoes the first irreversible step of glucose-6-phosphate dehydrogenase (G6PDH) to form 6PG which then accumulates in the tissue. The amount of [^{13}C-1]-6PG accumulated per given time period yields the rate of glucose utilization *via* the pentose shunt, assuming that the rate measured in the 6-AN perturbed system is the same as the rate when no 6-AN is administered (28).

We are interested in obtaining the flux of glucose through the shunt relative to flux through glycolysis (relative shunt flux). If one could assume that after administration of 6-AN, none of the [^{13}C-1]-6PG formed is metabolized further, and that no ^{13}C label is transported out of the tissue during the accumulation time, the relative shunt flux would be determined by the amount of ^{13}C label in 6PG relative to ^{13}C label incorporated in glycolysis metabolites. The first assumption is not reasonable considering that the the 6PGDH blockage by 6-ANADP is not total. This is supported by the fact that the amount of 6PG accumulated in a given time is proportional to the dose of 6-AN administered (27). The second assumption is reasonable if the time necessary for 6PG to accumulate to a detectable level is short enough. Since the action of 6PGDH results in the loss of the C1 label to CO_2, the calculation just suggested would underestimate the relative shunt flux.

The calculation just suggested would have the advantage of taking into account the amount of uptake of labeled glucose. Obviously, the amount of 6PG accumulated will also depend on the uptake of glucose in the tissue. In order to take into account the [^{13}C-1]-glucose uptake in the tissue, we propose to normalize the amount of [^{13}C-1]-6PG by the glucose fractional enrichment (ratio of labeled to total glucose) in the tissue. The ratio of [^{13}C-1]-6PG accumulated to glucose fractional enrichment then permits comparison of relative pentose shunt activities (given as G6PDH activity) of the tissue independently of variations in glucose uptake conditions. The amount of [^{13}C-1]-6PG is measured from the ^{13}C NMR spectrum of the tissue extract. The glucose fractional enrichment is obtained in the proton NMR spectrum of the tissue extract.

Chapter 3.

Methods

3.1. NMR methodology.

3.1.1. Sensitivity, signal to noise and quantitative measurement.

When using NMR as a tool for investigating metabolic pathways, optimization of the sensitivity is a prime goal towards which we strive. The way by which the maximization of the signal to noise is obtained depends on the conditions of the experiment. To test the metabolic hypotheses of our method we have used cell systems for dynamic NMR spectroscopy of the metabolic system with fields up to 11.7 T. We have also extracted the tissues frozen *in situ* which also enables NMR spectroscopy to be performed with the available high field narrow bore spectrometers.

Optimization of signal to noise: Ernst angle, T_1 measurements, signal processing.

In Fourier pulsed spectroscopy one obtains increased signal to noise relative to the continuous wave (cw) experiment due to coherent signal averaging. However, if the spin

is not fully relaxed between pulses a steady state Z magnetization M_z smaller than the equilibrium value M_0 occurs, resulting in a lower signal to noise than one could maximally obtain by the Fourier method. The value of M_z depends on the repetition delay T_R between pulses and the transverse relaxation time T_1 of the spin: longer T_R's permit return to equilibrium but increase acquisition time. The experimenter must trade off time for signal to noise. Maximization of the signal with respect to T_R which is chosen as short as acquisition permits is obtained by using the Ernst angle α_E (29) defined by

$$\cos\alpha_E = e^{-\frac{T_R}{T_1}} \tag{3.1}$$

We have generally used the Ernst angle which optimizes for the T_1 of the spin of interest in a given experiment, e.g. [^{13}C-4]-glutamate in the case of aerobic experiments. T_1's of compounds of interest were measured using an inversion recovery pulse sequence. T_2's were measured using a CPMG spin echo pulse sequence. In the relaxation times measurements, the variation of peak intensities with variable delay time was fitted to the following functions, using the fitting program provided by Bruker Instruments on the Aspect 3000 computer.

For T_1:

$$I(t) = I_0(1-2e^{-\frac{\tau}{T_1}}) \tag{3.2}$$

For T2:

$$I(\tau) = I_0 e^{-\frac{\tau}{T_2}} \tag{3.3}$$

Table 3.1 shows measured T_1's for the ^{1}H and ^{13}C of compounds of interest.

Table 3.1. Spin-lattice relaxation times (T_1) for the ^1H and ^{13}C of compounds of interest.

Compound	ppm	T1 (s)	#	Compound	ppm	T1 (s)	#
Alanine				**Glutamate**			
^{13}C: [^{13}C-2]	53.18	3.2	1	^{13}C: [^{13}C-1]	177.30	14.41	3
^{13}C: [^{13}C-3]	18.86	1.7	1	^{13}C: [^{13}C-2]	57.27	1.70	3
2-DG6P				^{13}C: [^{13}C-3]	29.63	1.08	3
^{31}P: [C-6]	7.52	3.11	13	^{13}C: [^{13}C-4]	36.10	1.28	3
Phosphate i	pH dep	2.91	13	^{13}C: [^{13}C-5]	183.99	14.94	3
DSS				^{13}C: [^{13}C-1]	177.30	n.m.	8
^{13}C: [^{13}C-1]	0.00	7.39	2	^{13}C: [^{13}C-2]	57.28	1.23	8
^1H: [^{12}C-1]	0.00	3.10	3	^{13}C: [^{13}C-3]	29.63	0.93	8
^1H: [^{13}C-1]	0.00	2.40	3	^{13}C: [^{13}C-4]	36.10	n.m.	8
Lactate				^{13}C: [^{13}C-5]	183.99	12.37	8
^{13}C: [^{13}C-2]	69.62	6.94	12	^1H: [^{12}C-2]	3.75	2.80	3
^1H: [^{12}C-3]	1.30	1.50	12	^1H: [^{12}C-4]	2.34	0.69	3
6PGluconate				^1H: [^{13}C-2]	3.75(c)	n.m.	3
^{13}C: [^{13}C-1]	179.50	5.28	5	^1H: [^{13}C-4]	2.34(c)	0.61	3
Glucose				**Glutamine**			
^{13}C: α-[^{13}C-1]	94.44	0.98	6	^{13}C: [^{13}C-1]	176.80	6.17	9
^{13}C: β-[^{13}C-1]	98.26	1.30	6	^{13}C: [^{13}C-2]	57.02	1.76	9
^{13}C: α-[^{13}C-2]	72.58	1.99	7	^{13}C: [^{13}C-3]	29.07	1.05	9
^{13}C: β-[^{13}C-2]	75.26	2.03	7	^{13}C: [^{13}C-4]	32.57	1.35	9
^1H: α-[^{12}C-1]	5.20	0.80	6	^{13}C: [^{13}C-5]	178.48	10.90	9
^1H: α-[^{13}C-1]	5.20(c)	0.60	6	**Glutathione**			
^1H: β-[^{12}C-1]	4.60	0.80	6	^1H:α-Cys-red	4.56	2.68	10
^1H: β-[^{13}C-1]	4.60(c)	0.60	6	^1H:α-Cys-ox	3.29	0.45	11

n.m. = not measured c = center of multiplet

#1 = From Sumegi (30) pca extract of yeast preparation, field is 11.7 T.

#2 = Standard solution 0.1M DSS in 0.1M phosphate buffered D_2O, pH 8, field is 9.3 T.

#3 = Standard solution 0.01M DSS, 0.3M glutamate in 0.1M phosphate buffered D_2O, pH 7, 9.3 T.

#4 = Yeast cell suspension after anaerobic consumption of 20 µmol of [^{13}C-1]-glucose, field is 9.3 T.

#5 = Standard solution 0.01M DSS, 0.1M 6-P-gluconate in 0.1Mphosphate buffered D_2O, pH 8, 9.3 T.

#6 = Standard solution 0.01M DSS, 0.1M [^{13}C-1]-glucose in 0.1M phosphate buffered D_2O, pH 7, 9.3 T.

#7 = Cell free preparation w/o coenzymes, 0.02M [^{13}C-1]-glucose, 0.1M imidazole buffer pH 7.4, 9.3T.

#8 = Aqueous fraction of yeast cell pellet extract, disolved in 0.1M phosphate buffered D_2O, pH 7, 9.3 T.

#9 = From reference (31) , pca extract of brain slices, field is 9.3 T.

#10 = Standard solution 0.01M DSS, 0.08M GSH in 0.1M phosphate buffered D_2O, pH 7, field is 11.7 T.

#11 = Standard solution 0.01M DSS, 0.08M GSSG in 0.1M phosphate buffered D_2O, pH 7, 11.7 T.

#12 = Cell free preparation at end of experiment, 0.1M imidazole buffer pH 7.4, 9.3T.

#13 = Aqueous fraction of rat brain extract, disolved in 0.1M phosphate buffered D_2O, pH 7, field is 9.3 T.

Digital processing of the FID signal was done using standard routines on either a Bruker Aspect 3000 computer with Bruker NMR data processing software or a SUN Sparc station with the *Felix* NMR data processing software from Hare Research (32). FID's were generally zero filled to twice their size after baseline correction for resolution enhancement. FID's were multiplied by an exponential decay generally using the matched filter condition for the spin of interest where the resulting spectral line is broadened by an amount equal to its natural linewidth, then Fourier transformed.

Quantitation.

The measured peak integral I_i for a spin i is proportional to the steady state magnetization $M_{z(i)}$. The peak intensity and integrals are corrected for T_1 steady state magnetization effects. These magnetization effects were incorporated by a saturation factor S_i (29):

$$S_i = \frac{1 - e^{-\frac{T_R}{T_1}} \cos\alpha}{(1 - e^{-\frac{T_R}{T_1}}) \sin\alpha} \qquad (3.4)$$

where α is the flip angle of the applied RF pulse, and T_R is the recycle delay or repetition time between pulses. The corrected peak area I_i is given by applying this saturation factor to the measured integral I_{mi} :

$$I_i = I_{mi} \times S_i \qquad (3.5)$$

In order to relate the corrected peak integral to the concentration of the compound in the sample, a reference peak of known concentration must be used. In the case of tissue extracts, the internal reference DSS (2,2-dimethyl-2-silapentane-sulfonate) is used. A volume of 50 or 100 µl of 0.1 M DSS in distilled water is added to the frozen tissue sample

to be extracted. The added DSS therefore follows the extraction procedure. Variation in concentrations due to loss of sample during the extraction are accounted for since they are accompanied by loss of the internal reference. DSS is hydrophilic and extracts into the aqueous phase of the aqueous-organic extraction. Calibration of the measurement for compounds of interest was performed by adding known amounts of the compound to tissue before extraction and measuring the concentration by NMR spectroscopy in the aqueous phase. The concentration of the compound in the NMR sample is calculated from the peak integrals of the compound of DSS with the following equation:

$$[L] = \frac{I_L}{n_L}\frac{n_{DSS}}{I_{DSS}}[DSS] \tag{3.6}$$

where [L] is the concentration of compound L, I_L is the T_1 corrected peak integral of compound L, n_L is the number of spins participating in the peak, I_{DSS} is the T_1 corrected integral of the DSS peak at 0 ppm, n_{DSS} is the number of spins participating in the DSS peak, and [DSS] is the concentration of DSS. In the proton spectrum, $n_{DSS}=9$ and in the carbon spectrum, $n_{DSS}=3$, since the DSS peak corresponds to a trimethyl $(CH_3)_3$ group. For example if the compound L measured is lactate, and the peak observed in the proton spectrum is [C-3]-lactate, then $n_L=3$. The concentration of the compound in the NMR tube is related to concentration in the brain sample expressed as μmol/gram wet weight with the following equation:

$$C_L brain = \frac{[L]v_{NMR}}{m_{sample}} \tag{3.7}$$

where v_{NMR} is the volume of the reconstituted aqueous sample in the NMR tube and m_{sample} is the wet weight (weighed before extraction) of the frozen brain sample.

Estimation of peak integral errors.

Peak integrals were obtained using the numerical integration routine provided in the

NMR data processing package *Felix* (32). Polynomial baseline correction was applied to the spectrum before integration when necessary to obtain flat baselines. Three sources of error are considered in the estimation of the error on the peak integral obtained. These are digitization, data truncation and instrumental noise and are estimated as outlined below according to Weiss and Ferreti (33). The digitization error, or error due to availability of data at discrete rather than continuous intervals, depends on the number of points per half width and is negligible if this number is above 3, which is the case in our integrations. The truncation error, or error due to incomplete sampling (impossibility to sample from $-\infty$ to $+\infty$) of the Lorentzian line in the numerical integration, depends the digital resolution $\Delta\omega$ of the spectrum and the number of points (n) used to cover the peak in the peak integration. The truncation error leads to underestimation of the peak area. Integration conditions were such that the relative truncation error (shown in equation 3.8) was approximately 1% for all peaks of interest .

$$\text{underestimation} = \frac{2\,tan^{-1}(\alpha(m+\frac{1}{2}))}{\pi} - 1 \qquad (3.8)$$

with (2m + 1) = n = total number of points used in the integration, and

$$\alpha = \frac{2\,\Delta\omega}{\Delta\omega_{\frac{1}{2}}} \qquad (3.9)$$

where $\Delta\omega$ = digital resolution (hertz per point) and $\Delta\omega_{1/2}$ = width at half height of the peak.

The error on the peak area was dominated by noise error. The noise error depends on the previous factors and on the signal to noise ratio (SNR) of the peak. The following expression was used to estimate the relative error on the peak area dominated by noise (33):

$$\text{relative error} = \frac{\sigma(\text{integral})}{\text{integral}} = \frac{\alpha\sqrt{2m+1}}{\pi\,SNR} \qquad (3.10)$$

3.1.2. Proton observation of carbon nuclei: inverse detection.

Signal to noise improvement by observation of protons instead of carbon.

The higher gyromagnetic ratio of the proton relative to the carbon nucleus implies that higher sensitivity is achieved in the same amount of time by observing protons instead of carbon nuclei. In order to verify that reasonable sensitivity improvement relative to carbon detection was achieved in our experiments by using the proton detection sequence, we measured signal to noise ratios obtained with both detection methods under as similar as possible conditions on a phantom sample, and then compared the SNR improvement to the theoretical improvement expected. Below, the theoretical SNR improvement is derived.

The expression for the theoretical signal to noise SNR or Ψ of the NMR experiment is given by Alderman (34) as a function of probe, instrument and sample parameters:

$$\Psi = M_0 \sqrt{\frac{\mu_0 \omega_0 Q \Gamma}{8FkT\Delta f}} \qquad (3.11)$$

with the following definitions:

Physical constants:

μ_0 = permeability of free space = $4\pi\ 10^{-7}$ ($A^{-1}\ m^{-2}\ T$)

ω_0 = Larmor frequency = $\gamma_0 B_0$

γ_0 = gyromagnetic ratio $\quad \gamma_{0(proton)} = 26.751 \times 10^7$ radian $s^{-1}\ T^{-1}$

$\gamma_{0(carbon\text{-}13)} = 6.7283 \times 10^7$ radian $s^{-1}\ T^{-1}$

B_0 = constant magnetic field

k = Boltzmann's constant = 1.38×10^{-23} J K^{-1}

Probe parameters:

Q = quality factor (dimensionless)

F = amplifier noise figure = noise out/G noise in (G=amplification) (dimensionless)

T = temperature of probe

Δf = bandwidth of detection

Γ = factor taking into account the distribution of B_1 in the sample. (dimension = m^3)

In the ideal case of a perfectly homogeneous B_1 perpendicular to B_0, Γ is given by:

$$\Gamma = \sin^2 \alpha \frac{V_{sample}^2}{V_{resonator}} \tag{3.12}$$

with α = flip angle, V_{sample} = volume of the sample, and $V_{resonator}$ = probe volume.

Sample parameters:

M_0 = equilibrium magnetization

$$M_0 = \frac{N\gamma_0^2\hbar^2 I(I+1)}{3kT} B_0 \tag{3.13}$$

$\hbar$ = Plank's constant = 1.0546×10^{-34}

I = quantum spin number = 1/2 for proton and carbon

T = sample temperature

N = number of spins per unit volume in sample (dimension = m^{-3})

Equations 3.11 and 3.13 enable us to express the signal to noise Ψ as a function of the gyromagnetic ratio. This is done by replacing ω_0 with $\gamma_0 B_0$ and replacing M_0 with the right side of equation 3.13 in equation 3.11. The signal to noise estimated using this calculation comes out proportional to the gyromagnetic ratio to the power 5/2, as shown below.

$$\Psi = M_0 \sqrt{\frac{\mu_0 \omega_0 Q \Gamma}{8FkT\Delta f}} = \frac{N\gamma_0^2\hbar^2 I(I+1)}{3kT} B_0 \frac{\mu_0^{1/2}\gamma_0^{1/2}B_0^{1/2}Q^{1/2}\Gamma^{1/2}}{\sqrt{8FkT\Delta f}}$$

$$\Psi = \frac{N\hbar^2 I(I+1)}{3kT} \sqrt{\frac{\mu_0 Q \Gamma}{8FkT\Delta f}} \gamma_0^{3/2} B_0^{3/2} \tag{3.14}$$

In theory then, if one were able to devise an experiment where all experimental parameters concerning the probe, the sample and the acquisition channels were identical except for the gyromagnetic ratio of the nucleus observed, one would get $(\gamma_{proton}/\gamma_{carbon})^{5/2} = 32$ times better signal to noise from the proton experiment. In practice, for a given experimental setup, this improvement is hard to achieve because for a given proton carbon probe, probe parameters (Q, filling factor) are usually different for

each channel.

The SNR improvement was measured for the probe used in the inverse detect experiments on the Bruker AM-500 spectrometer . A phantom sample of 50% [^{12}C-1]-glucose / 50% [^{13}C-1]-glucose in phosphate buffered D_2O was used. The proton and carbon channels were tuned to the sample and the length of proton and carbon 90° flip angles were determined prior to the measurement . For detection on the carbon channel, a single pulse sequence with a 90° pulse and a recycle delay T_R of 7.32s permitting the ^{13}C glucose transverse magnetization to fully relax ($T_R >> T_1$ of α- and β-[^{13}C-1]-glucose) was used without proton decoupling. The spectral width was 10000 Hz, the data record size was 16K points and 64 scans were accumulated. For detection on the proton channel, the proton inverse detect sequence was used as well as a single pulse sequence with a 90° pulse for comparison. For both sequences, the recycle delay T_R was 7.97s (permitting full transverse relaxation of the glucose protons). The spectral width was 5556 Hz, the data record size was 16K points and 64 scans were accumulated. The SNR of the inverse proton observe experiment was found to be 20 times higher than SNR of the direct carbon detect experiment. Taking into account the difference in spectral width:

$$\sqrt{\frac{\Delta f_{13C}}{\Delta f_{1H}}} = \sqrt{\frac{10000}{5556}} = 1.32$$

would increase the theoretical improvement by a factor of 1.32 from the improvement given by the ratio of γ's (32 x 1.32 = 42.24). Therefore the experimental improvement in SNR is only half of the theoretically expected improvement. The lower value of 20 for the ratio of SNR's is assumed to be due in part to differences in the proton and carbon coils quality factor Q, B_1 distribution factor G and/or amplifier noise figure F since all other parameters must be the same.

Application: proton inverse detect pulse sequence.

The proton inverse detect pulse sequence used is based on the sequence first proposed by Bendall (35) for selective detection of protons coupled to ^{13}C nuclei, by suppression of signal from protons not coupled to ^{13}C. The sequence is shown in 3.1.

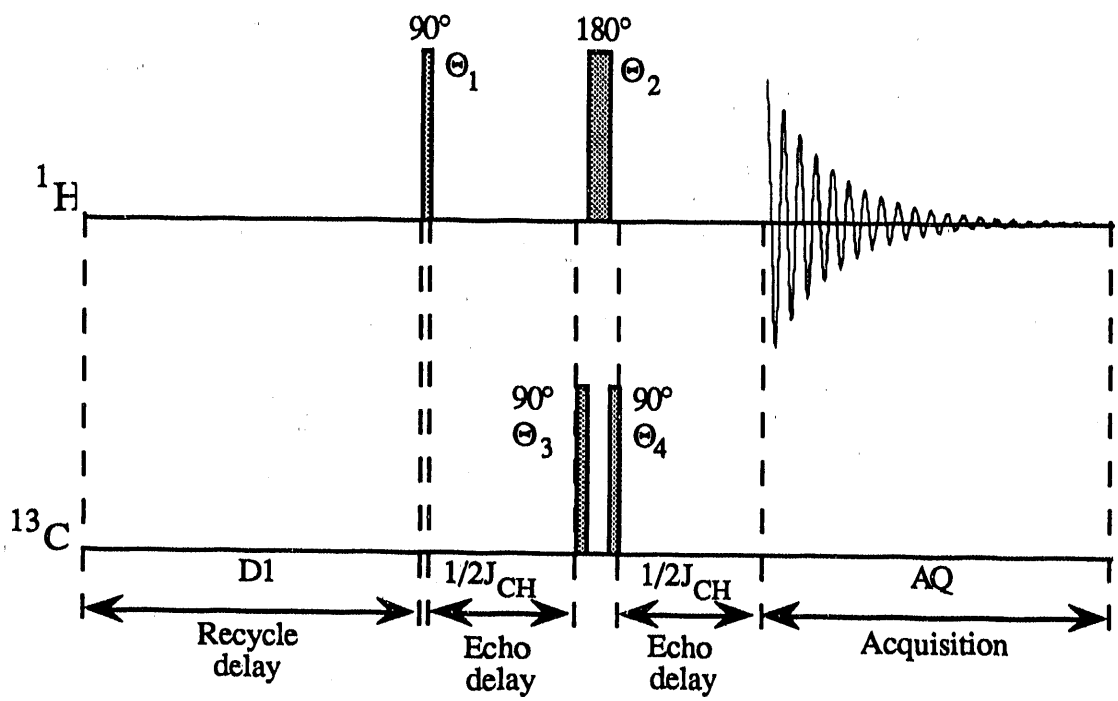

Figure 3.1. Proton inverse detect sequence for selective detection of protons coupled to ^{13}C. The time scale of the pulses and echo delays is exaggerated relative to recycle delay and acquisition (typical values are D1 ≈ 2s, 90° ≈ 8μs, $1/2J_{CH}$ ≈ 4 ms, AQ ≈ 2s) Θ_i are the phases of the pulses described below. J_{CH} is the scalar ^{13}C-^{1}H coupling constant of the ^{1}H of interest.

The phase sequence is the following (Θ_i refer to pulse phases in figure 3.1):

	Θ_1 ^{1}H90°	Θ_2 ^{1}H180°	Θ_3 ^{13}C90°	Θ_4 ^{13}C90°	^{13}C 180°	^{13}C refocus	^{12}C refocus	REC
1st scan	x	x	x	x	on	+y	-y	+y
2nd scan	x	-x	x	x	on	+y	-y	+y
3rd scan	x	x	x	-x	off	-y	-y	-y
4th scan	x	-x	x	-x	off	-y	-y	-y

In the original pulse sequence (35), a 180° carbon pulse simultaneous with the 180° proton pulse is turned on and off on alternate scans, and the "^{13}C 180° on" scan is subtracted from the "^{13}C 180° off" scan. The proton inverse detect pulse sequence that was adapted to the Bruker AM-series spectrometer realizes the ^{13}C 180° carbon on/off pulse with two consecutive 90° pulses (36). If the phases are are the same ($\Theta_3 = \Theta_4$ = x, in the 1st and 2nd scans) the result is the "^{13}C 180°" on case, whereas if they are opposite (Θ_3 = x and Θ_4 = -x, in the 3rd and 4th scans) the result is the "^{13}C 180° off" case. Subtraction is realized by inverting the receiver phase command when the ^{13}C 180° is off (REC = -y in the 3rd and 4th scans as opposed to +y in the 1st and 2nd scans) and summing the FID's. Alternating between +x and -x for the ^{1}H 180° pulse phase (Θ_2) compensates for imperfections in pulse length. Quadrature phase cycling is applied, resulting in a total of 16 scans for one full quadrature cycle. Since the subtraction is realized by inverting the receiver phase and summing the FID's, the effect of subtraction on signal to noise should not be different from the effect of averaging FID's that is obtained in an ordinary spin echo sequence i.e. SNR should increase as the square root of the number of acquisitions.

Suppression of the protons connected to ^{12}C results by subtraction of scans in which the phase of the ^{13}C satellites is opposite the phase of the ^{12}C-protons (^{13}C-180° on) from scans in which the phase is the same (^{13}C-180° off). The proton portion of the pulse sequence is a spin echo, and ^{12}C-protons will always refocus with the same phase after the

^{1}H-180° pulse (-y for an initial ^{1}H-90°$_{+x}$ pulse), since they are unaffected by ^{13}C pulses. On the other hand because of scalar coupling J_{CH}, after a ^{1}H-90°$_{+x}$ pulse, protons connected to ^{13}C have two components precessing in opposite directions corresponding to the +z and -z eigenstates of the ^{13}C magnetization. After an echo delay of $(2J_{CH})^{-1}$ the two components have a relative phase difference of 180° and are pointing in opposite directions on the x axis. If no ^{13}C pulse is applied, the two components refocus with the same phase as the ^{12}C-protons (-y). The ^{13}C-180° pulse, interchanges the ^{13}C eigenstates and reverses the precession of the two ^{13}C-proton components, which then refocus with a phase opposite to the ^{12}C-proton (+y). Decoupling may be applied on the carbon channel during acquisition. When carbon decoupling is applied, the ^{13}C satellite chemical shifts collapse to the center of the multiplet. This was not done in our case because the ^{13}C satellites of [^{13}C-4]-glutamate are in a relatively uncluttered zone of the extract spectrum, and appear more clearly at their coupled position than at their decoupled position.

Figure 3.2 demonstrates suppression of the ^{12}C protons by using the inverse detect sequence on a sample of 50% [^{12}C-1]-glucose -50% [^{13}C-1]-glucose in phosphate buffered D_2O. It is notable that the inverse detect sequence also accomplishes reasonable water suppression, since the water protons are not connected to ^{13}C.

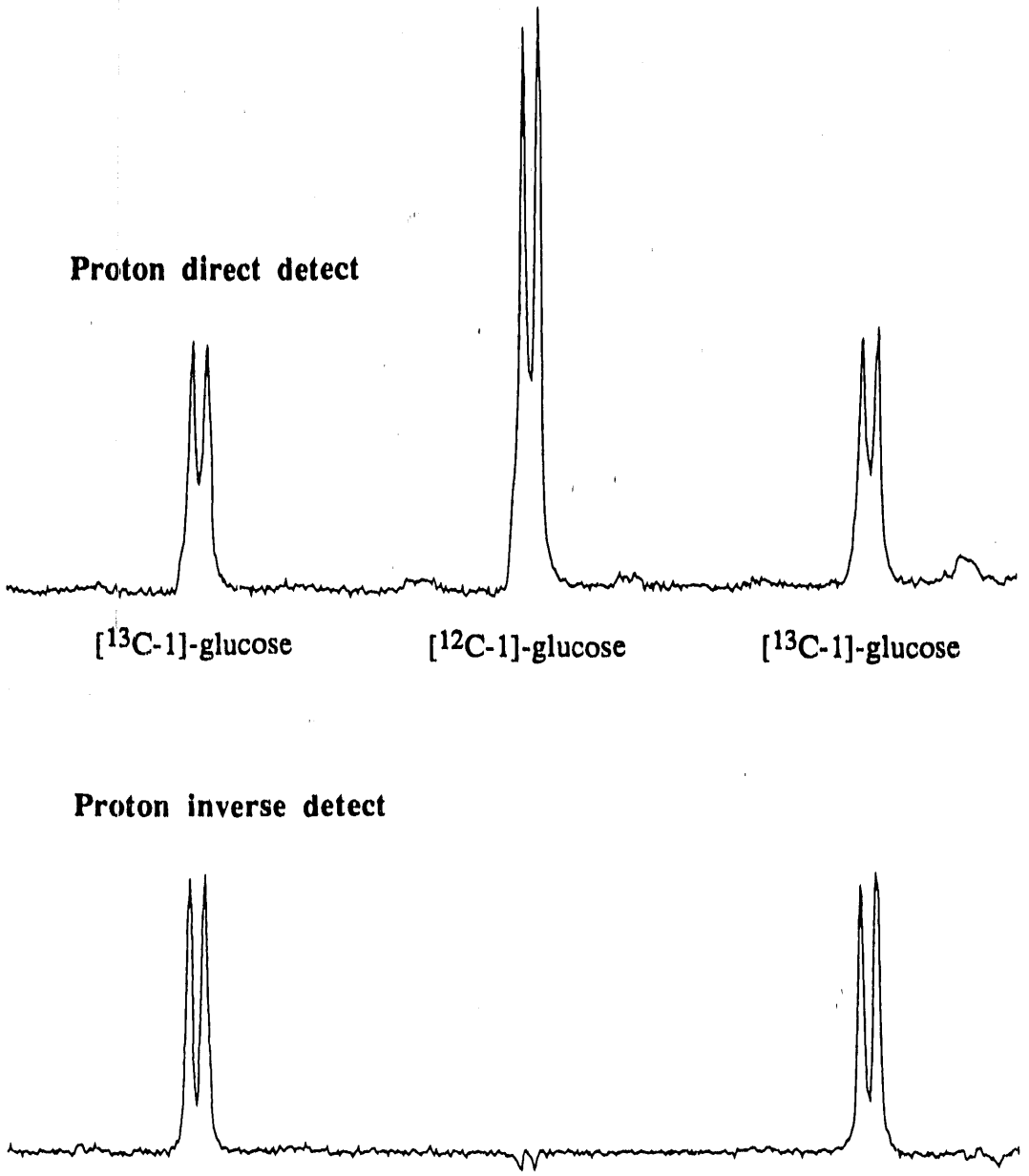

Figure 3.2. 50%:50% mixture of [^{12}C-1]-glucose:[^{13}C-1]-glucose in D_2O phosphate buffer. Upper spectrum: direct proton detect pulse sequence (single pulse). Lower spectrum: inverse detect pulse sequence described in text.

3.2. Cell preparations.

3.2.1. Cell free brain preparations.

The purpose of the cell free preparations is to have in a small test tube a viable

system containing the glycolysis, pentose shunt and glutathione-reductase-peroxidase enzymes. In this system, we verify the model for distribution of label from [^{13}C-1] and [^{13}C-2]-glucose into lactate carbons and measure relative glucose flux through the pentose shunt with high field (11.7 Tesla) NMR spectroscopy. The preparation of cell free systems from rat brain containing these cytosolic enzymes is based on preparations used by Dickens and Glock (37) for observation of the oxidative steps of the pentose shunt. Imidazole buffer is used instead of phosphate buffer so that strong buffering capacity is obtained without using a high concentration of phosphate which would act as an inhibitor.

Sprague Dawley rats (200-300g) were lightly anesthetized with metofane (methoxyflurane) and decapitated. The whole brain was removed and rinsed in ice cold imidazole buffer 0.1M with 0.02M Na-phosphate ph 7.4 (imidazole-Pi buffer). The cerebellum was removed and the rinsed brain (the remaining two hemispheres and midbrain) was weighed then homogenized in an ice bath with a Potter tube with 4 ml per gram brain wet weight of ice cold imidazole-Pi buffer. The homogenate was centrifuged at 4ºC at 8000g for 10 minutes. The clear supernatant constitutes the cell free preparation. One obtains approximately 5 ml of supernatant per gram of wet weight brain in this preparation. The dynamic NMR measurement was done with 0.8 ml supernatant placed in a 5 mm tube to which was added [^{13}C-1]-glucose and coenzymes so that final concentrations in 1 ml were the following: glucose 20mM, ATP 3mM, NAD+ 0.3mM, $NADP^+$ 0.3mM, thiamine pyrophosphate 3mM, nicotinamide 3mM, $MgCl_2$ 2mM. GSSG added was 1.5mM. The final enzyme dilution from amount per gram wet weight brain to amount per ml of aliquot in the NMR tube is therefore approximately a factor of 6. The supernatant is kept ice cold until the measurement which was done at 37° C. Stability of the preparations was evaluated by the glucose consumption kinetics. Preparations were stable for approximately the first six hours after homogenization. If the glucose consumption rate after addition of labeled glucose was slowed relative to rates from preparations used immediately post preparation, the samples were discarded and the data not taken into

account.

After addition of [^{13}C-1]-glucose, 2 minute acquisition intervals are acquired alternately on the carbon and proton channels. Proton decoupling is gated on during acquisition on the carbon channel and a either a 1331 solvent suppression pulse sequence or presaturation of the water peak is used on the proton channel.

3.2.2. Yeast preparations.

Wild strain yeast cells *Saccharomyces cerevisiae* and *Candida utilis* are grown in aerobic suspension at 30° C to mid-log phase. The growth medium is 1% yeast extract, 2% peptone with 2% dextrose in water. At mid-log phase the cells are placed in an ice bath, centrifuged for 10 minutes at 4° C, 7700 g then washed twice and resuspended in ice cold growth medium without dextrose. Before experiments the temperature of the cell suspensions is brought to 30° C. [^{13}C-2]-glucose (10 mg) is pipetted in cell suspension (30 ml of 1.4×10^8 cells/ml) which is maintained aerobic by agitation. After 10 minutes, suspensions are placed in ice bath, centrifuged at 4° C. The cell pellet is frozen in liquid nitrogen and then extracted with chloroform-methanol. The aqueous fraction reconstituted in D_2O phosphate buffer pH 7 is observed by ^{13}C NMR spectroscopy.

3.3. Whole animal experiments.

3.3.1. Infusion of [^{13}C-2]-glucose with evaluation of the glutamate pool.

Sprague Dawley rats (200-300g) were fasted with free access to water for 24 hours prior to the experiment in order to reduce endogenous glycogen stores. Approximately twenty minutes prior to surgery and glucose infusion, the rats received 2 mg/kg propranolol I.P. in order to block adrenaline induced cardiac arrhythmia and reduce increases in circulating endogenous glucose (38). The rats were lightly anesthetized by metofane inhalation just prior to surgery. Under metofane anesthesia, the rats were

tracheotomized for transfer to nitrous oxide anesthesia administered with a rat respirator connected to a gas regulator delivering 30% O_2 in N_2O. When nitrous oxide anesthesia was established, electrodes were placed on the limbs for cardiac monitoring. When rats showed heart failure, the study was discontinued, and the animals sacrificed under anesthesia. Under nitrous oxide anesthesia, the jugular vein was catheterized for infusion of glucose, 2-deoxyglucose (2DG) and t-bytyl hydroperoxide (TBHP). TBHP is the peroxide $(CH_3)_3$-C-O-OH which is expected to be scavenged by the cellular glutathione peroxidase and therefore stimulate pentose shunt activity for production of NADPH. Three series of experiments were done.

In the first series, a bolus of 15 mg/kg of 2DG was injected I.V. *via* the jugular vein at the onset of the experiment. This was followed immediately by infusion of [^{13}C-2]-glucose in the control case. In oxidatively stressed rats, glucose infusion was preceded by a bolus of 33 mmol/kg TBHP. A total volume of approximately 1 ml glucose in isotonic saline was infused constantly over a period of 30 minutes at the rate of 33 µl/minute for a total glucose dose of 500 mg/kg (100 mg for a 200 g rat). At the end of glucose infusion, the skull was frozen in liquid nitrogen under anesthesia and frozen brain tissue removed and extracted with chloroform-methanol. The aqueous fraction was reconstituted after lyophilization in phosphate buffered D_2O with an internal DSS reference (see section 3.1). ^{13}C, ^{1}H and ^{31}P NMR spectroscopy was performed on a Bruker AM-400 (9.3 T) spectrometer.

The protocol for the second series was identical to the first one except that in the second series unlabeled glucose was used and the dose of the 2DG bolus at the onset of the experiment was varied. 2DG doses administered were: 500 mg/kg, 100 mg/kg and 50 mg/kg. Controls and TBHP stressed animals were done for each 2DG dose. The purpose of this series was to determine a minimum acceptable dose of 2DG for which the 2DG6P peak would yield a reasonable signal to noise ratio in the ^{31}P NMR spectrum of the extract.

This was done because in the first series the 2DG6P peak was not detected in the brain extracts. A dose of 50 mg/kg was found acceptable.

The protocol for the third series was identical to the first one except that in the third series a 50 mg/kg dose of 2DG was used and a total dose of 900 mg/kg of [^{13}C-2] glucose was infused in 30 minutes.

Model for the plasma glucose levels obtained during [^{13}C-2]-glucose infusion.

Plasma glucose concentrations during the infusion of [^{13}C-2]-glucose were estimated by using a one compartment model representing the rat's glucose distribution compartment. The model is shown in figure 3.3.

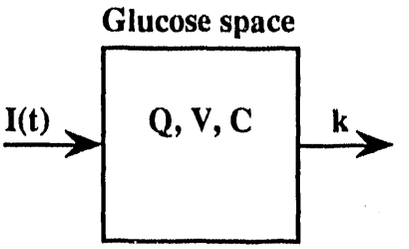

Figure 3.3. Model for plasma glucose concentrations. I(t) is the glucose input function; Q, V and C are respectively the total amount of exchangeable glucose, the apparent volume of the glucose distribution compartment and the glucose concentration; k is the rate constant for glucose turnover.

The model is described by the equation of conservation of mass:

$$\dot{Q} = I - kQ(t) \qquad (3.15)$$

where Q is the mass of the exchangeable glucose pool, I is the constant infusion rate in units of [mass.time^{-1}] and k is the rate constant for transport out of the glucose distribution space in units of [time^{-1}]. Integration of 3.15 yields:

$$Q(t) = Q(0)e^{-kt} + \frac{I}{k}(1 - e^{-kt}) \tag{3.16}$$

The exchangeable glucose pool is assumed to be in a single compartment comprised of plasma, extracellular fluid and cytoplasm with an apparent distribution volume V (39). Since by definition, the glucose is rapidly exchanging in the distribution space, the glucose concentration is assumed to be the same in all parts of the distribution space. Therefore plasma concentration is obtained by dividing both sides of equation 3.16 by the apparent volume of glucose distribution V:

$$C(t) = \frac{Q(t)}{V} = \frac{Q(0)}{V}e^{-kt} + \frac{I}{Vk}(1 - e^{-kt}) \tag{3.17}$$

This equation is plotted in figure 3.4. In the case where the total dose of glucose infused was 500 mg/(kg body weight), the glucose input function I was constant at 3 mg min^{-1} in a volume of 33 µl min^{-1}. Initial plasma glucose concentration C(0) = Q(0)/V was taken to be the low normal value for the rat (1.5 mg/ml = 8.3 mM) since rats were fasted 24 hours prior to the experiment. The total volume infused was 1 ml in a period of 30 minutes. Variations in volume due to the volume of infusate are neglected. The volume of distribution of glucose for mammals is taken as 180 ml (kg body weight)$^{-1}$, which for a 200 gram rat corresponds to V = 36 ml. The estimate for the initial mass of the exchangeable glucose pool is Q(0) = C(0)V = 54 mg = 300 µmol. Glucose turnover rate for the rat was taken as 58±4 µmol (kg body weight)$^{-1}$ min^{-1} from Brooks et al. (40). The rate constant k from equation 3.16 may be defined in units of [min^{-1}] by multiplying the glucose turnover rate in units of [µmol (kg body weight)$^{-1}$ min^{-1}] by the rat's body weight and dividing it by the initial amount of glucose in the rat glucose distribution space. For the 200 gram rat, the plasma glucose turnover rate is then 11.6 µmol min^{-1} which thus corresponds to a rate constant k = 11.6/300 = 0.039 min^{-1}. The values taken for the simulation are summarized below:

$I = 0.016$ mmol min^{-1}	constant infusion rate
$V = 0.036$ l	apparent glucose distribution volume
$k = 0.039$ min^{-1}	rate constant for glucose transport out of the glucose distribution compartment
$C(0) = 8.3$ mM	initial plasma glucose concentration

and the simulation is shown in figure 3.4.

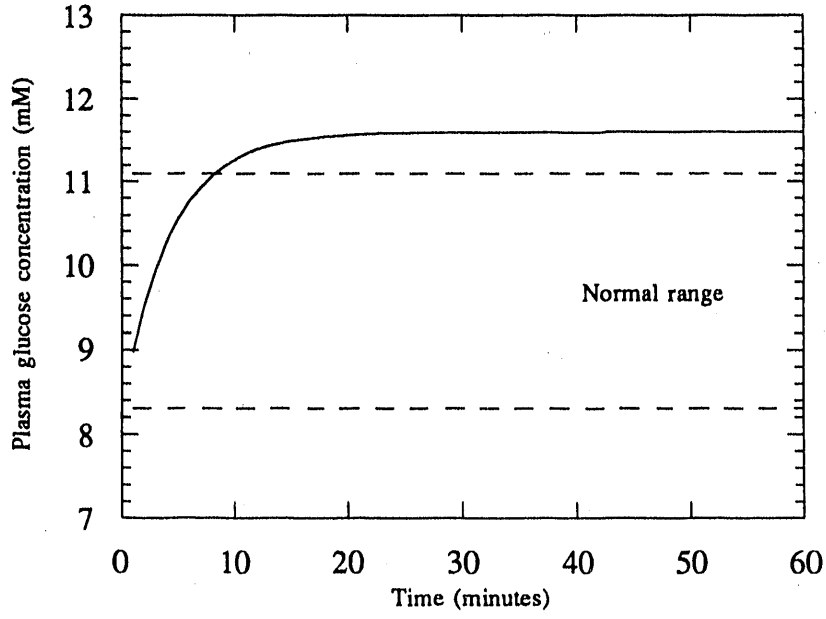

Figure 3.4. Simulation of plasma glucose concentrations (mM) during constant infusion of 3 mg/min of [^{13}C-2]-glucose in a 200 g rat. The horizontal lines delimit the normal range of concentrations for the rat.

Figure 3.4. shows that after 30 minutes of infusion, the plasma glucose is estimated to be about 11.6 mM which is 5% above the high normal level of plasma glucose concentration and considered hyperglycemic. In the hyperglycemic state one expects an increase in insulin secretion resulting in increased glucose utilization by insulin-sensitive tissues and consequently increased glucose turnover. The β-adrenergic receptor blocker

propranolol which is known to inhibit insulin and glucagon secretion (41) is injected prior to infusion. Insulin secretion due to hyperglycemia is therefore assumed to be attenuated in our experimental protocol. Likewise any glucagon secretion should be inhibited. Therefore we expect the turnover rate not to be affected by high insulin levels. Endogenous glucose production due to glucagon should also be inhibited.

In the case where the total dose of glucose infused was 900 mg/kg, the infusion rate was about doubled to 6 mg min^{-1} by doubling the concentration of the infusate (the infusion volume rate remained the same at 33 $\mu l\ min^{-1}$) and the steady state plasma glucose concentration was estimated to be 23.2 mM which is about double the high normal level. In this case the rat is highly hyperglycemic. Again, insulin secretion due to hyperglycemia is assumed to be attenuated in our experimental protocol. It has been reported that cerebral glucose utilization rates are unaffected by hyperglycemia levels up to 31 mM in the rat (42), and it is therefore unlikely that a hyperglycemia level of 23.2 mM would affect pentose shunt activity in the rat brain.

3.3.2. 6-aminonicotinamide studies.

Sprague Dawley rats (200-300g) were fasted with free access to water for 24 hours prior to the beginning of the experiment (considered as the beginning of surgery for infusion) in order to reduce endogenous glycogen stores. Approximately twenty minutes prior to surgery, the rats received 2 mg/kg propranolol I.P. in order to block adrenaline induced cardiac arrhythmia and increases in circulating endogenous glucose (38). Two hours prior to surgery and glucose infusion, 35 mg/kg of 6-AN was administered I.P., in order to give sufficient time for the inhibitor 6-ANADP to form in the brain. The procedure for the placement of the catheter in the jugular vein under metofane and nitrous oxide anesthesia was identical to one described in the previous section. [^{13}C-1]-glucose was infused at a rate of approximately 250 mg kg/hour for 3 hours resulting in a total dose of

approximately 750 mg/kg in three hours. Oxidatively stressed rats received a 33 mmol/kg I.V. bolus of TBHP immediately before the beginning of [^{13}C-1]-glucose infusion. Another group of rats received a bolus dose of 110 mg/kg FDG before glucose infusion. Control rats received only the glucose. At the end of infusion, the skull was frozen in liquid nitrogen under anesthesia and frozen brain tissue removed and extracted with chloroform-methanol. The aqueous fraction was reconstituted after lyophilization in phosphate buffered D_2O with an internal DSS standard (see section 3.1). [^{13}C-1]-6-phospho-gluconate is observed in the ^{13}C spectrum. Spectroscopy was performed on a Bruker AM-400 (9.3T) NMR spectrometer.

Chapter 4.

Results

4.1. Cell free brain preparations.

The cell free brain preparations contain the cytosolic brain enzymes for glycolysis, pentose shunt and the glutathione-peroxidase-reductase systems; absent are enzymes from the subcellular fractions, in particular mitochondrial enzymes (citrate cycle) and membrane bound enzymes. We have studied these systems under anaerobic conditions to verify the model for distribution of label from [^{13}C-2]-glucose in the lactate pool and measurement of glucose flux through the pentose shunt from that distribution. The distribution of label in lactate under anaerobic conditions is assumed to reflect the distribution of label in pyruvate under aerobic conditions and this assumption is used to evaluate the distribution of label expected in glutamate under aerobic conditions (see section 2.3). Under aerobic conditions, our model for the measurement *in vivo* relies on glutamate to be a reporter for measurement of pentose shunt activity by the relative enrichments in its C4 and C5 positions. The advantage for NMR detection of glutamate is that glutamate has a relatively large pool size in the brain (43). Glucose carbons are also rapidly incorporated into the

glutamate pool (44). The ^{13}C enrichments of glutamate carbons depend on labeling of initial pyruvate entering the cycle, relative flux *via* either pyruvate dehydrogenase or pyruvate decarboxylase into the cycle, amount of cycling and equilibrium between α-ketoglutarate and glutamate. This part of our study addresses the initial labeling of pyruvate by observation of the lactate pool and evaluates the effect of oxidative stress from oxidized glutathione or t-butyl hydroperoxide on the labeling.

4.1.1. Use of [^{13}C-1]-glucose.

In order to monitor flux of glucose through the pentose shunt under anaerobic conditions (21), 20 μmol [^{13}C-1]-glucose was added simultaneously with the coenzymes ATP, NADP, $NADP^+$, thiamine pyrophosphate, and nicotinamide to 800 μl of cell free preparation and placed in the spectrometer at 37°C for acquisition alternately *via* the carbon and proton channels. Oxidized glutathione (GSSG) was added at a concentration of 1.5 mM to stress the system relative to controls. The upper part of Figure 4.1. shows the time course of a typical proton spectrum series. The flux X of glucose through the shunt was measured as described in section 2.2.1. The time course of the measured flux is plotted in figure 4.2 and compares controls to glutathione stressed cell free preparations. In both cases the flux through the shunt was higher at the beginning of the experiment and then took lower values. The high flux (43±8% for controls, 69±22% for GSSG treated) at the beginning may be explained by a high $NADP^+$/NADPH ratio when $NADP^+$ has just been added to the sample. Each time point represents the cumulated flux. The overall amount of glucose consumed *via* the pentose shunt is given by the flux at the end of the experiment when all the glucose has been consumed. The cumulated flux in the GSSG stressed preparations was 1.6 times higher than controls at the beginning of the experiment and 2.2 times higher at 60 minutes. At 60 minutes all of the glucose has been consumed, so the amount of glucose consumed *via* the shunt in the GSSG treated preparations was 13±1%

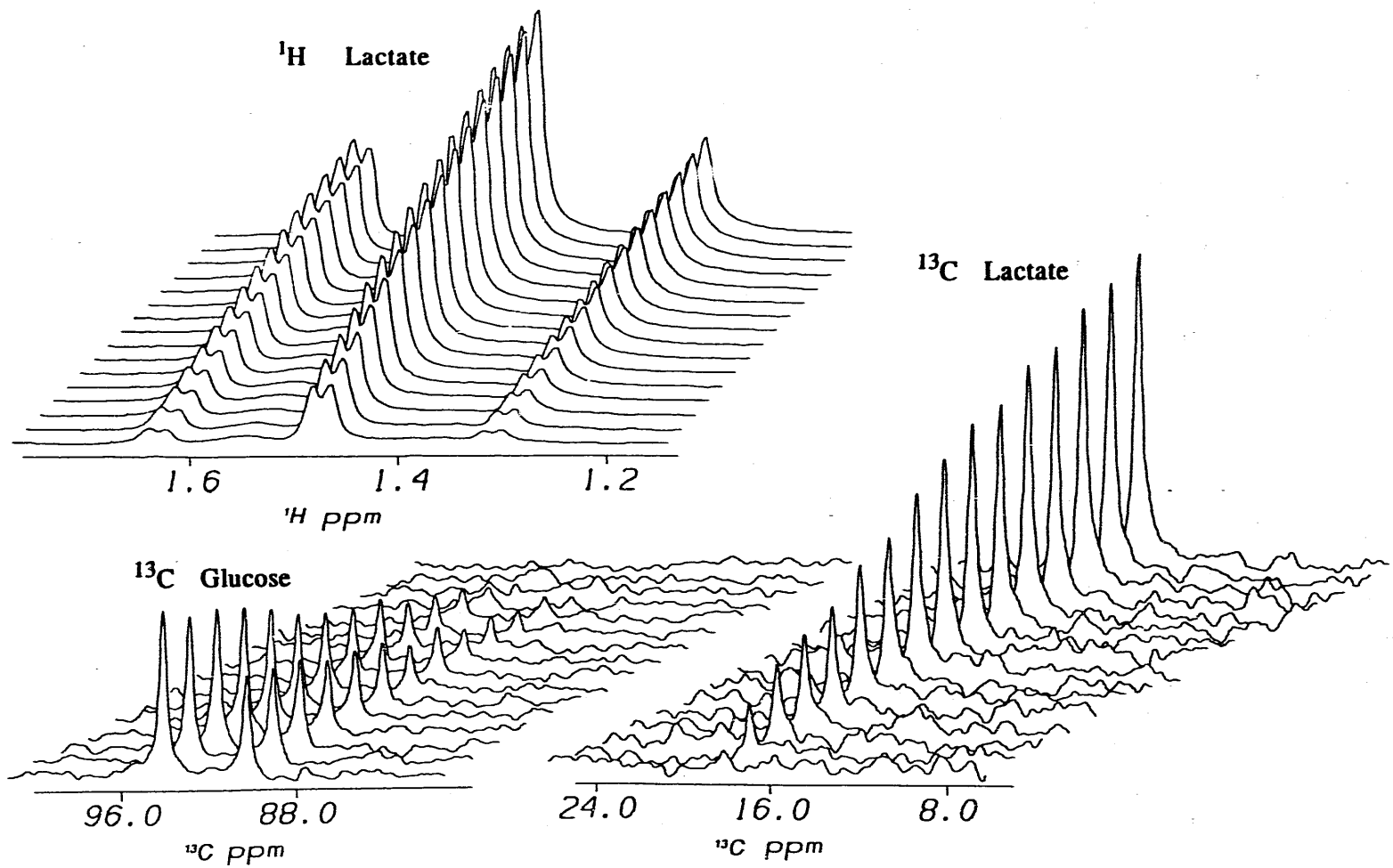

Figure 4.1. Cell free rat brain preparation after addition of [^{13}C-1]-glucose. Top: Time course of ^{1}H NMR spectra in the C3 lactate region, showing lactate production. The central peak is [^{12}C-3]-lactate, and the satellites are [^{13}C-3]-lactate. Bottom: Time course of ^{13}C NMR spectra in the C1 glucose and C3 lactate regions, showing glucose consumption and lactate production. On the left are α- and β-[^{13}C-1]-glucose peaks, on the right is the [^{13}C-3]-lactate peak.

of 20 μmol i.e. 2.6 μmol and 6±1% of 20 μmol i.e. 1.2 μmol in the controls.

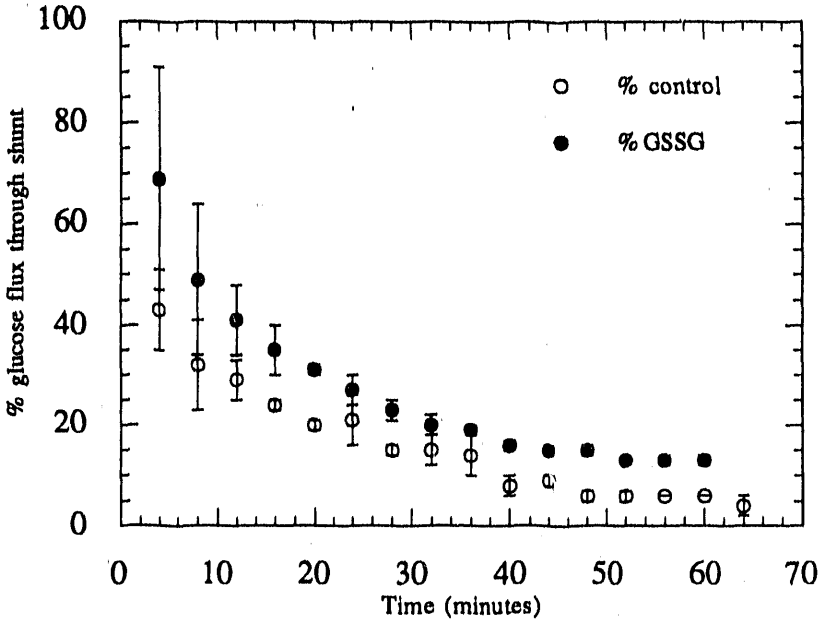

Figure 4.2. Percentage flux of glucose via the pentose shunt under oxidative stress in cell free preparations under anaerobic conditions. [^{13}C-1]-glucose used. Filled circles represent the flux when 1.5 mM oxidized glutathione (GSSG) was added at the onset of the experiment (n=2). Empty circles represent controls that received no GSSG (n=2).

4.1.2. Use of [^{13}C-2]-glucose.

Dynamic monitoring of the flux.

The flux of glucose via the shunt in these experiments was determined after addition of [^{13}C-2]-glucose using the model developed in section 2.2.2. Conditions of the experiment were identical to the previous experiments that use [^{13}C-1] label. Figure 4.3(a) shows the changes with time of the flux of glucose through the pentose shunt calculated using equation 2.17 based on the ratio r_1 of [^{13}C-3]-lactate to [^{13}C-2]-lactate. One observes an increase in flux through the shunt when glutathione has been added to the preparation, similarly to the previous case.

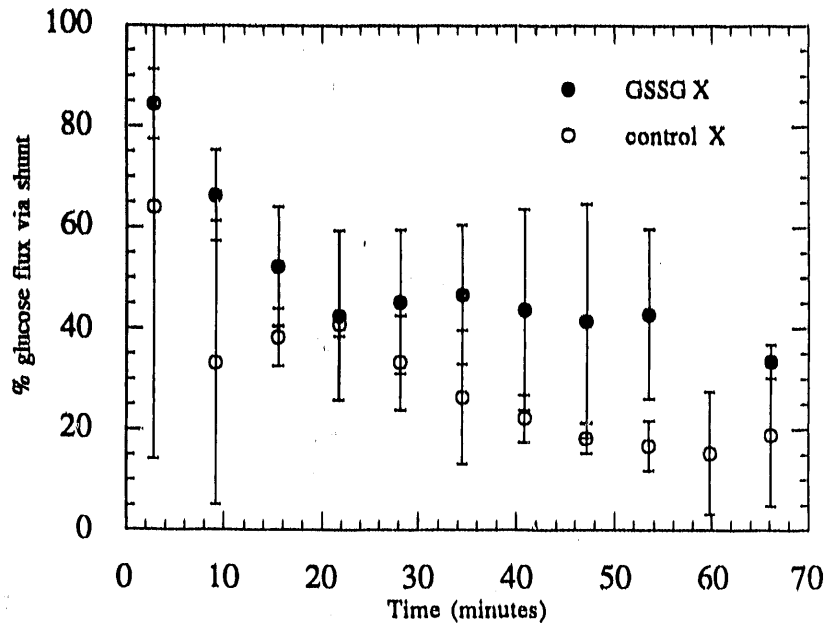

a

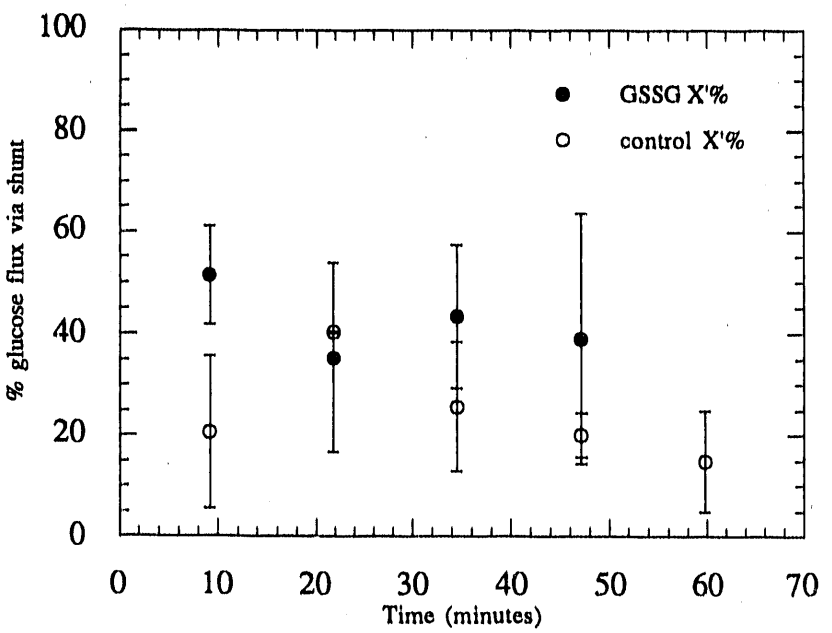

b

Figure 4.3. Percentage flux of glucose via the pentose shunt under oxidative stress in cell free preparations under anaerobic conditions. [^{13}C-2]-glucose used. Filled circles represent the flux when 1.5 mM oxidized glutathione (GSSG) was added at the onset of the experiment (n=2). Empty circles represent controls that received no GSSG (n=2). **a**: equation 2.17 was used to calculate X. **b**: equation 2.18 was used to calculate X.

In the beginning of the experiment flux was 1.3 times higher in the GSSG case than the controls. When most of the glucose had been consumed, the flux was 3 times higher in the GSSG case than the controls. The flux calculated using equation 2.18 based on the ratio r_2 of [^{13}C-3]-lactate to [^{12}C-3]-lactate is shown in figure 4.3(b). In this case the calculation was based on integrals from the proton spectrum only and since data are acquired alternately on the carbon and proton channels there are half as many data points in the plot. The fluxes calculated with this method were lower than those with the previous method, but still showed a factor of 1.5 (at the beginning) to 2 (at 60 minutes) increase in the case of GSSG. The results using equation 2.17 for calculation of the fractional flux of glucose through the shunt based on [^{13}C-2]- and [^{12}C-3]-lactate and glucose consumed are shown in figure 4.4. The calculation yields a similar differential between the GSSG treated and the control preparations as was observed with the previous two methods, but the percentages given are too high (above 100% at the beginning of the experiment). This can be explained by the presence of unlabeled lactate in the preparation before addition of the labeled glucose.

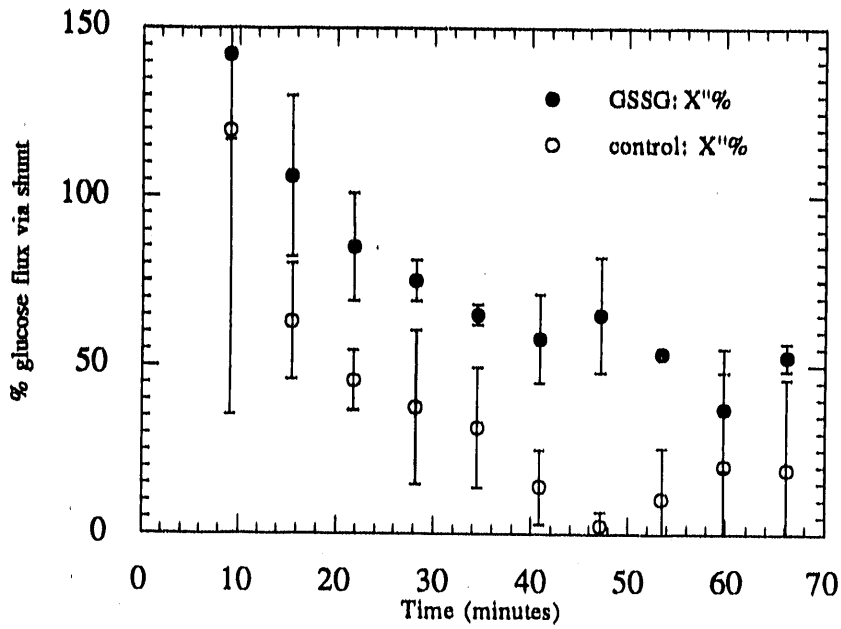

Figure 4.4. Percentage flux of glucose via the pentose shunt under oxidative stress in cell free preparations under anaerobic conditions. [^{13}C-2]-glucose used. Filled circles represent the flux when 1.5 mM oxidized glutathione (GSSG) was added at the onset of the experiment (n=2). Empty circles represent controls that received no GSSG (n=2).

Endpoint measurement of the flux.

The effect of a higher concentration of GSSG was studied in experiments where spectra were not acquired dynamically during glucose consumption, but only at the final time point (when all glucose has been consumed). In this case, the cell free brain solutions were prepared in 0.2 M imidazole / 20 mM phosphate buffer. Each cell free sample of 0.8 ml was placed in a 5 mm NMR tube and the tube placed in a water bath maintained at 37°C. At the onset of the experiment, [^{13}C-2]-glucose (20 mM) was added simultaneously with the coenzyme preparation. The coenzyme preparation was the same as the one used in the previous experiments. In the stressed preparations, 50 µl of GSSG were added at a concentration of 20 mM. Controls received 50 µl of buffer in the place of GSSG. The tubes were then capped and shaken in the water bath for a period of 200 minutes. At the

end of the 200 minutes, the tubes were placed in a ice cold water bath and 100 µl of DSS 0.1 M were added to all tubes. Carbon and proton NMR spectroscopy was then done at room temperature within twelve hours from the end of incubation.

The glucose flux through the shunt was calculated using equation 2.18. Glucose flux through the shunt was 17 ± 4% (n=2) for controls and 28 ± 5% (n=3) for the GSSG treated preparations.

4.2. Yeast preparations.

The yeast preparations, as opposed to the previous preparation, constitute a complete cell system including cytosolic enzymes and intact mitochondria and are used here to investigate the complete model from [^{13}C-2]-glucose to glutamate on a well studied and controllable system that can be observed at high field. The yeast cells have in common with brain cells the fact that under aerobic conditions they pool glutamate and the characteristics of their pentose shunt pathway are reported to be of the classical type (45).

Incorporation of [^{13}C-2]-glucose into glutamate under aerobic conditions.

In order to determine the incorporation of [^{13}C-2]-glucose into the glutamate pool in Saccharomyces cerevisiae (SC) 10 mg of labeled glucose were incubated with 30 ml preparations of 1.4x10^{8} cells/ml SC in medium with no other carbon source. After 10, 20 and 30 minutes of aerobic incubation at 37°C the cells were placed in an ice bath, centrifuged at 4°C and the pellet obtained was frozen in liquid nitrogen and extracted by the chloroform-methanol method for observation by NMR (see methods). A ^{13}C NMR spectrum is shown in figure 4.5. Analysis of the spectrum takes into account 25 peaks which have a signal to noise level above 3. A total of 16 of these peaks were identified and assignments are shown in figure 4.5. Assigned peaks belong to alanine, aspartate, glutamate, glutamine, glycerol, succinate and trehalose groups. The sections of the

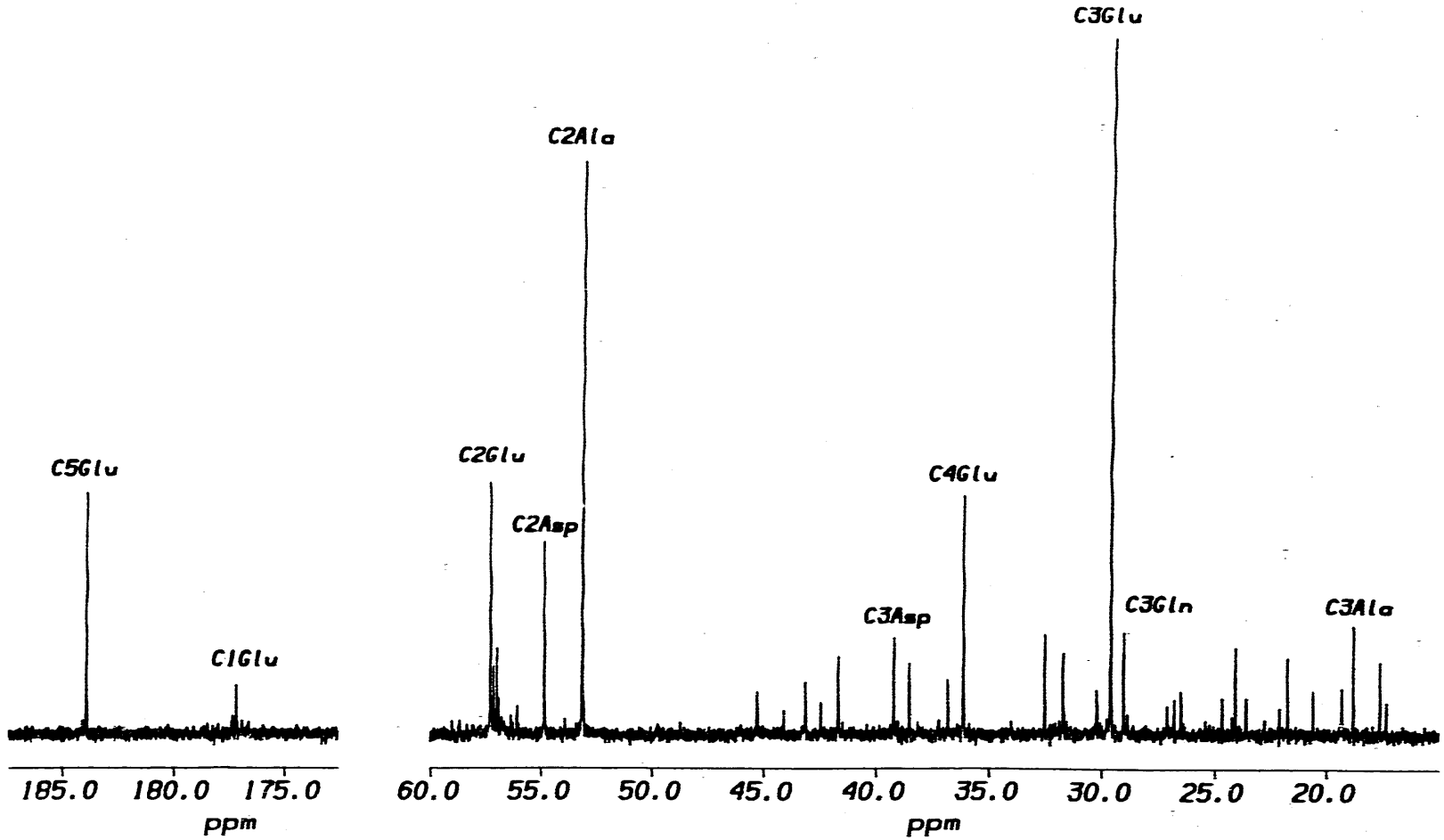

Figure 4.5. ^{13}C NMR spectrum of the aqueous phase of Saccharomyces cerevisiae yeast pellet extract after 10 min of aerobic incubation with [^{13}C-2]-glucose. Resonances shown are : CiGlu = carbons 1 to 5 of glutamate, CiAsp = carbons 2 to 3 of aspartate, CiAla = carbons 2 to 3 of alanine, C2Gln = carbon 2 of glutamine. Not shown are resonances [C-2] of glycerol at 74.75 ppm, [C-2]-trehalose at 72.74 ppm, [C-2]-glutamine at 57.02 ppm, [C-2,3]-succinate at 36.84 ppm, and DSS at 0.00 ppm.

spectrum not shown in figure 4.5 include [^{13}C-2]-trehalose, [^{13}C-2]-glycerol and the internal reference DSS peaks. Peaks visible but not labeled in figure 4.5 are [^{13}C-2]-glutamine at 57.02 ppm and [^{13}C-2,3]-succinate at 36.84 ppm. Carbons C1 to C5 of glutamate are all observed. Assignments are based on NMR spectra obtained of the pure compounds in the same buffer used to reconstitute extracts and on the literature (46) & (47). All glucose had been consumed by 10 minutes. The observed incorporation of label into these compounds is consistent with aerobic metabolism of glucose to pyruvate, entry of pyruvate in the citrate cycle, active glutamate transaminase producing glutamate from α-ketoglutarate, and active aspartate transaminase, producing aspartate from oxaloacetate. It is notable that the peaks do not show ^{13}C-^{13}C coupling patterns, which is due to the large pool of unlabeled substrate (see section 2.4.1). This observation is also found in aerobic studies of SC where [^{13}C-1]-glucose was the carbon source (48).

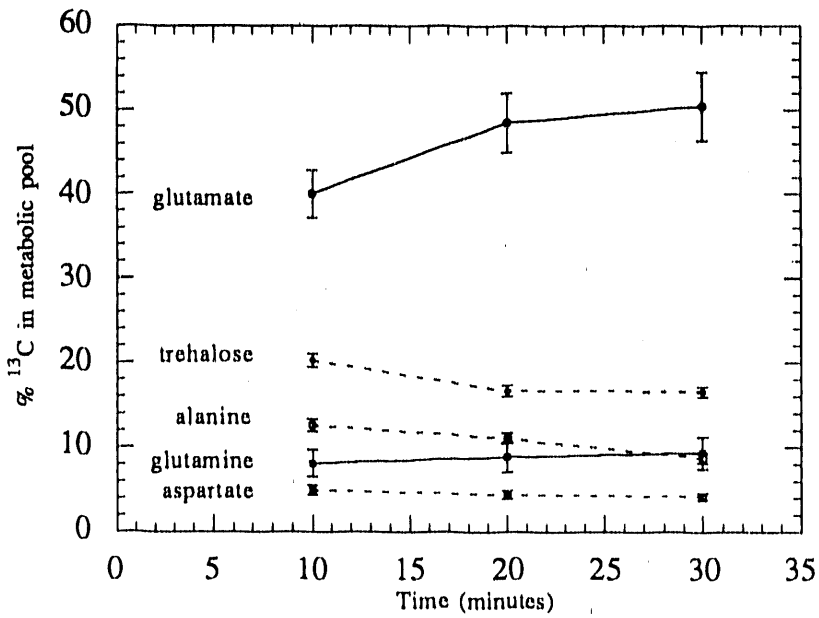

Figure 4.6. Percentage of label incorporated into metabolic pools with time of aerobic incubation (n=2 for each time point) of SC yeast.

Figure 4.6 shows how the percentages of label incorporated into the metabolic

pools of glutamate, trehalose, alanine, glutamine and aspartate varied with incubation time. This ratio expressed in percentage is the sum of integrals of all spectral peaks of a given compound over the sum of integrals of all peaks. The percentage of the total carbon label in glutamate increased with time, while labeled trehalose decreased. This would indicate a transfer of label from trehalose to glutamate under the conditions of the experiment consistent with aerobic utilization of glucose that was first stored in the form of trehalose. It is notable that the five metabolic pools shown above account for about 80 to 90% of the label incorporated as measured by the sum of integrals over the 25 main carbon peaks observed.

Figure 4.7 shows the relative enrichments of glutamate carbons after 10 minutes of aerobic incubation with [^{13}C-2]-glucose under the control conditions. The ratio of C4 to C5 peak areas of glutamate was used to calculate the relative amount of glucose flux through the shunt and found to be 13 ± 2 % (n=2) under the control conditions.

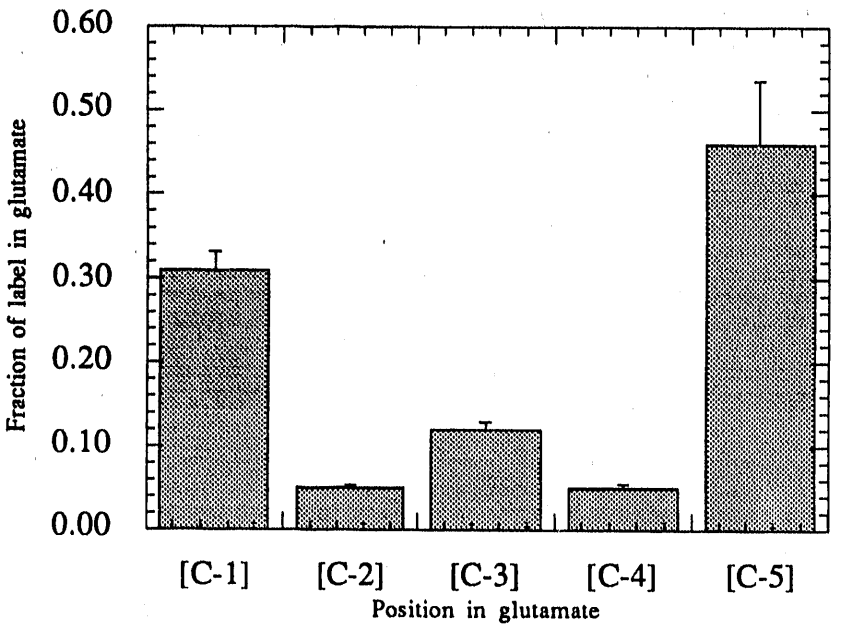

Figure 4.7. Relative fractional enrichments of ^{13}C label in the 5 positions of glutamate after 10 minutes of aerobic incubation of Saccharomyces cerevisiae with [^{13}C-2]-glucose (n=2). Fraction of label in position i = [^{13}C-i]-glutamate/Σ[^{13}C-i]-glutamate.

Flux of glucose through the pentose shunt with oxidative stress.

In order to observe the effect of increasing oxidative stress on the distribution of label in the glutamate pool and flux of glucose through the pentose shunt, SC cells were incubated for ten minutes with 10 mg of [^{13}C-2]-glucose under the same aerobic conditions as the previous experiment except that t-butyl-hydroperoxide (TBHP) was added to preparations at the onset of the experiment. Controls did not receive any TBHP. The TBHP concentrations studied were 0.1, 1 and 10 mM and the effect on the flux of glucose through the shunt is shown in figure 4.8.

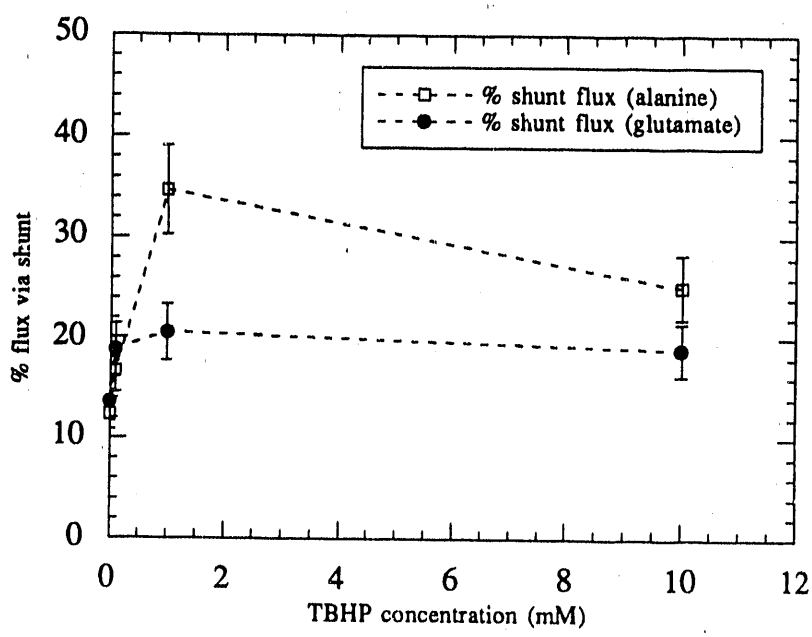

Figure 4.8. Flux of glucose through shunt with oxidative stress (TBHP) in SC yeast preparations (n=3). Flux was measured in two ways: from the ratio of C3 to C2 alanine peaks (❑)and from the ratio of C4 to C5 glutamate peaks.(•).

The flux of glucose through the pentose shunt was calculated using the two methods developed in section 2.3. The first uses the ratio of [^{13}C-4] to [^{13}C-5]-glutamate and the second the ratio of [^{13}C-3] to [^{13}C-2]-alanine. Using the glutamate enrichment method for calculation, flux of glucose *via* the pentose shunt was shown to increase by a factor of 1.6 (from 13 ± 2% to 21 ± 3%) with a dose of 1 mM TBHP. Flux remained unchanged with a further increase to 10 mM TBHP. Using the alanine enrichment method for calculation, the flux was shown to increase by a factor of 3 (from 12 ± 2% to 35 ± 3%) with a dose of 1 mM TBHP. The flux at 10 mM TBHP was 25 ± 3%, a factor of 2 above the control value.

The yeast cells were also stressed with 0.1 mM phenazine methosulfate, which is a strong electron acceptor (49). In this case the flux through the shunt was 25 ± 3% calculated by the glutamate method and 33 ± 4% calculated by the alanine method. These

values correspond to increases comparable to the increases measured for a 1 mM TBHP stress.

Saccharomyces cerevisiae vs. Candida utilis.

Candida utilis (CU) is a yeast variety similar to Saccharomyces cerevisiae except that it is primarily aerobic in its growth requirements and has high pentose shunt enzyme activities (45).

Candida utilis cells were prepared and incubated aerobically for 10 minutes with [^{13}C-2]-glucose under control conditions identical to those for SC in the previous experiments. A ^{13}C NMR spectrum of the aqueous fraction of the CU cell pellet extract after incubation with [^{13}C-2]-glucose is shown in figure 4.9. The main peaks are comparable to the main peaks found in the SC cell extract, however the relative intensities reflect higher flux of glucose through the pentose shunt. Oxidative stress of CU cells relative to control conditions was realized by adding 1.5 mM GSSG at the onset of the experiment. The flux of glucose through the pentose shunt in S. cerevisiae under control and TBHP stressed conditions and in CU under control and GSSG stressed conditions are compared in figure 4.10.

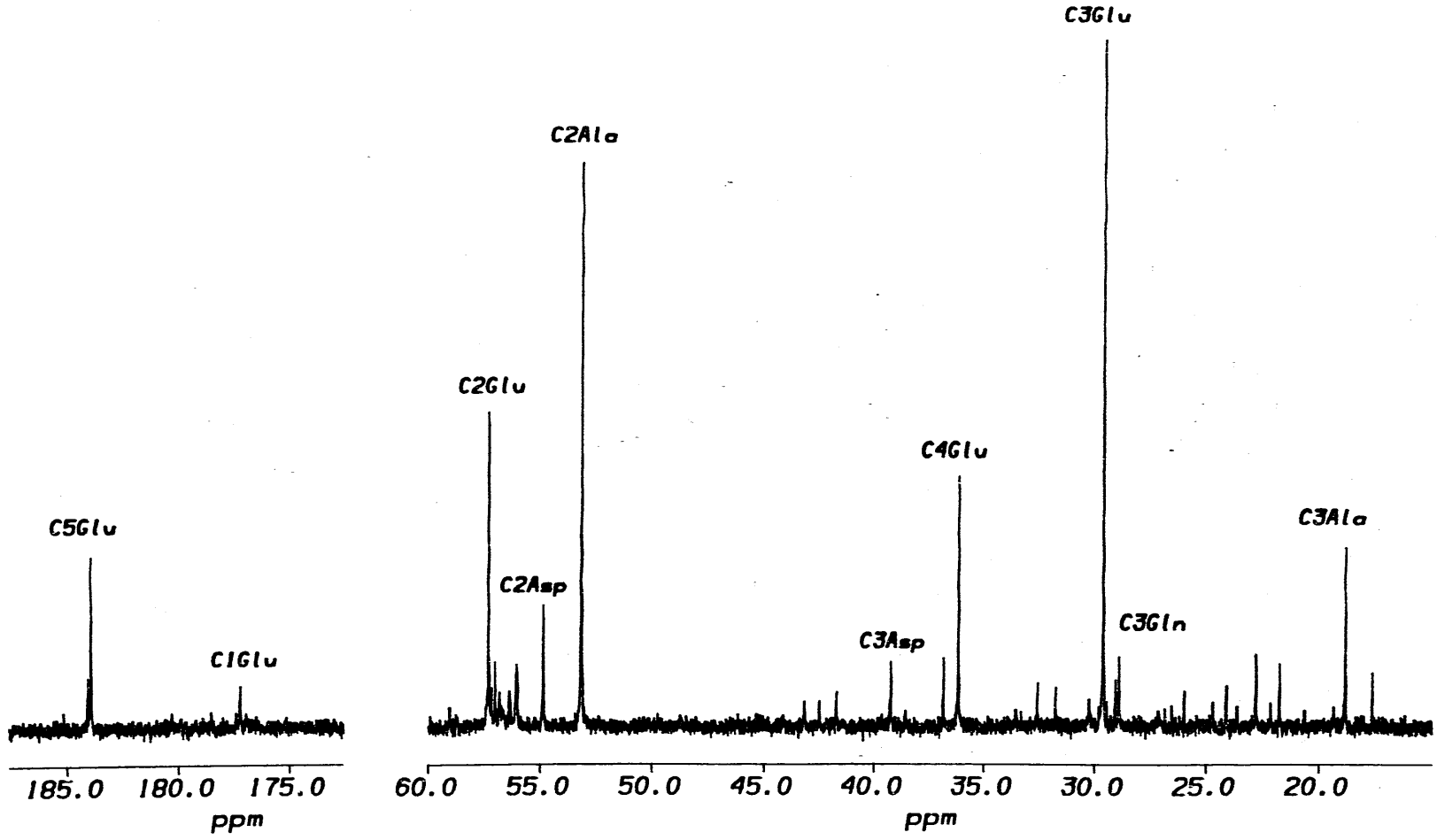

Figure 4.9. ^{13}C NMR spectrum of the aqueous phase of Candida utilis yeast pellet after 10 min of aerobic incubation with [^{13}C-2]-glucose. Resonances shown are : CiGlu = carbons 1 to 5 of glutamate, CiAsp = carbons 2 to 3 of aspartate, CiAla = carbons 2 to 3 of alanine, C3Gln = carbon 3 of glutamine. Not shown are resonances [C-2] of glycerol at 74.75 ppm, [C-2]-trehalose at 72.74 ppm, [C-2]-glutamine at 57.02 ppm, [C-2,3]-succinate at 36.84 ppm, and DSS at 0.00 ppm.

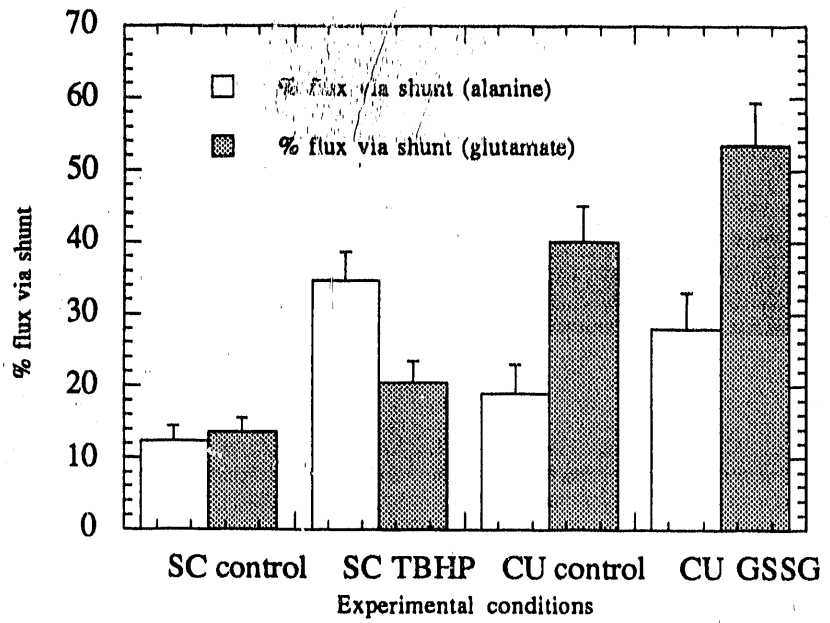

Figure 4.10. Flux through pentose shunt for Saccharomyces cerevisiae under control conditions (SC control, n=2) and 1 mM TBHP stress (SC TBHP, n=2) and Candida utilis under control conditions (CU control, n=4) and 1.5 mM GSSG stress (CU GSSG, n=3)).

The comparison of the two species shows that CU had 3 times more glucose flux through the pentose shunt than did SC under identical aerobic control conditions, when measured with the glutamate enrichment method. This increase was only 1.6 times when measured by the alanine enrichment method. In CU, 1.5 mM GSSG increased flux through the shunt by a factor of 1.3 to 1.5 (using either method). The glutamate method shows a continuing increase of flux from control SC (13 ± 2%) to GSSG stressed CU (53 ± 5%).

4.3. Whole animal experiments.

4.3.1. Glutamate fractional enrichment.

The previous studies show that the percentage flux of glucose through the pentose

shunt can be measured by observation of glutamate relative enrichment in partial and whole cell systems, and the relative increases of the flux when oxidative stress is applied can also be measured. In order to experimentally evaluate the relative enrichment methods of pentose shunt measurement in a whole animal *in vivo*, the following experiments were undertaken. Nitrous oxide anesthetized rats were infused for one half hour with a total of 500 or 900 mg/kg of [^{13}C-2]-glucose, the brain was frozen under anesthesia and removed for aqueous organic extraction. Oxidatively stressed rats received 30 mmol/kg TBHP I.V. at the onset of the experiment while control rats received none. The aqueous phase of the extract was analyzed by NMR spectroscopy for measurement of the relative areas of metabolic intermediates. A ^{13}C NMR spectrum of the aqueous phase of a control rat brain extract is shown in figure 4.11. The spectrum shows peaks from glucose derived metabolites that were also present in the yeast extracts (alanine, aspartate, glutamate, glutamine and lactate) and the peaks from metabolites that are more specific to brain tissue: γ-aminobutyrate (GABA) and N-acetyl aspartate (NAA). The α-and β-[^{13}C-2]-glucose peaks from glucose uptake into the brain are also present but not shown in figure 4.11. Analysis of the ^{13}C NMR spectrum took into account a total of 33 resonance peaks (excluding the internal reference DSS peak), 21 of which were assigned to the above mentioned metabolites. The assigned peaks account for 75 to 80% of the total carbon. The eight metabolic pools just mentioned account for about 75 to 80% of the ^{13}C label as measured by the sum of integrals over the 33 main carbon peaks observed. Figure 4.12 shows the distribution of label among these metabolic pools in a typical experiment. The presence of lactate is due to anaerobic lactate production during the freezing and extraction procedure. The amount of lactate varied considerably with the efficiency of freezing relative to interruption of blood flow. Brain extracts from rats in which the head was sectioned before freezing show considerably more lactate (around 43%) than extracts from rats in which the brain was frozen under anesthesia before sectioning (around 6%).

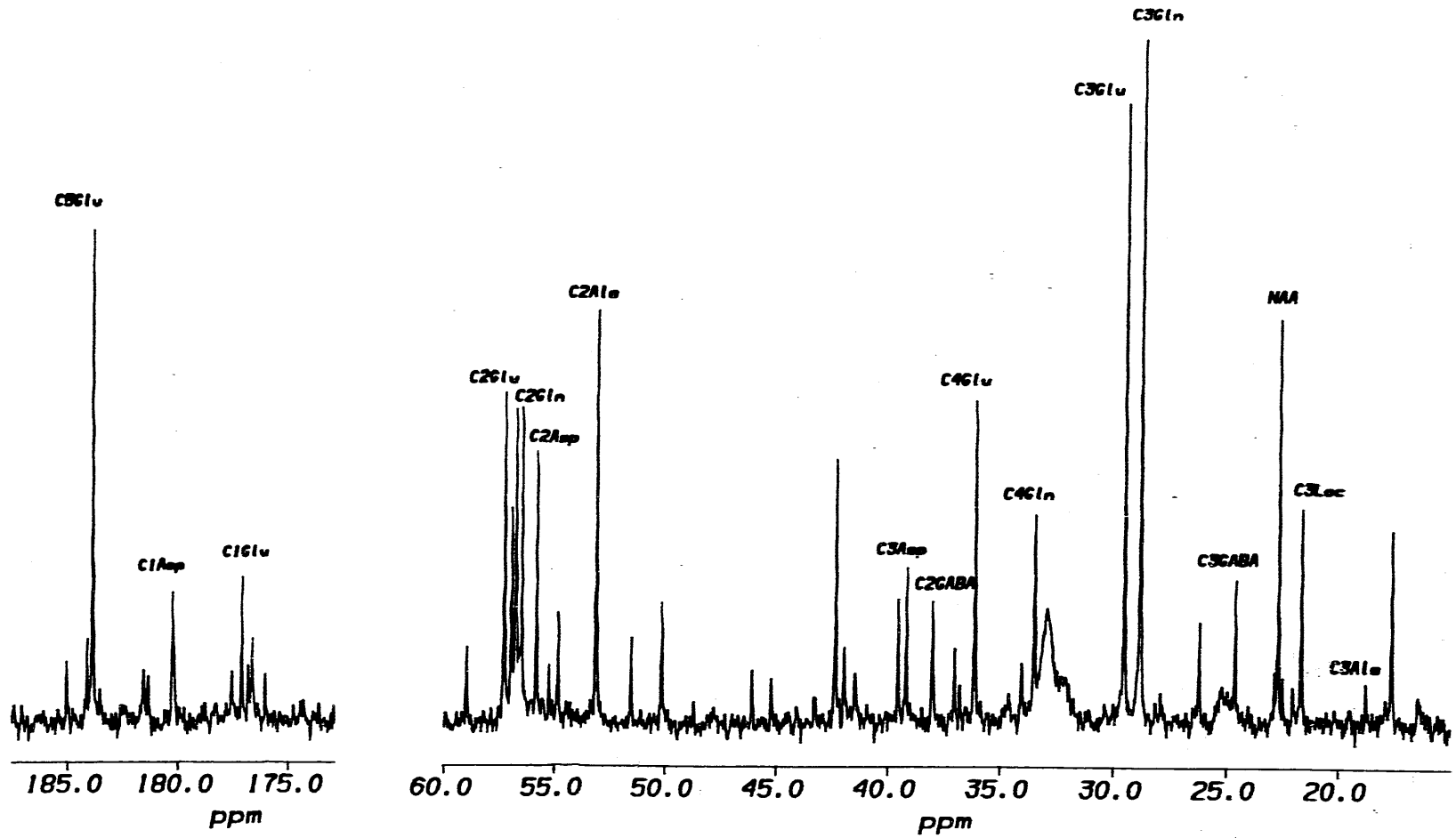

Figure 4.11. ^{13}C NMR spectrum of the aqueous phase of a rat brain extract after 1/2 hour I.V. infusion with [^{13}C-2]-glucose. Resonances shown are : CiGlu = carbons 1 to 5 of glutamate, CiAsp = carbons 1 to 3 of aspartate, CiAla = carbons 2 to 3 of alanine, CiGln = carbons 2 to 3 of glutamine, CiGABA = carbons 2 to 3 of γ-aminobutyrate, NAA = CH3 N-acetyl-aspartate, C3Lac = carbon 3 lactate. Not shown are resonances α-and β-[C2]-glucose at 72.58 and 75.26 ppm, [C2]-lactate at 71.14 ppm and DSS at 0.00 ppm.

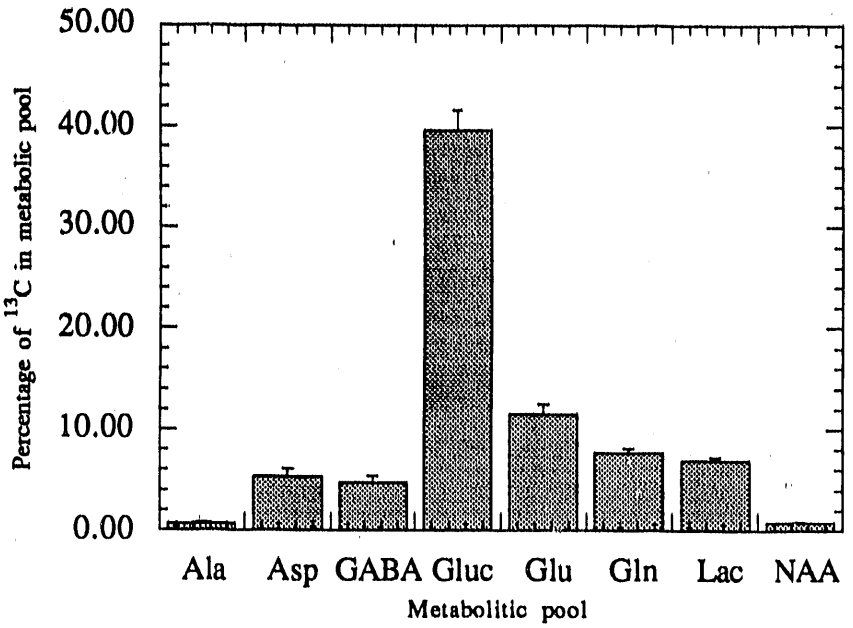

Figure 4.12. Typical distribution of ^{13}C label in the eight main metabolic pools of the rat brain after 30 minute I.V. infusion with [^{13}C-2]-glucose, expressed as percent of total observed ^{13}C. Ala = alanine, Asp = aspartate, GABA = γ-aminobutyrate, Gluc = glucose, Glu = glutamate, Gln = glutamine, Lac = lactate, NAA = N-acetyl-aspartate.

Figure 4.13 shows the relative enrichments of glutamate carbons after 30 minutes of I.V. infusion with [^{13}C-2]-glucose under the control conditions. The ratio of C4 to C5 peak areas of glutamate is used to calculate the relative amount of glucose flux through the shunt and found to be 25 ± 4 % under the control conditions. The relative enrichments of alanine C2 and C3 were not used to measure flux of glucose through the pentose shunt in this case because the C3 enrichment was too low to give a peak with sufficient signal to noise ratio.

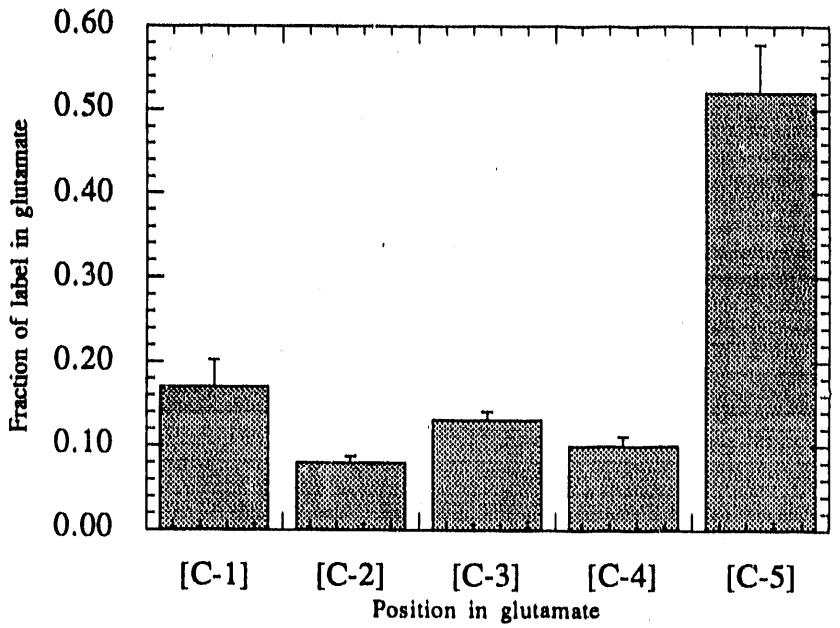

Figure 4.13. Relative fractional enrichments of ^{13}C label in the 5 positions of glutamate in the rat brain extract after 30 minutes of I.V. infusion with [^{13}C-2]-glucose under control conditions (n=2). Fraction of label in position i = [^{13}C-i]-glutamate/Σ[^{13}C-i]-glutamate.

The distribution of ^{13}C label found in the glutamate from rat brain is similar to that found in yeast cells. When 33 mmol/kg TBHP was infused I.V. prior to glucose infusion, the percent glucose flux through the shunt was 32 ± 5% which did not constitute a significant increase relative to flux under control conditions.

Proton spectroscopy.

The evaluation of glucose flux through the pentose shunt by measurement of C4 and C5 glutamate peak areas is possible in the brain extracts as was shown in the previous section. Due to the low receptivity of the ^{13}C spin, acquisition of the ^{13}C spectrum with sufficient signal to noise ratio implies long acquisition times, which are feasible *in vitro* but make such a measurement *in vivo* difficult. The proton spin, which theoretically gives a

32-fold increase in sensitivity relative to ^{13}C, yields sufficient signal to noise ratios from glutamate in short acquisition times, but only provides information on the protonated positions: C2, C3 and C4. Measurement of glucose flux is therefore not feasible from the proton spectrum alone, but one can obtain relative variations of C4 enrichment. If these are normalized by the total flux of glucose, then an increase in C4 enrichment is related to increase in glucose flux through the pentose shunt. In order to evaluate the feasibility of this type of measurement *in vivo*, proton spectra were acquired on the brain extracts.

Figure 4.14 shows a proton spectrum from 4.7 to 1.1 ppm of the aqueous phase of a rat brain after 30 minutes I.V. infusion with [^{13}C-2]-glucose. The pulse sequence used to obtain this spectrum was a : [recycle delay -presaturation pulse applied at the water frequency (4.8 ppm) -single 45° pulse -acquisition]. In this case the protons connected to unlabeled (^{12}C) carbons are predominant and ^{13}C satellites are obscured by the ^{12}C protons. Figure 4.15 shows the spectrum obtained by applying the inverse detection pulse sequence set for detection of [^{13}C-4]-glutamate proton satellites (see methods section 3.1.2.) compared to the single pulse sequence in the 0.6 ppm area surrounding the [^{13}C-4]-glutamate proton peak at 2.5 ppm. The right side of figure 4.15 shows the same comparison in the DSS region and demonstrates that DSS ^{13}C satellites can be used for quantitative determination in the inverse detect spectrum. As would be expected considering the results of the analysis of the ^{13}C spectra, comparison of [^{13}C-4]-glutamate peaks in the ^{1}H spectra did not reveal significant differences between control and TBHP stressed animals.

The direct detect ^{1}H spectrum is also necessary for determination of the fractional enrichment of glutamate carbons because it permits measurement of [^{12}C-4]-glutamate concentrations. The fractional enrichment of the C4 carbon of glutamate was determined in the rat brain extracts. The [^{12}C-4]-glutamate concentration was obtained from the ^{1}H direct detect spectra and the [^{13}C-4]-glutamate concentrations from the ^{13}C spectra. Since the

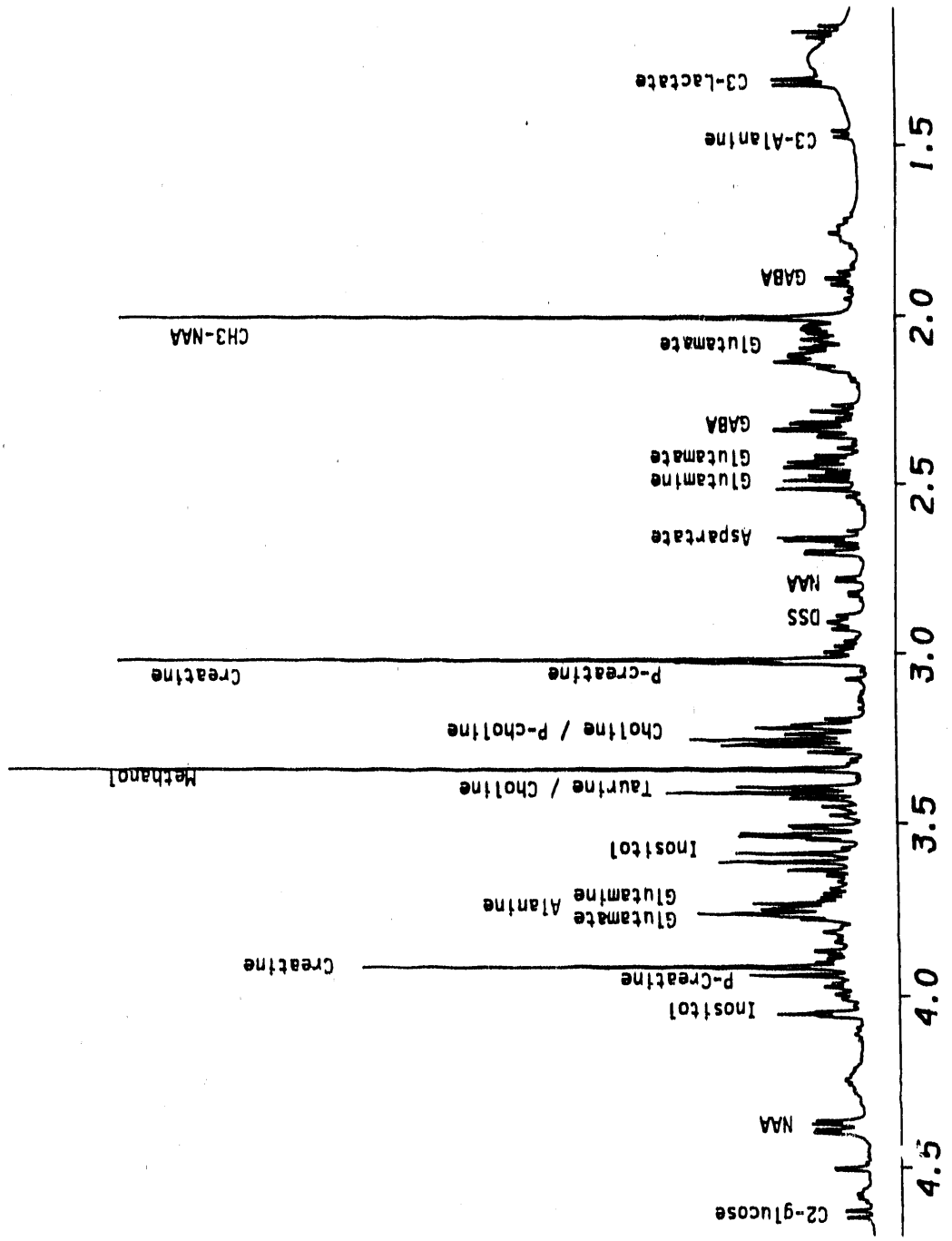

Figure 4.14. ^{1}H NMR spectrum of the aqueous phase of a rat brain extract after 30 minutes I.V. infusion with [^{13}C-2]-glucose. Abbreviations: NAA = N-acetyl aspartate, GABA = γ-aminobutyrate. Methanol present is residual solvent.

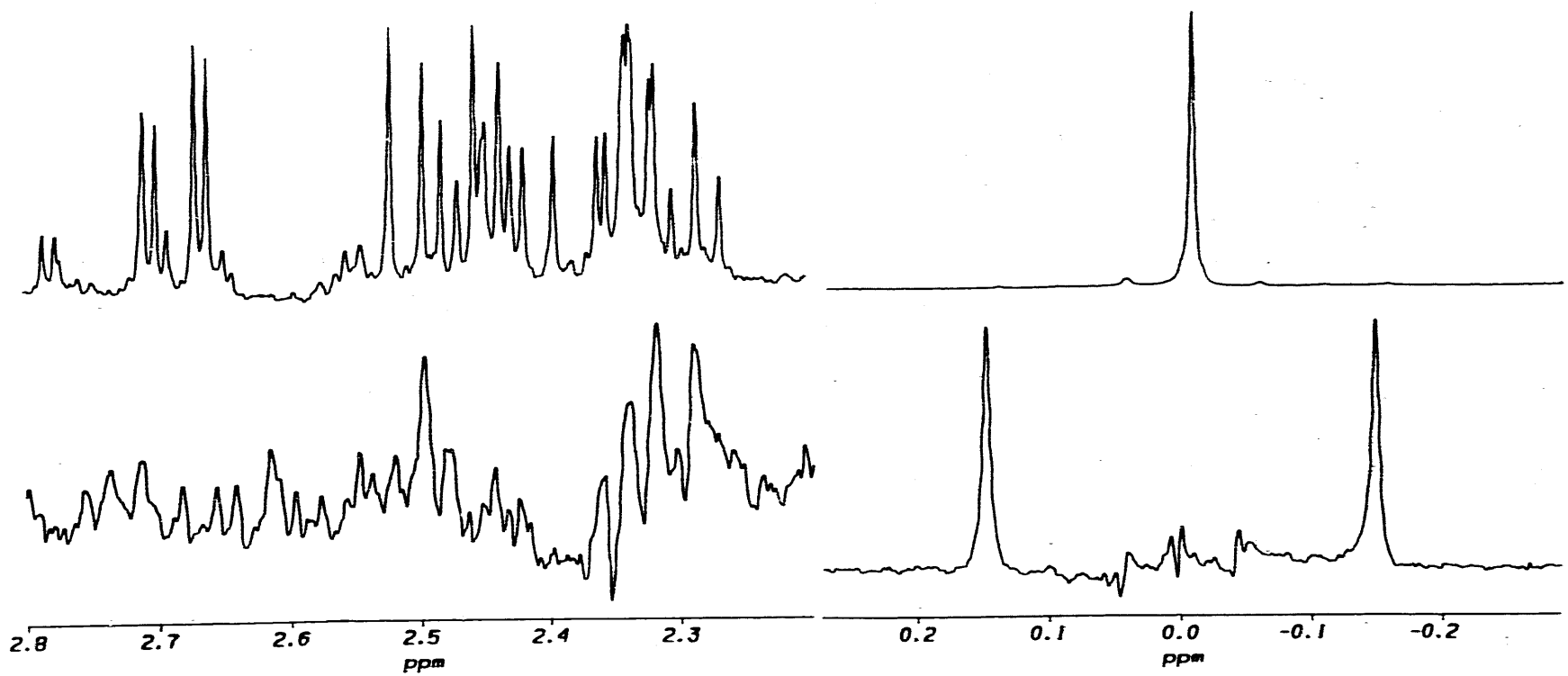

Figure 4.15. ^{1}H NMR spectra of the aqueous phase of a rat brain extract after 30 minutes I.V. infusion with [^{13}C-2]-glucose. Upper spectra: single pulse with water presaturation sequence - Lower spectra: inverse detect sequence. Left side: [^{13}C-4]-glutamate region - Right side: DSS internal reference region.

level of hyperglycemia is not expected to affect cerebral glucose utilization rates in the rat (42), data from the lightly hyperglycemic (11.6 mM) and the strongly hyperglycemic (23.2 mM) rat brains were pooled together here. The fractional enrichment of [^{13}C-4]-glutamate was 10 ± 4% (n=4). The total glutamate pool was 9±2 μmol/g wet weight brain (n=4) determined from the proton direct detect spectra. Therefore approximately 0.9 μmol/(g wet weight brain) of glutamate was labeled in C4 corresponding to about 0.2% of the 552 μmol of label infused (for the lightly hyperglycemic rats) or 0.1% (for the strongly hyperglycemic rats).

4.3.2. Metabolic blockade: the 6-aminonicotinamide method.

In order to evaluate the 6-aminonicotinamide method for determination of glucose flux through the pentose shunt (section 2.4), the following experiments were done. 6-AN was injected I.P. 2 hours previous to 3 hours constant I.V. infusion of a total of 750 mg/kg [^{13}C-1]-glucose. Oxidatively stressed rats received a 33 mmol/kg I.V. bolus of TBHP immediately prior to glucose infusion. In order to test whether FDG would affect the shunt activity, FDG stressed rats received a 110 mg/kg FDG bolus immediately prior to glucose infusion. Control rats received only the [^{13}C-1]-glucose infusion 2 hours after the 6-AN injection. At the end of glucose infusion, the brain was frozen and extracted. ^{13}C NMR spectra were acquired from the aqueous phase of the extracts. A typical ^{13}C spectrum of the aqueous phase of rat brain extract from a 6-AN treated rat infused with [^{13}C-1]-glucose is shown in figure 4.16. The [^{13}C-1]-6PG peak area was measured to determine the amount of [^{13}C-1]-6PG accumulated per gram brain (see section 3.1.1). This amount was then normalized by either the glucose dose or the glucose fractional enrichment to account for glucose uptake in the brain (see section 2.4.) The results are presented in table 4.1.

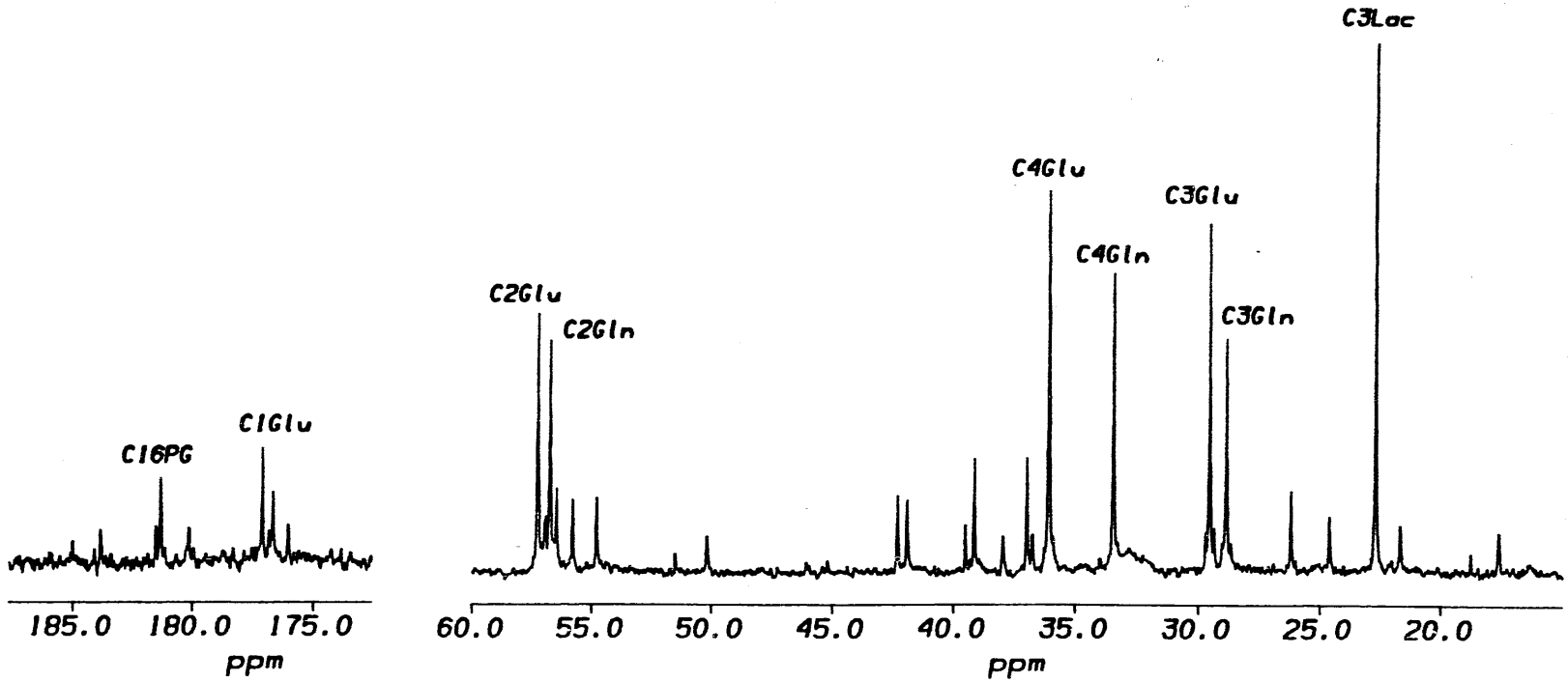

Figure 4.16. ^{13}C NMR spectrum of the aqueous phase of a 6-AN treated rat brain extract after 3 hours I.V. infusion with [^{13}C-1]-glucose. Resonances shown are : CiGlu = carbons 1 to 4 of glutamate, CiGln = carbons 2 to 3 of glutamine, C3Lac = carbon 3 lactate. Not shown are resonances α-and β-[C1]-glucose at 98.52 and 94.71 ppm and DSS at 0.00 ppm. Leftside scale increased twofold.

Table 4.1. Results of the 6-AN study. The first column (6PG) gives the amount of [^{13}C-1]-6PG per gram wet weight brain in μmol/g ww br. The second column (6PG per glucose dose) gives the ratio of the first column to the glucose dose expressed in mmol/kg. The third column gives the ratio of the first column to the glucose fractional enrichment of the brain expressed as a fraction.

Experimental conditions	6PG (μmol/g br)	6PG per glucose dose	6PG per fract. enrichmt.
Control (n=3)	4 ± 1	1.0 ± 0.3	9.6 ± 0.3
TBHP (n=1)	9 ± 1	2.4 ± 0.3	28.0 ± 0.3
FDG (n=2)	6 ± 1	1.1 ± 0.1	9.8 ± 0.2

Table 4.1. shows small increases in the amount of 6PG accumulated for the TBHP and FDG treated animals. When the 6PG is normalized for glucose by either the glucose dose or the glucose fractional enrichment then the FDG treated animals show no significant difference from the controls. On the other hand the TBHP rat shows an increase by a factor of 3 of the glucose fractional enrichment normalized 6PG, attributed to increase in relative flux of glucose through the pentose shunt.

Chapter 5.

NMR determination of glutathione redox state in tissues.

The tripeptide γ-glutamyl-cysteinyl-glycine, known as glutathione (GSH), is the cofactor for the one of the cell's main antioxidant enzymatic systems: glutathione peroxidase. The cell's resistance to damage from peroxides depends in part on the amount of reduced glutathione present in the cell and the cell's capacity to regenerate reduced GSH once glutathione has been oxidized in the peroxide destruction reaction. As we have mentioned earlier, the cell's capacity to regenerate reduced GSH depends on the production of NADPH. The glutathione redox state is the ratio of reduced to oxidized glutathione and it reflects the cell's capacity at a given time to defend itself against the arrival of peroxides. In the following, we develop a method to monitor the glutathione redox state based on the proton NMR detection of the reduced and oxidized forms. We have applied this method to the cell free preparations in which glutathione has been added, and this suggests that the method could be applied to tissues *in vivo*, on the condition that the peaks specific to the

reduced and oxidized forms of glutathione may be distinguished in the proton spectrum *in vivo*.

5.1. NMR determination of glutathione redox state.

The active group of GSH in the redox reaction is the cysteinyl's thiol SH group which when oxidized forms a disulfide bridge linking two glutathione molecules together in the oxidized GSSG form.

2 GSH (red) $\rightleftharpoons$ GSSG (ox)

The chemical formulas of the reduced (GSH) and oxidized (GSSG) forms of glutathione are shown below (with no assumptions on three dimensional conformation), where Gly, Cys and Glu represent respectively the glycine, cysteine and glutamine groups.

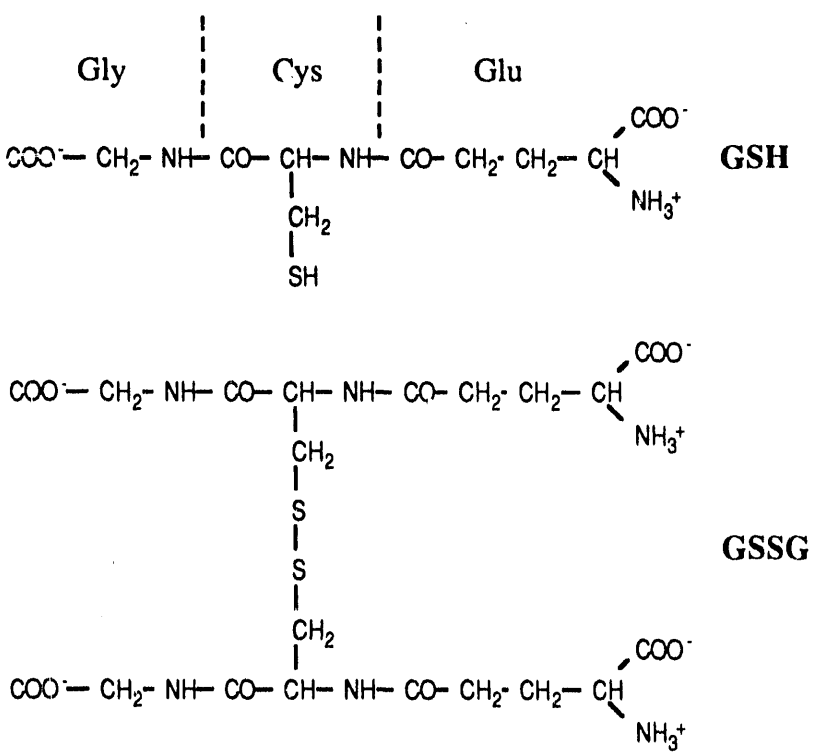

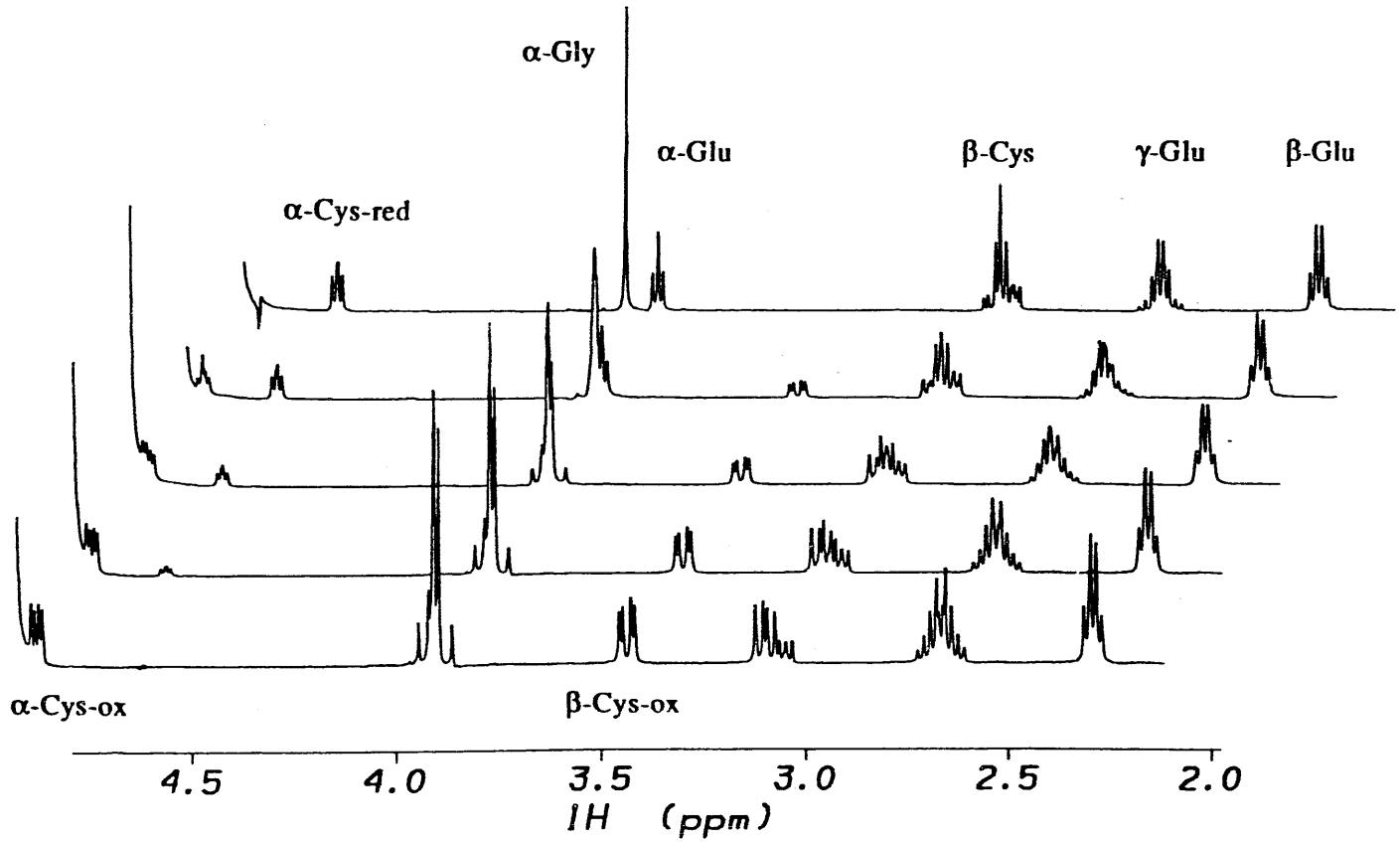

Figure 5.1. ^{1}H NMR spectra of solutions of glutathione with varying concentrations of reduced and oxidized forms. From top to botom: 80 mM GSH; 60 mM GSH + 20 mM GSSG; 40 mM GSH + 40 mM GSSG; 20 mM GSH + 60 mM GSSG; 80 mM GSSG. Abbreviations: Cys = cysteinyl , Gly = glycyl, Glu = glutamyl; α, β and γ refer to the position relative to the C-terminal carboxy of the amino acid group; ox and red refer respectively to the oxidized and reduced forms of glutathione.

The spectral differences between the reduced and oxidized forms of glutathione distinguish the two species in solution. Quantitative determination of the relative amounts of the two species in solution is therefore possible on the condition that the peaks specific to each species be detectable in the spectrum. Figure 5.1 demonstrates the spectral differences between the reduced and oxidized forms of glutathione. Solutions of glutathione in phosphate buffered D_2O were prepared with varying ratios of the reduced to the oxidized form with an internal DSS chemical shift reference standard, and the proton NMR spectra of the solutions are shown in figure 5.1. Initial assignments of the spectra are based on previous studies (50) & (51) and proton-proton coupling correlations that were obtained in the 2-D COSY spectrum of glutathione by us. We interpret the spectral differences in the following manner. The α– and β-cysteinyl proton frequencies are sensitive to the change in redox state of the glutathione molecule due to the proximity of the disulfide bridge. The α-cysteinyl H peak at 4.57 ppm in the reduced form is shifted downfield by 0.18 ppm to 4.75 ppm (close the the residual water peak) in the oxidized form. For glutathione in the reduced form, the β-cysteinyl H_2 chemical shift is centered at 2.96 ppm. The conformation of the oxidized form of glutathione is such that the two β-cysteinyl H_2 groups are not equivalent. One is shifted downfield by 0.34 ppm from 2.96 ppm to 3.30 ppm, while the other remains at 2.96 ppm.

Whether the above conformational interpretation is correct or not, the data show that the peak centered at 4.57 ppm has a relative area corresponding to 1 proton and is specific to GSH, and that the peak centered at 3.30 ppm has a relative area corresponding to 2 protons, and is specific to GSSG. With the appropriate correction for the number of protons per peak, these two peaks were used to evaluate the ratio of reduced to oxidized forms of glutathione in the prepared solutions. If I_{GSH} is the area of the peak at 4.57 ppm and I_{GSSG} is the area of the peak at 3.30 ppm, the ratio of GSH to GSSG is given by:

$$\frac{[GSH]}{[GSSG]} = \frac{I_{GSH}}{0.5 I_{GSSG}} \qquad (5.1)$$

Figure 5.2 compares the value for the GSH/GSSG ratio obtained with equation 5.1 to the expected value for the ratio.

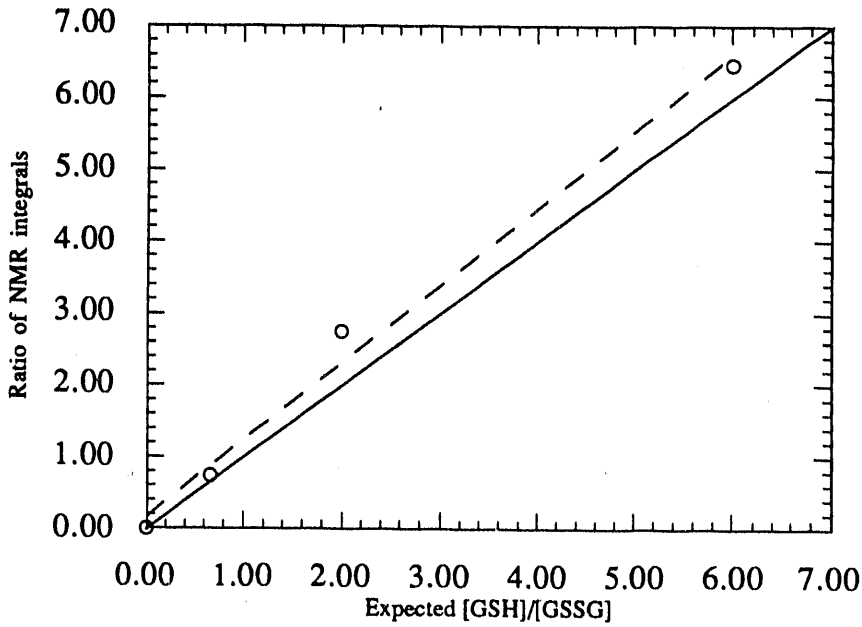

Figure 5.2. The experimental ratio of GSH to GSSG peak intensities (equation 3.14.) is plotted against the expected ratio. The dotted line is the fit of the data points to a linear function and the solid line is the identity function. The point with zero coordinates corresponds to noise which was not integrated, since no peak was visible.

The fact that the GSH peak at 4.57 ppm rides on the wings of the residual water peak contributes to the higher than expected ratio values. These data suggest that it should be possible to follow the reduction of GSSG to GSH after addition of GSSG to a cell system. The characteristic peaks should be observable after subtraction of the first spectrum of a dynamic series from the subsequent spectra of the series. The contribution to the spectrum of the water peak and peaks from metabolites whose concentration and chemical shift remain constant during the experiment should be removed by the spectral subtraction.

5.2. Measurement of glutathione redox state in cell free preparations.

In the cell free preparations it was possible to evaluate the glutathione redox state by subtraction spectroscopy as just described. In the endpoint measurement case, the proton spectrum from a control preparation is subtracted from the spectrum of the GSSG treated preparation. This procedure is illustrated in figure 5.3 which shows an example of spectra from control and GSSG treated preparations and the subtraction spectrum. The subtraction spectrum clearly shows the α- and β-cysteinyl proton peaks in the reduced and oxidized forms of glutathione from which the redox state of glutathione is determined. The percent of GSSG that was reduced during the experiment was found to be 87 ± 11% (n=3), assuming that all of the glutathione added was in the oxidized form. This assumption is reasonable considering that the GSSG solution was verified by proton NMR for presence of GSH before addition to the cell free preparations, and no GSH was detected. The GSH/GSSG ratio or glutathione redox state was 10 ± 6 (n=3).

In the experiments in which the pentose shunt flux was monitored continually during glucose consumption, it was also possible to monitor the decrease of the GSSG peak. Since in these experiments, the initial GSSG concentration was lower than in the end-point experiments, consecutive proton FIDs were added together in groups of 3 to increase signal to noise. In order to suppress peaks from other metabolites whose concentration doesn't vary, the last spectrum was subtracted from each of the previous ones. The series of subtraction spectra for a typical experiment is shown in figure 5.4. Figure 5.4 shows the decrease with time of the β-Cys GSSG peak at 3.3 ppm which reflects the reduction of GSSG to GSH.

The cerebral concentration of glutathione is reported to be between 0.9 and 3.4 μmol/g brain for the rat (43) and 2 μmol/g brain in humans (52). At this concentration in the human brain, the glutathione peaks should be detectable *in vivo* in a reasonable volume

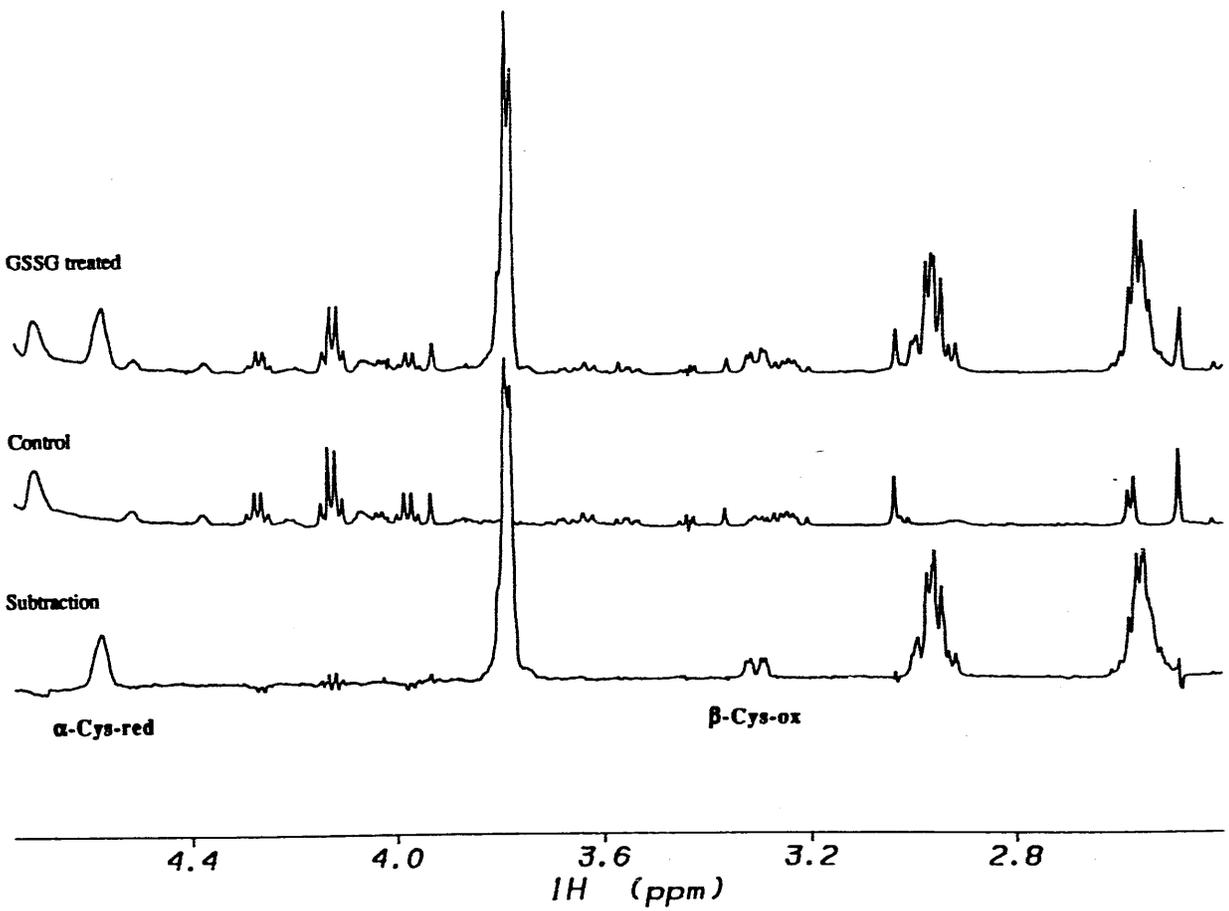

Figure 5.3. Determination of glutathione redox state in the cell free preparations by subtraction of the ^{1}H NMR spectra. Top spectrum: GSSG treated preparation. Middle spectrum: control preparation. Bottom: Subtraction spectrum: GSSG treated - control. α-Cys-red = α-cysteinyl group of reduced GSH; β-Cys-ox = β-cysteinyl group of oxidized GSSG.

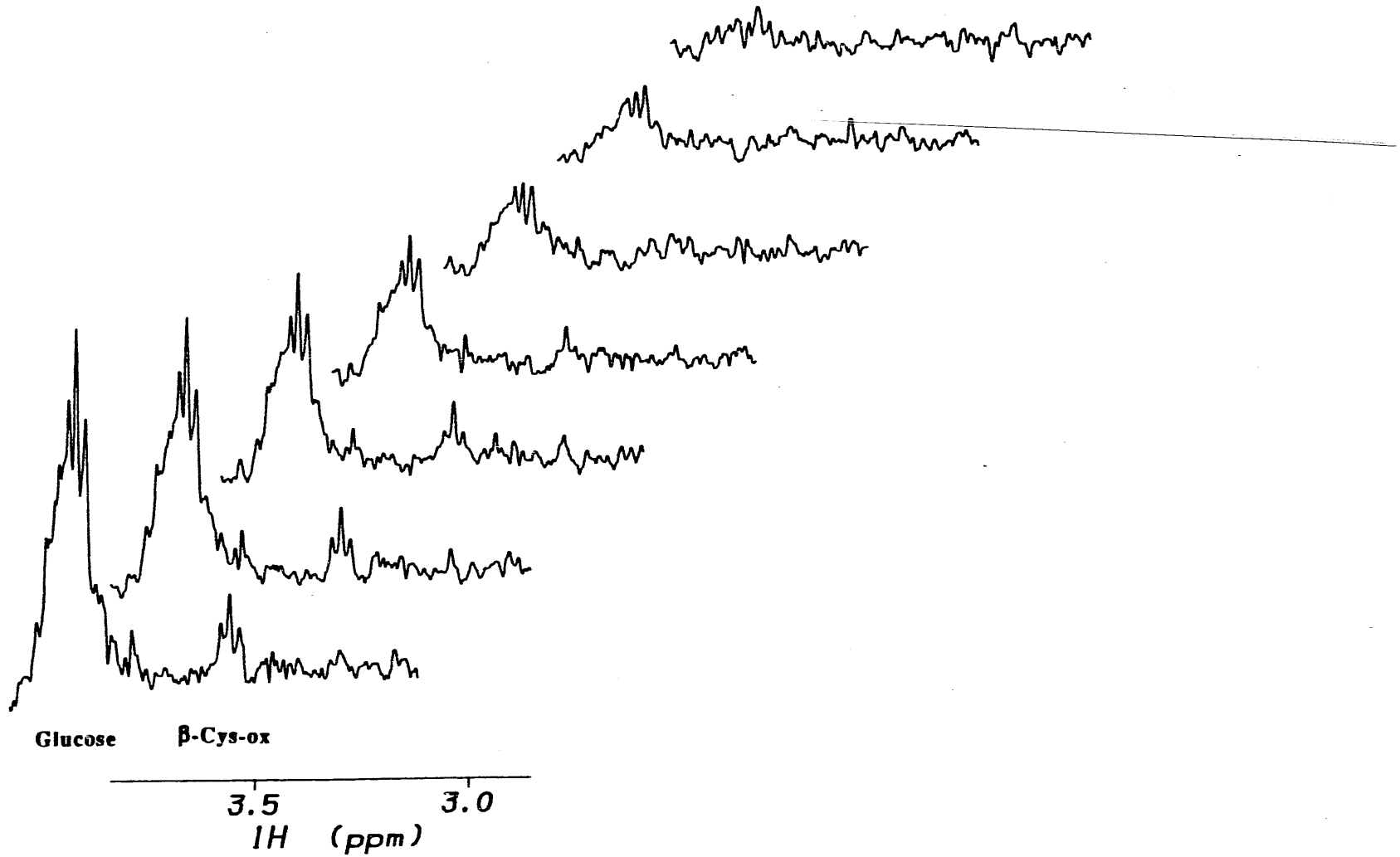

Figure 5.4. Time series of ^{1}H NMR subtraction spectra in the cell free preparations after addition of 20μmol [^{13}C-2]-glucose and 1.5 mM GSSG. Each spectrum is the sum of 3 acquisition intervals corresponding to 21 minutes of acquisition.

β-Cys-ox = β-cysteinyl group of oxidized glutathione.

and with a reasonable acquisition time, but the proximity of the chemical shift of α-Cys of GSH to the water peak and that of β-Cys of GSSG to choline, P-choline and taurine peaks requires that a suitable spectral editing technique be used to distinguish the glutathione peaks.

Chapter 6.

Conclusions.

6.1. NMR measurement of pentose shunt.

We have proposed to develop and evaluate NMR methods for measurement of the relative flux of glucose via the pentose phosphate pathway in living tissues. We have presented methods based on the incorporation of ^{13}C label into major metabolic pools after administration of [^{13}C-2]-glucose. The proposed methods were evaluated in cell preparations and whole animals using tissue extracts, and we have shown that the methods can be used for measurement of relative pentose shunt flux under anaerobic or aerobic conditions. The value of the NMR measurements over radioactive tracer measurements resides in that NMR permits non-invasive sequential monitoring of the metabolic state of the tissue.

6.1.1. Anaerobic measurements in cell free systems.

In the brain cell free preparations, we have used both [^{13}C-1] and [^{13}C-2]-glucose for measurement of the relative flux of glucose through the shunt. The relative shunt flux

has been previously measured under anaerobic conditions using NMR detection of lactate fractional enrichments and [^{13}C-1]-glucose as a substrate as described in section 2.2.1 (equation 2.5) in perfused rabbit lens (21) and perfused rat C6 glioma cells (53). The brain cell free system is only comparable to these systems in as much as the cytosolic glycolysis, pentose shunt and glutathione peroxidase-reductase enzymes were present in all systems and these systems were all studied in anaerobia. One obvious distinction is the fact that in the cell free preparations, cytosolic enzymes and cofactors are diluted relative to the physiological state and this implies that in order for it to function, cofactors are added to the preparation. The concentrations of the cofactors affect the activities of the enzymes. In our preparations, the enzymes and cofactors are diluted approximately by a factor of 6 from their amount per gram wet weight brain. The selection of concentrations of cofactors used in our studies and the choice of pH (7.4) were based on previous enzymatic studies of cell free preparations (37), (54) & (55) and were designed to insure activity of all steps of the glycolysis and pentose shunt pathways. These concentrations are given again below:

Mg^{++}	2 mM
NAD^+	0.3 mM
$NADP^+$	0.3 mM
ThiaminePP	3 mM
ATP	3 mM
nicotinamide	30 mM

Of particular importance for the regulation of the oxidative steps of the pentose shunt are the relative amounts of $NADP^+$ and NADPH, since under physiological conditions, the $NADP^+$/NADPH ratio controls glucose-6-phosphate dehydrogenase activity. In our experiment $NADP^+$ was prepared without any NADPH in the coenzyme solution which is added to the NMR cell free aliquot. This accounts for the high value of 50% (control) to 80% (GSSG stressed) flux through the shunt at the onset of the experiment when the $NADP^+$/NADPH ratio is highest. The variations of the

$NADP^+$/NADPH ratio during the time course of glucose consumption were not monitored in the cell free preparations. The physiological concentrations for $NADP^+$ and NADPH in the rat brain are reported (43) to be respectively 5 and 17 nmol/g wet weight brain which gives a physiological $NADP^+$/NADPH ratio of 0.3.

In the rabbit lens incubated in bicarbonate medium, the flux was reported to have an equilibrium basal level of 5.6 ± 5.8 % (21), although in the first several hours of incubation, the flux ranged from 20 to 40%. These initially high values for the flux in the rabbit lens, similar to the ones found in the cell free brain preparations were not commented upon by the authors. In the C6 glioma cells, the flux through the shunt was found to be 10.01 ± 0.85 %, but no dynamic assessment of the flux was done.

In the cell free preparations the value for the overall flux of glucose was found to be 6% under the control conditions. Since in the preparations the cytosolic enzyme and cofactor system is not under physiological conditions no direct comparison is made to the above mentioned studies in perfused tissues which also used the [^{13}C-1]-glucose/C3 lactate enrichment method. However studies of pentose shunt activity in brain mince have been done under conditions similar to the cell free preparations but using [^{14}C-1] and [^{14}C-2]-glucose as the substrate and observing release of $^{14}CO_2$ (56) to evaluate pentose shunt activity. In the brain mince experiments, 150 mg of brain are incubated in 2ml of 0.15 M phosphate buffer containing the following cofactors:

Mg^{++}	5 mM
NAD^+	0.5 mM
$NADP^+$	0.5 mM
ATP	5 mM
nicotinamide	50 mM

With [^{14}C-1]-glucose as the added substrate and the above cofactor concentrations, the effect of GSSG on the pentose shunt activity was evaluated. The amount of $^{14}CO_2$ released from the preparation was increased by a factor of 2.2 (from 302 nmol $^{14}CO_2$ in

the control to 667 nmol $^{14}CO_2$ in the GSSG treated case) when 2.5 mM GSSG was added to the brain mince. We observed an increase of the relative shunt flux by a similar factor of 2.3 (from 6% in the control to 14% in the GSSG case) when 1.5 mM GSSG was added to the cell free preparation. Although the release of $^{14}CO_2$ from [^{14}C-1]-glucose is indicative of pentose shunt activity it cannot be used as such to measure the relative flux of glucose through the shunt. The results obtained in the brain mince and cell free preparations confirm the role of the pentose shunt in the maintenance of levels of reduced glutathione in the brain and support the hypothesis of the shunt's involvement in protection against oxidative stress. Similar values are found between increases due to GSSG in similar preparations (cell free preparation and brain mince) using different methods for evaluation of the shunt flux.

When the [^{13}C-2]-glucose/lactate enrichment method is used for measurement of the relative shunt flux in the cell free preparations, values comparable to those obtained with the [^{13}C-1]-glucose/lactate enrichment method are found. Table 6.1 compares results obtained by the two methods at the onset and towards the end of the experiment.

Table 6.1. Relative flux of glucose through the pentose shunt in cell free preparations using the C1 and C2 methods of measurement. Increase in flux due to addition of GSSG is shown in 3rd and 6th columns.

	control C1	GSSG C1	incr C1	control C2	GSSG C2	incr C2
onset	50%	80%	1.7	65%	85%	1.3
end	6%	14%	2.3	15%	35%	2.3

The results as presented in table 6.1 show that the increase due to GSSG is about the same using both measurement methods but values found for the C2 method are higher than those for the C1 method.

One possible source for bias in the measurement by the C2 method is the presence of alanine whose C3 protons resonate at a frequency close to the $^{13}C3$ lactate satellite at 1.46 ppm. The unaccounted for presence of alanine would introduce a bias towards higher values of relative shunt flux. This can be avoided by taking the [^{13}C-3]-lactate satellite resonance at 1.24 ppm and multiplying by 2 to obtain the total satellite peak area.

6.1.2. Aerobic yeast studies.

In the aerobic yeast, we have used [^{13}C-2]-glucose for measurement of the relative flux of glucose through the shunt by the method of NMR observation of the relative enrichments of glutamate carbons, which we propose in section 2.3. Two species of yeast were studied and the effect of oxidative stress from of t-butyl hydroperoxide and oxidized glutathione was evaluated.

Results from NMR and radiotracer methods compared in Saccharomyces cerevisiae.

The relative flux of glucose through the shunt has been evaluated by others in Saccharomyces cerevisiae (SC) using radioactive tracer methods under similar conditions (57) & (58) and found to be comparable or inferior to the flux found in our measurement. In our experiments where SC cells are grown to mid-log phase in the presence of 2% dextrose as the carbon source and 1% yeast extract as the nitrogen source, the relative shunt flux is found to be 13 ± 2%.

Wang et al. (57) find 12%, for SC grown with glucose and $(NH_4)SO_4$. Their method of measurement of the relative flux is based on the $^{14}CO_2$ released from [^{14}C-1] and [^{14}C-6]-glucose.

Gancedo and Lagunas (58) measured relative shunt flux in SC cells with 2% glucose as the carbon source and compared the effects of the nitrogen source. When $(NH_4)_2$ HPO4 was the nitrogen source, a relative shunt flux of 2.5 ± 0.3% was found,

whereas when 1% yeast extract was the nitrogen source, the relative shunt flux was 0.9 ± 0.4%. These values, which are 5 to 10 times lower than the value found by us, were obtained using the method of measurement developed by J. Katz et al. (59).

Comparable values of relative flux of glucose through the pentose shunt are found with measurements using the NMR and radioactive tracer techniques. Differences are probably due to both the differences in experimental conditions and the methods used for evaluation of the shunt.

Saccharomyces cerevisiae and Candida utilis compared by the NMR method.

When the Candida utilis (CU) variety of yeast is compared to SC under identical control aerobic conditions in our experiments, the relative shunt flux is found to be 40 ± 3% which is three times higher than SC's flux. This is explained by the higher pentose shunt enzymatic activities found in CU. Table 6.2 compares the reported (45) pentose shunt enzymatic activities of Saccharomyces cerevisiae and Candida utilis.

Table 6.2. Enzymatic activity in μmoles/min/mg protein of the pentose phosphate pathway enzymes in S. cerevisiae and C. utilis (from (45)).

Enzyme	S. cerevisiae	C. utilis	Ratio CU/SC
Glucose-6-P dehydrogenase	0.06	2.15	36
6-P-gluconate dehydrogenase	0.12	0.35	3
Transketolase	0.2	1.45	7
Transaldolase	0.02	0.2	10
Aldolase*	3.0	1.1	0.36

*Aldolase is an enzyme of the glycolytic pathway.

Table 6.2 shows that the shunt enzymatic activities are 3 to 36 times higher in CU than in SC cells. Since table 6.2 gives values from individual assays of each enzyme, one would expect that the overall effect of the enzymes in concert would be limited by the

lowest activity. Accordingly, the factor of 3 increase in overall shunt activity found in CU corresponds to the lowest increase in enzymatic activity found i.e. the activity of 6-phospho-gluconate dehydrogenase.

Effect of oxidative stress.

The effect of oxidative stress from TBHP, phenazine methosulfate and GSSG on the relative flux of glucose through the pentose shunt was studied in SC and CU cells. To our knowledge, variations of shunt activity in yeast cells as a function of this type of oxidative stress has not been evaluated by other methods. We find a small progressive increase (factor of 1.6) of relative shunt flux from 0 to 1mM TBHP in SC A similar increase of the relative shunt flux by a factor of 1.3 was found when CU cells were stressed with 1.5 mM GSSG. The effect on shunt flux with variable concentrations of GSSG was not studied. In the S.C. cells the flux then plateaus with a further increase of TBHP up to 10 mM. This may be explained by the use of other mechanisms of defense against peroxides (catalase) by the yeast cells which do not involve glutathione and the pentose shunt.

6.1.3. Whole animal brain studies.

When the glutamate relative enrichment method is applied to the rat brain the value found for the relative glucose flux is 25 ± 4% for the control rats (n=2) which were not stressed with TBHP. The relative shunt flux has been evaluated by others in a variety of brain preparations, using a variety of methods. The results of studies by others are summarized in table 6.3.

Table 6.3. Summary of relative fluxes of glucose through the pentose phosphate pathway measured in brain tissue.

System studied	Relative shunt flux	Reference
Normal human brain	negligible	Sacks (60)
Isolated monkey brain	5-8%	Hostetler (61)
Isolated rat brain	34.6%	Hakim (62)
Isolated calf brain	the major pathway	Moss (63)
Incubated bovine brain slices	negligible	Krass (64)
Bovine pituitary/pineal slices	3-5%	Krass (64)
Adult rabbit brain slices	0.3%	Guerra (65)
Fetal rat brain slices	3.5%	Guerra (65)
Adult rat brain slices	0.3%	Zubairu (66)
Juvenile rat brain slices	0.7%	Zubairu (66)
Adult rat cerebellum slices	0.35%	Hothersall (67)
Adult rat hemisphere slices	0.77%	Hothersall (67)
Rat superior cervical ganglion	16%	Härkönen (68)
Rat brain extract	3-5%	Hostetler (69)
Rat brain extract	1.3%	Gaitonde (70)
Rat brain extract	2.3%	Gaitonde (28)
Rat brain extract	7.8%	Gaitonde (71)

Table 6.3 has results distributed into 3 groups depending on the type of preparation that was studied. The first 4 rows group results obtained in *in vivo* studies in which the anesthetized subject's principal cerebral vessels are catheterized for administration of substrates or sampling of metabolic products. The second 9 rows group results obtained from incubated brain slice preparations. The last 3 rows group results obtained from rat brain extracts studies similar to the studies done in this thesis work, where analysis of

metabolic products is done on the brain extract after *in vivo* administration of substrates. Table 6.3 shows that a wide range of values are found in the literature for the relative shunt flux in the brain. Factors which may have affected our measurement are discussed in the following.

Results from the study of this thesis do not reflect regional differences in activity in the brain but only an average from all areas of the sample. In this study, the brain samples were the whole brain excluding cerebellum but including the brain stem structures which contain the nucleus coeruleus and the raphe nuclei. It is in these structures that the enzymatic activity of pentose shunt enzymes is reported to be highest (72). High pentose shunt activities from these small local areas could be weighting the average towards a higher value than would be obtained if only the cerebrum was studied.

It is possible that propranolol, which is administered to the rats prior to surgery, might have an effect on pentose shunt activity. Propranolol is a β-adrenergic antagonist. One study shows that β-adrenergic agonists increase the oxidative pentose phosphate pathway and that the β-adrenergic antagonist atenolol reduces the agonist-induced increase (73). This suggests that propranolol might also have a reducing effect on pentose shunt activity.

In the studies where extracts of brain tissue are used for the measurement, it is possible that the the tissue undergoes an ischemic state during the tissue freeze-isolation procedure. If ischemia increases the relative shunt flux, then possibly large increases in shunt flux might have occurred during the brain removal procedure.

Although the technique of anesthesia by N_2O was chosen as the one that would least perturb glucose uptake as opposed to barbiturates (which are known to decrease glucose consumption) (2) it is possible that N_2O anesthesia might have increased the shunt activity.

The rats all received a bolus I.V. dose of 2-deoxyglucose (2DG) before onset of glucose infusion. We have previously reported (74) that 2-^{19}F-2-deoxyglucose (^{19}FDG) affects glucose uptake and pentose shunt activity in the rabbit brain in a dose dependent manner. This suggests that the 2DG administered in this study might also affect pentose shunt activity in the rat brain. The results and conclusions of the previous study are summarized and discussed relative to the results of the present study in the following.

In our previous study, anesthetized male New Zealand white rabbits were administered I.V. loading doses of either 70 mg/kg or 120 mg/kg of ^{19}FDG prior to an ^{18}FDG injection *via* the femoral artery. Control rabbits received no ^{19}FDG. Control and FDG loaded rabbits were imaged simultaneously by PET using a 3 mm transverse section after identical doses of 8.5 mCi of ^{18}FDG were given in I.V. boluses. Dynamic brain images were obtained continually post injection, and arterial input function samples were obtained from a femoral line opposite the input line out to 40 minutes post ^{18}FDG injection. Data were also taken at the liver 40 minutes post ^{18}FDG injection. The dynamic PET data were used along with arterial blood concentration data to derive kinetic constants for the 3 compartment model shown below:

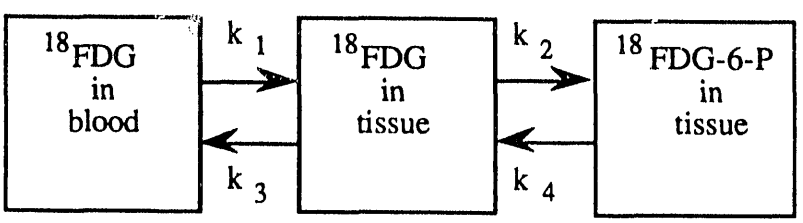

After the 40 minute PET study, the brains of the 70 mg/kg and 210 mg/kg ^{19}FDG loaded rabbits were rapidly excised and frozen in liquid nitrogen immediately post euthanasia. Brain samples were extracted with chloroform-methanol and the aqueous fraction was reconstituted in buffered D_2O with 5mM TFA as an internal ^{19}F NMR reference. ^{19}F NMR spectra were collected from the aqueous fractions on an 11.7 Tesla spectrometer.

The effect of FDG loading on ^{18}FDG uptake and kinetics is shown in tables 6.4 and 6.5.

Table 6.4. Comparison of relative organ uptakes of ^{18}FDG in control and ^{19}FDG-loaded rabbits (from Bolo et al. (74)).

Organ	Control	^{19}FDG (70 mg/kg)	^{19}FDG (210 mg/kg)
Brain	100%	78%	57%
Liver	100%	120%	120%

Table 6.5. Comparison of kinetic rate constants in control and ^{19}FDG-loaded rabbits (from Bolo et al. (74)).

Parameter (min^{-1})	^{19}FDG (210 mg/kg) Rabbit	Control Rabbit	% Difference (FDG/control)
k_1	0.092	0.089	+3%
k_2	0.239	0.154	+55%
k_3	0.027	0.042	-36%
k_4	0.00015	0.0043	-97%
f_v*	0.183	0.146	+25%

*f_v is the vascular fraction (percent of activity in a given organ due to blood)

The data from tables 6.4 and 6.5 show that ^{18}FDG brain kinetics are perturbed and ^{18}FDG brain uptake is decreased with ^{19}FDG loading. This suggests decreased glucose uptake and perturbed glucose kinetics in the brain with ^{19}FDG loading.

^{19}F NMR spectra of the brain extracts showed the presence of a peak at -121.11 ppm assigned to 2-^{19}F-6-phospho-gluconate (2F-6P-DG) in the 210 mg/kg extract but not in the 70 mg/kg brain extract. 2F-6P-DG is the product of metabolism of FDG by the glucose-6-phosphate dehydrogenase enzyme of the pentose shunt. If the pentose shunt activity had been the same in the 70 mg/kg loaded rabbit brain as in the 210 mg/kg rabbit brain, then we would expect to see a peak with an intensity 7.5% of the intensity of the

FDG peak in the 70 mg/kg brain extract spectrum. This would have been detectable above noise level under the conditions of the experiment. Since no peak above noise level was observed in the -121.11 ppm region of the 70 mg/kg brain extract spectrum, we conclude that pentose shunt activity was lower in the 70 mg/kg FDG loaded rabbit brain than in the 210 mg/kg FDG loaded rabbit brain. This suggests that there is a dose dependent increase of pentose shunt activity in the rabbit brain with ^{19}FDG loading.

It is possible that 2DG also perturbs glucose uptake kinetics and increases pentose shunt activity in the rat brain in a dose dependent manner. The doses given in our study were 15 and 50 mg/(kg body weight) which are below the 70 mg/kg for which no ^{19}FDG metabolism via the pentose shunt was observed in the rabbit brain. Further studies are needed to assess the effect of 2DG on pentose shunt activity in the brain.

6.2. Applications.

6.2.1. Tumor metabolism studies.

Increases in pentose shunt enzymatic activity have been associated with cellular proliferation in carcinogenesis and the changes in metabolism of tumors relative to normal tissue. (75 - 79). Although cause and effect relationships between cancer and pentose shunt activity are not established, one may explain activated pentose shunt in relation to cellular division in general, where lipid biosynthesis and production of nucleotides are active processes. The *in vivo* monitoring of pentose shunt activity has the potential to help distinguish tumors from normal tissue and aid in following the metabolic evolution of treated cancerous tissues.

6.2.3. Ischemia in cardiac muscle and brain.

It has been suggested that the highly reactive oxygen derived free radicals superoxide anion, hydroxyl radical and hydrogen peroxide play a role in cerebral ischemia and trauma (80 - 84). Free radical production has been implicated in injury to brain tissue after transient ischemia (7) & (8). The fact that the pentose shunt is involved in scavenging peroxides therefore suggests that pentose shunt activity may be increased in cerebral ischemia. Although pentose shunt flux in the heart is reported to be low (85), shunt activity might also be increased in the case of cardiac ischemia. One study (86) showed that in hearts perfused with [^{13}C-2]-glucose, [^{13}C-3]-lactate appeared in detectable amounts immediately after ischemia was induced. These results are in accord with presence of glucose flux through the shunt during the ischemic period. By applying the model developed in this study (equation 2.17) to the data of that study, one obtains a value of approximately 11% flux of glucose through the shunt after 30 minutes of ischemia.

6.2.2. Cardiac and skeletal muscle studies.

A review of studies of the pathologies of the neuromuscular apparatus (87) indicates that many affected muscle fibres of patients with muscular dystrophies, congenital myopathies, inflammatory myopathies, metabolic myopathies, endocrine myopathies, or with diseases of the lower motor neuron, display an enhanced activity of both oxidative enzymes of the pentose phosphate pathway. Further understanding of the metabolic mechanisms involved in these pathologies should result from *in vivo* metabolic monitoring of pentose shunt activity of muscular tissues.

6.3. Potential for human studies *in vivo*.

In the following, we investigate the potential for and limitations of applying the methods developed in this study to human studies *in vivo*. The hypothetical experiment here is non-invasive ^{13}C NMR detection of [^{13}C-5]- and [^{13}C-4]-glutamate after administration of [^{13}C-2]-glucose. The strategy for evaluating the feasibility of human studies is first to estimate the steady state amount of ^{13}C label incorporated into C4 and C5-glutamate from infused [^{13}C-2]-glucose by using the mathematical model developed in this study and then to estimate the signal-to-noise obtainable from the ^{13}C labeled glutamate by comparison with results obtained from ^{13}C NMR human studies from the current literature. We finally estimate the total amount of infused [^{13}C-2]-glucose required for such a study by using a one compartment mathematical model of plasma glucose concentrations that takes into account the human glucose turnover rate.

Model for C4 and C5-glutamate fractional enrichment as a function of [^{13}C-2]-glucose flux through the pentose shunt.

In order to estimate the signal-to-noise obtained from ^{13}C-glutamate after infusion of [^{13}C-2]-glucose, we first estimate the amount of ^{13}C-glutamate that is produced in the tissue. This is done using the model developed in chapter 2 and applying the assumption of negligible production of pyruvate, acetyl-CoA, and glutamate from endogenous unlabeled sources. This assumption may apply well in brain tissue, but does not apply in skeletal muscle tissue in which endogenous unlabeled glycogen provides most of the glucose.

In the model developed in chapter 2, measurement of the relative shunt flux from glutamate carbons relied on relative enrichments instead of fractional enrichments to avoid undetermined terms arising from undetermined production of unlabeled pyruvate and glutamate from endogenous sources. However measurement of the relative shunt flux was

expressed as a function of fractional enrichments of lactate carbons (equations 2.26 and 2.27), assuming 100% fractional enrichment of the [^{13}C-2]-glucose substrate, negligible production of lactate from unlabeled endogenous sources and a negligible endogenous lactate pool at the onset of infusion. If we assume negligible production of pyruvate from unlabeled endogenous sources, and that steady state enrichment of the pyruvate pool is attained, then the fractional enrichments of C2- and C3-pyruvate (F_{P2} and F_{P3}) are given respectively by equations 2.33 and 2.34 shown again below.

$$F_{P2} = \frac{3(1-X)}{6-X} \tag{2.33}$$

$$F_{P3} = \frac{2X}{6-X} \tag{2.34}$$

If we also assume negligible production of acetyl-CoA and glutamate from unlabeled endogenous sources and that steady state enrichment of the acetyl-CoA and glutamate pools is attained, then F_{P2} is equivalent to F_{C1} (fractional enrichment of acetyl-CoA C1) which is also equivalent to F_{G5} (fractional enrichment of glutamate C5), and F_{P3} is equivalent to F_{C2} (fractional enrichment of acetyl-CoA C2) which is also equivalent to F_{G4} (fractional enrichment of glutamate C4). Therefore by applying these assumptions, the following expressions are obtained for the fractional enrichments of C4- and C5-glutamate as a function of relative shunt flux:

$$F_{G4} = \frac{2X}{6-X} \tag{6.1}$$

$$F_{G5} = \frac{3(1-X)}{6-X} \tag{6.2}$$

The fractional enrichment of the C4 carbon of glutamate was found to be 10±4% (n=4) in the rat brain extracts. This 10% fractional enrichment of C4-glutamate found

corresponds to 28% relative flux through the pentose shunt if we apply equations 6.1 and 6.2. The average value found for relative shunt flux in the rat brains is also 28±5% (n=4) if one pools the data from the different groups of rats. This suggests that the assumptions underlying this model are plausible in the case of the rat brain extracts. An approximate 100% FE of the glucose substrate pool may be explained by considering that infusion of 99% [^{13}C-2]-glucose was via the jugular vein, and therefore glucose uptake in the brain was mostly on the first pass before glucose dilution from endogenous glucose production occurred in the plasma. Under these assumptions one can say that the FE of C4 and C5 glutamate was determined by the relative flux of glucose through the pentose shunt.

In the case where C4 and C5-glutamate FE's are determined only by the relative glucose flux through the shunt, the maximum FE for C4 and C5-glutamate are obtained. If the FE of glucose entering the brain is lower than 100% - say x% - but there is no pyruvate or glutamate dilution, than the C4 and C5 glutamate will be reduced by x%. Further reduction of C4- and C5-glutamate FE will result from dilution of pyruvate or glutamate pools. In order to evaluate conditions for measurement of pentose shunt flux in the human, we will model the situation in the case where FE is determined by pentose shunt flux, and then consider reductions in signal to noise that would occur when the glucose FE is reduced.

Assuming that the C4- and C5-glutamate FE's are determined by the shunt flux, we use the equations 6.1 and 6.2 to calculate the amount of label in C4- and C5-glutamate produced in the human brain after constant infusion of [^{13}C-2]-glucose. Assuming that that the glutamate concentration in the human brain is approximately 10 μmol/g brain weight (43), then the plot of steady state concentrations of [^{13}C-4]- and [^{13}C-5]-glutamate as a function of relative flux of glucose through the pentose shunt is given by multiplying FE's by 10mM. The plot of [^{13}C-4]- and [^{13}C-5]-glutamate concentrations obtained this way is given in figure 6.2.

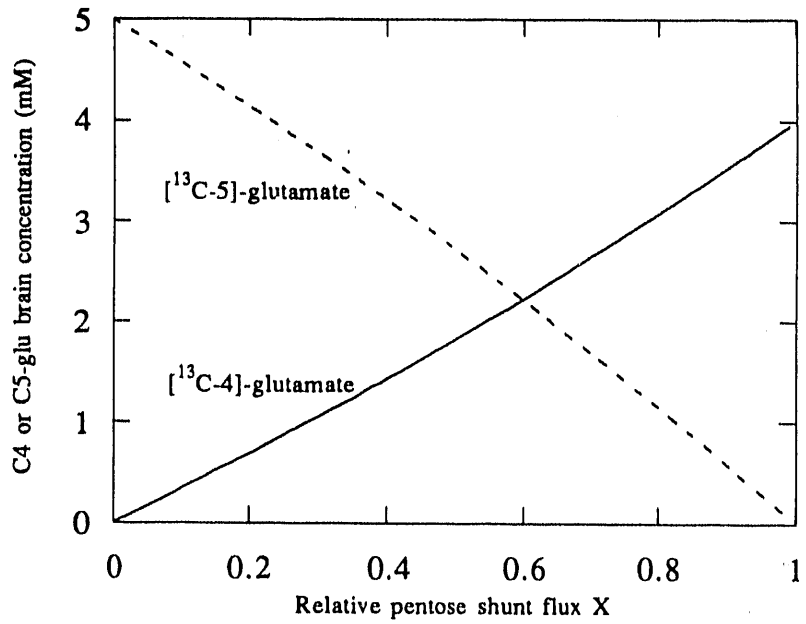

Figure 6.2. Estimate of human brain concentrations of [^{13}C-4] and [^{13}C-5]-glutamate assuming the glutamate carbon fractional enrichments are determined by flux of glucose through the pentose shunt.

The measurement of the relative flux of glucose through the pentose shunt depends on the detection of both [^{13}C-4]- and [^{13}C-5]-glutamate. Figure 6.2 shows that for very low and very high values of relative shunt flux, low tissue concentrations of either species are obtained. These low concentrations will be the main limiting factor for NMR detection. For low shunt flux, the measurement is limited by detection of [^{13}C-4]-glutamate, and for high shunt flux, the measurement is limited by detection of [^{13}C-5]-glutamate.

Another limiting factor for NMR detection is saturation due to long T_1 relaxation time (discussed in section 3.1.1). Since the T_1 of [^{13}C-5]-glutamate in the extract is 12.37s (10 times higher than the C4's T_1 in the extract), the T_1 saturation effect for [^{13}C-5]-glutamate may also be important in tissues. The value of the T_1 of [^{13}C-5]-glutamate in

the brain *in vivo* must be measured to evaluate the saturation effect on SNR in the brain. For low shunt flux values, low detectability of [^{13}C-5]-glutamate due to saturation is compensated by high concentration. For example in the brain extract spectra from our study where 25% shunt flux was measured, the [^{13}C-5]-glutamate was observed with a SNR 1.5 times higher than [^{13}C-4]-glutamate (see figure 4.11), even though saturation effects were substantial. For high shunt flux values, low detectability of [^{13}C-5]-glutamate due to saturation would imply increasing recycle delay times to increase SNR.

Conditions for ^{13}C detection of [^{13}C-4]-glutamate in human studies.

In section 1.3 we estimated the lowest detectable (at a SNR level of 5) concentration of a small metabolite in human brain ^{1}H NMR studies to be about 0.9 μmol/g brain in 8 ml of detected volume with an acquisition time of 4 minutes. This was based on *in vivo* human ^{1}H brain studies done at a field of 2 Tesla. In the same manner we now estimate the lowest detectable concentration in a human brain ^{13}C NMR study based on a ^{13}C NMR human study done at 2.1 Tesla (88). In the study by Gruetter et al. (88), ^{13}C spectra were obtained in a 144 ml volume of the brain using ISIS localized spectroscopy (89), after infusion of 20 to 40 grams of [^{13}C-1]-glucose. The blood was assumed to make up only approximately 3% of the volume of detection which excluded major blood vessels, and therefore signal from blood glucose was neglected. The β-glucose peak was observed with a signal to noise of about 5 (evaluated from the spectrum), with an acquisition time of 14.5 minutes. The brain [^{13}C-1]-glucose concentration was determined by the authors to be 1.03 ± 0.25 mM. Assuming that 62% of the glucose was in the β-configuration, the concentration of β-[^{13}C-1]-glucose peak with a SNR of 5 was about 0.6 mM. Hence a SNR of 5 was obtained from a species with a concentration of 0.6 mM in a volume of 144 ml with an acquisition time of 14.5 minutes at a field strength of 2.1 Tesla. This SNR obtained under these conditions is used to estimate conditions for detection of [^{13}C-4]-

glutamate. Assuming that [^{13}C-4]-glutamate and [^{13}C-1]-glucose have about the same T_1 (in solution the T_1's are respectively 1.28 s and 0.98 s) the same SNR should be obtained from [^{13}C-4]-glutamate as from [^{13}C-1]-glucose under the same conditions.

Conditions for measurement of pentose shunt flux.

Let's evaluate the conditions required for detection of [^{13}C-4]-glutamate, given the conditions of the Gruetter measurement mentioned above (88). When NMR spectroscopy is performed *in vivo*, the Brownian motion of electrolytes (in high concentrations) in the biological sample induce extra noise in the receiving coil. This noise is dependent on the Larmor frequency ω_0 (90) and the expression for the signal to noise ratio is therefore different than the one used in section 3.1.2. In the *in vivo* case, the signal-to-noise ratio (SNR) is still proportional to the concentration (C), the detection volume (V) and the square root of the acquisition time ($t^{1/2}$ since the acquisition time is proportional to the number of acquisitions) but the dependence on field strength (B_0) is linear (as opposed to B_0 to the power 3/2 shown in equation 3.14), because the noise term in the denominator contains B_0 (90). Therefore, if in the following expression:

$$SNR = kCVt^{1/2}B_0 \qquad (6.3)$$

we insert the values for C, V, t and B_0 that were obtained by Gruetter et al., the proportionality constant becomes:

$$k = 0.00724\ ml^{-1}\ mM^{-1}\ min^{-1/2}\ T^{-1}$$

Considering that 4 Tesla spectrometers possessing a wide enough bore to permit human brain studies are presently available, and that shunt flux in the human brain *in vivo* is likely to be smaller than the 25% that was found in the rat brain extract studies, let us evaluate the SNR as a function of time and sample volume for a situation where the relative shunt flux is 5% and the field is 4 Tesla. In accord with equation 6.1 these would be the conditions for detection of 0.17 mM of [^{13}C-4]-glutamate at 4 Tesla. We note that in order

to neglect signal from blood glucose, the volume of detection must exclude major blood vessels, otherwise the contribution of blood glutamate to the signal must be accounted for. The plots for SNR under these conditions is shown in figure 6.3.

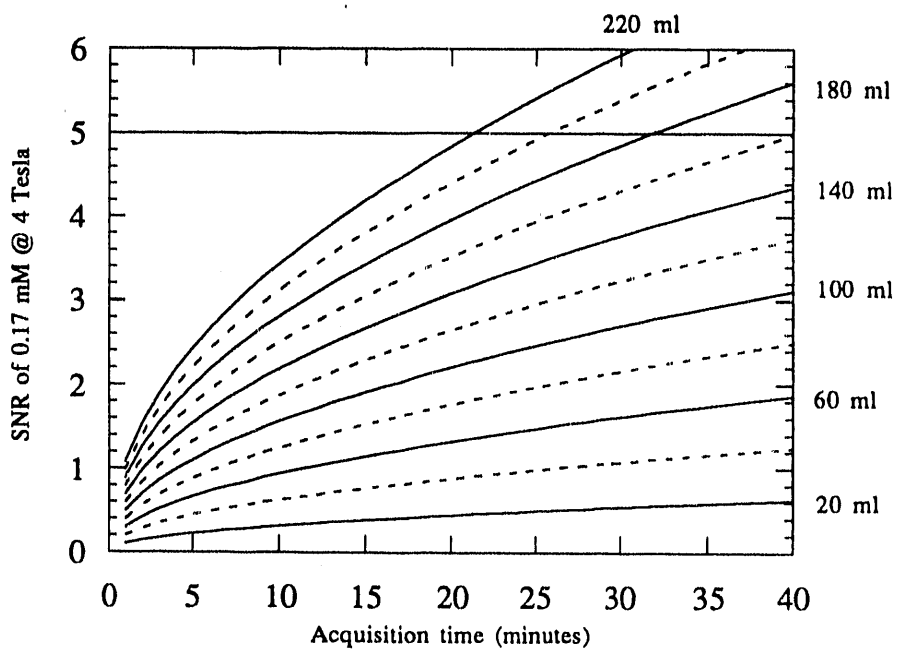

Figure 6.3. 5% flux of glucose through the pentose shunt @ 4 Tesla. Estimation of the ^{13}C signal to noise obtainable from 0.17 mM [^{13}C-4]-glutamate in the human brain as a function of acquisition time for different detection volumes at a field strength of 4 Tesla after 30 minutes of constant infusion of [^{13}C-2]-glucose. Curves are plotted for volumes from 20 to 220 ml with 20 ml increments. The horizontal line corresponds to the SNR limit of 5.

Figure 6.3 based on equation 6.3 enables one to rapidly estimate graphically the experimental conditions needed for obtaining sufficient SNR to measure pentose shunt activity. A signal-to-noise ratio of 5, sufficient to infer 5% flux of glucose through the pentose shunt is estimated to be acquired at a spectrometer field strength of 4 Tesla, in a localized volume of about 185 ml (5.7 cm on a side) with an acquisition time of 30 minutes if 100% plasma glucose fractional enrichment is obtained. In the following section we

estimate that 82% plasma glucose FE is attained in the human with constant 99% [^{13}C-2]-glucose infusion. If 82 % plasma glucose fractional enrichment is obtained, then the detection volume should be increased accordingly to 226 ml (6.1 cm on a side) to obtain the same signal-to-noise level with the same acquisition time. A signal to noise ratio of 5 is considered as sufficient for such a study.

It is of interest to project the conditions of the measurement beyond the present state of NMR technology. Assuming that the signal-to-noise increases linearly with field strength from 4 to 10 Tesla, we can consider the improvement in time resolution that would be obtained in a hypothetical 10 Tesla wide bore spectrometer for human studies. At 10 Tesla the same signal-to-noise of 5 would be obtained from the same volume (226 ml), with 5% pentose shunt flux in only 4.8 minutes.

The signal-to-noise obtained is mainly limited by the concentration of [^{13}C-4]-glutamate which depends on relative shunt flux. At 25% of glucose flux through the pentose shunt for example, a SNR of 5 is obtained in a volume of 63 ml (3.9 cm on a side) with 10 minutes of acquisition time at 4 Tesla. At 82% plasma glucose fractional enrichment, this becomes 77 ml (4.3 cm on a side). In order to give an idea of the conditions of detection as a function of the relative shunt flux the SNR obtained is plotted as a function of the relative shunt flux at a field strength of 4 Tesla with a 15 minute acquisition time in figure 6.4.

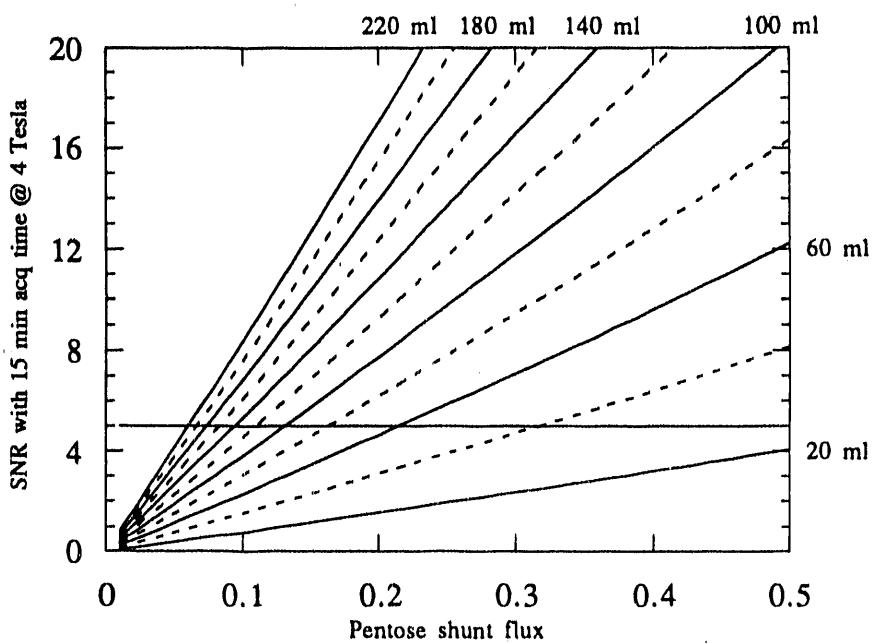

Figure 6.4. Estimate of the signal-to-noise ratio obtainable at a spectrometer field strength of 4 Tesla with an acquisition time of 15 minutes as a function of relative flux of glucose through the pentose shunt.. Plots are given for different detection volumes from 20 to 220 ml in increments of 20 ml. Horizontal line corresponds to the SNR limit of 5.

Figure 6.4 shows that for values of relative glucose flux through the pentose shunt below about 10%, a volume of 131 ml (5.1 cm on a side) or more is needed to obtain a signal to noise of 5 at a field strength of 4 Tesla with 15 minutes acquisition time. At 82% plasma glucose FE, this becomes 160 ml (5.4 cm on a side). For shunt flux values above 10%, smaller volumes or acquisition times may be used. As was mentioned above, for high shunt flux values, the brain concentration of [^{13}C-5]-glutamate is low (below 1 mM for 80% flux), and this limits measurement of relative shunt fluxes above that value. However for high flux values, a lower boundary for the shunt flux may be obtained. If in an experiment, detection of [^{13}C-4]-glutamate were obtained without detection of [^{13}C-5]-glutamate, this would imply that the shunt flux is above a limit close to 80%, depending on the conditions of detection and the T_1 of [^{13}C-5]-glutamate in the tissue.

Amount of [^{13}C-2]-glucose required for in vivo human studies.

In the following an estimate of the amount of [^{13}C-2]-glucose that would be necessary for ^{13}C NMR detection of [^{13}C-5]- and [^{13}C-4]-glutamate in human studies *in vivo* is obtained. For this estimation, a one compartment model for the glucose distribution space with two phases of constant infusion of 99% [^{13}C-2]-glucose is used. It was shown above that the ^{13}C-glutamate FE at a given shunt flux is proportional to the plasma glucose FE, so the objective here is to obtain a high level of plasma glucose FE without having total plasma glucose go beyond a level which might perturb cerebral glucose metabolism. This is taken to be about 10 mM = 180 mg/dl.

In an experimental setting, high levels of plasma glucose can be maintained by applying a modification of the hyperglycemic glucose clamp technique (91) which reduces endogenous production of glucose with dosed insulin infusion (92). Therefore in the model we use for the estimation, we assume endogenous glucose production to be negligible (93). In the hyperglycemic glucose clamp a priming dose of glucose is administered for 14 minutes, followed by continuous infusion at a rate which is adjusted to maintain constant the plasma glucose concentration. In our simplified model of the glucose clamp we use two phases of constant infusion instead of the infusion at a variable rate which would be used in a real glucose clamp. The first phase corresponds to the priming dose. The second phase corresponds to the continuous infusion. The values of plasma glucose concentration and fractional enrichment are evaluated in the single compartment model.

1/ Priming dose:

In the single compartment model, we call I the constant glucose infusion rate (units of [mass time^{-1}]), a the infused glucose fractional enrichment, V the apparent glucose distribution volume and k the glucose turnover rate constant (units of [time^{-1}]). The total mass of exchangeable glucose Q(t) is given by:

$$Q(t) = Q(0)e^{-kt} + \frac{I}{k}(1 - e^{-kt}) \tag{6.4}$$

The mass of labeled glucose Q*(t) is given by:

$$Q^*(t) = \frac{aI}{k}(1 - e^{-kt}) \tag{6.5}$$

The plasma glucose fractional enrichment is therefore:

$$FE = \frac{Q^*(t)}{Q(t)} = \frac{\frac{aI}{k}(1 - e^{-kt})}{Q(0)e^{-kt} + \frac{I}{k}(1 - e^{-kt})} \tag{6.6}$$

The following values for an average 70 kg person are taken for the estimation:

V = 12.6 liters (180 ml glucose distribution space/kg body weight)

$k = 0.012\ min^{-1}$ (from glucose turnover of 2.0 mg (kg body weight)$^{-1}$ min^{-1} with a plasma glucose concentration of 90 mg/dl = 5 mM)

Q(0) = 11.34 g (Q(0) = CV with C = 90 mg/dl)

a = 99% (commercially available)

The priming dose is taken as 2 mg (kg body weight)$^{-1}$ for each mg/dl increase in plasma glucose from DeFronzo et al. (91). Taking a 70 kg subject with an initial 90 mg/dl plasma glucose concentration and a desired final glucose concentration of 180 mg/dl this corresponds to an infusion rate I = 12.86 mg (kg body weight)$^{-1}$ min^{-1} for a period of 14 minutes i.e. a total of 12.6 g.

2/ Continuous infusion:

After the priming dose has been applied for 14 minutes the plasma glucose concentration is estimated to be 168 mg/dl. Equation 6.4 is used again for estimating the total glucose mass Q(t) except that the new initial glucose mass Q(0) is taken as as the glucose mass after infusion of the priming dose. The following equation that takes into

account the amount of label in the glucose space after the priming dose is used for estimating the mass of labeled glucose:

$$Q^*(t) = Q^*(0)e^{-kt} + \frac{aI}{k}(1 - e^{-kt}) \qquad (6.6)$$

We take the initial mass of labeled glucose $Q^*(0)$ as the mass of labeled glucose after infusion of the priming dose. In the model we assume that inhibition of insulin secretion due to hyperglycemia is obtained by infusion of somatostatin. We therefore also assume that the glucose turnover remains unchanged in the hyperglycemic state. Values used for the estimate of the second phase of infusion are summarized below:

V = 12.6 liters	(180 ml glucose distribution space/kg body weight)
$k = 0.012\ min^{-1}$	(from glucose turnover of 2.0 mg (kg body weight)$^{-1}$ min^{-1} with a plasma glucose concentration of 90 mg/dl = 5 mM)
Q(0) = 21168 mg	(estimation from priming infusion)
$Q^*(0)$ = 11482 mg	(estimation from priming infusion)

These values yield a required constant infusion rate of I = 3.89 mg (kg body weight)$^{-1}$ min^{-1} to obtain 180 mg/dl = 10 mM steady state plasma glucose concentrations i.e. 272 mg min^{-1} in a 70 kg subject.

Figure 6.5 shows the simulation of plasma glucose concentrations and fractional enrichment using the two phase infusion.

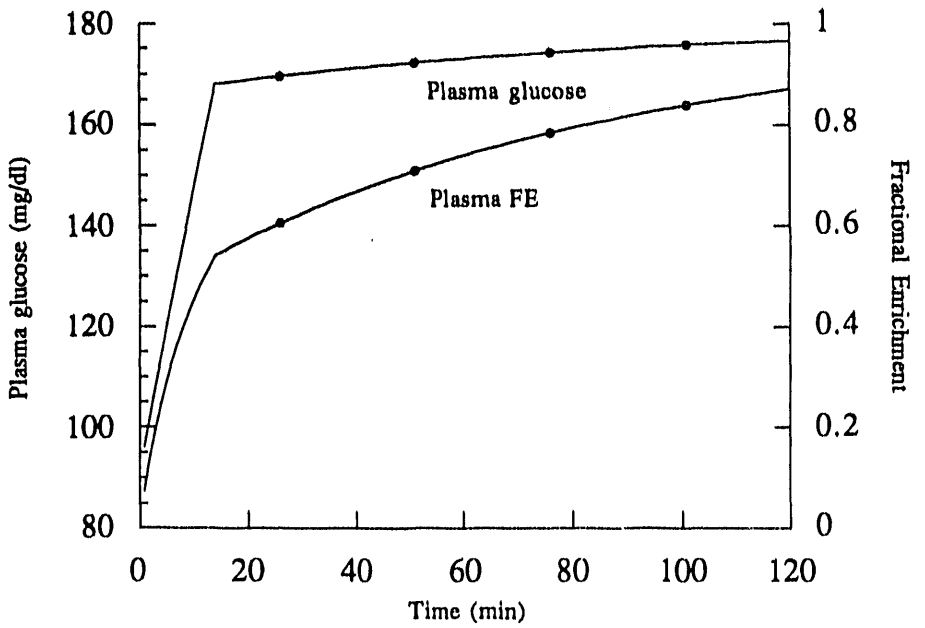

Figure 6.5. Simulation of plasma glucose concentration (mg/dl) and ^{13}C fractional enrichment obtained with the two phase infusion model.

Figure 6.5 shows that the steady state plasma glucose concentration obtained after 60 minutes of infusion is only 4% short of the desired level of 180 mg/dl. The plasma glucose fractional enrichment obtained after 60 minutes is 74%, and is 82% by 90 minutes. For a total infusion time of 90 minutes, (after 60 minutes, steady state is practically attained and a minimum of 30 minutes are taken for NMR acquisition) the total [^{13}C-2]-glucose dose is estimated from the two phase infusion model to be about 33 g for a 70 kg subject i.e. 471mg (kg body weight)$^{-1}$.

Medical science NMR studies of this type in the human subject at a field strength of 2 to 4 Tesla require 90 to 120 minutes or more of 99% ^{13}C labeled substrate infusion with large NMR detection volumes (at least 6 cm on a side), and therefore require on the order of 20 to 50 grams of ^{13}C labelled substrate (94) & (92). These conditions are almost impracticable considering the high cost of ^{13}C enriched substrates at the present time. The price of one gram of [^{13}C-2]-glucose at present is about $400. This results in a total cost

of $13200 for 33 grams of [^{13}C-2]-glucose. Yet at a field strength of 10 Tesla, the increase in sensitivity relative to that at 4 Tesla would result in a reduction in required acquisition time by a factor of 6. The consequent decrease in required ^{13}C label would make the conditions of the study more practical.

The estimates given in this study suggest that the method of measurement of relative glucose flux through the pentose shunt based on relative enrichments of glutamate carbons C4 and C5 is applicable to non-invasive human studies. This study predicts the limitations imposed on volume of detection, amount of pentose shunt flux, field strength, acquisition time and ^{13}C labeled glucose dose. Considering these limitations, *in vivo* studies of the pentose phosphate pathway in the human brain and in organ regions or tumors of about 200 cc volume appear feasible at the present time.

Bibliography

1. N. Z. Baquer, J. S. Hothersall, P. McLean. Function and regulation of the pentose phosphate pathway in brain. *Curr. Topics Cell. Regul.* **29**, 265-289 (1989).

2. B. Siesjo, *Brain Energy Metabolism* (John Wiley and Sons, Ltd., Bath, England, 1978).

3. H. Herken, K. Lange, H. Kolbe. Brain disorders induced by pharmacological blockade of the pentose phosphate pathway. *B.B.R.C.* **36**, 93-100 (1969).

4. S. S. Sternberg, F. S. Philips. 6-aminonicotinamide and acute degenerative changes in the central nervous system. *Science* **127**, 644-646 (1958).

5. L. Stryer, *Biochemistry* (W.H. Freeman and Co., New York, 1988).

6. N. Z. Baquer, J. S. Hothersall, P. McLean, A. L. Greenbaum. Aspects of carbohydrate metabolism in developing brain. *Develop.Med. Child Neurol.* **19**, 81-104 (1977).

7. B. D. Watson, M. D. Ginsberg. Ischemic injury in the brain. Role of oxygen radical-mediated processes. *Ann. N. Y. Acad. Sc.* **559**, 269-81 (1989).

8. W. Cao, J. M. Carney, A. Duchon, R. A. Floyd, M. Chevion. Oxygen free radical involvement in ischemia and reperfusion injury to brain. *Neurosc. Let.* **88**, 233-238 (1988).

9. R. Marttilla, M. Röyttä, H. Lorentz, U. Rinne. Oxygen toxicity protecting enzymes in the human brain. *J. Neural Transmission* **74**, 87-95 (1988).

10. R. Del Maestro, W. McDonald. Distribution of superoxide dismutase, glutathione peroxidase and catalase in developing rat brain. *Mech. Ageing and Dvpt.* **41**, 29-38 (1987).

11. R. Sohal, B. Sohal, U. Brunk. Relationship between antioxidant defenses and longevity in different mammalian species. *Mech. Ageing and Dvpt.* **53**, 217-227 (1990).

12. G. Rao, E. Xia, A. Richardson. Effect of age on the expression of antioxydant enzymes in male Fischer F344 rats. *Mech. Ageing and Dvpt.* **53**, 49-60 (1990).

13. C. Hanstock, D. Rothman, J. Prichard, T. Jue, R. Shulman. Spatially localized ^{1}H NMR spectra of metabolites in the human brain. *Proc. Nat. Acad. Sc. USA* **85**, 1821-1825 (1988).

14. L. Lewis, B. Ljundgren, K. Norberg, B. Siesjö. *J. Neurochem.* **23**, 659-671 (1974).

15. B. L. Horecker, A. H. Mehler. Carbohydrate Metabolism. *Ann. Rev. Biochem.* **24**, 207-274 (1955).

16. J. Williams, P. Blackmore, C. Duke, J. MacLeod. Fact, uncertainty and speculation concerning the biochemistry of D-erythrose-4-phosphate and its metabolic roles. *Int. J. Biochem.* **12**, 339-344 (1980).

17. J. Williams, K. Arora, J. Longenecker. The Pentose Pathway: A Random Harvest. Impediments which oppose acceptance of the classical (F-type) pentose cycle for liver, some neoplasms and photosynthetic tissue. The case for the L-type pathway. *Int. J. Biochemistry* **19**, 749-817 (1987).

18. B. Landau, in *The Pentose Phosphate Pathway*(Academic Press, Orlando, Fla., 1985) pp. 153-177.

19. L. M. McIntyre, D. R. Thorburn, W. A. Bubb, P. W. Kuchel. Comparison of computer simulations of the F-type and L-type non-oxidative hexose monophosphate shunts with ^{31}P experimental data from human erythrocytes. *Eur. J. Biochem.* **180**, 399-420 (1989).

20. G. Brooks. Lactate production under fully aerobic conditions: the lactate shuttle during rest and exercise. *Federation Proc.* **45**, 2924-2929 (1986).

21. J. A. Willis, W. F. Williams, T. Schleich. Dynamic assesment of hexose monophosphate shunt activity in the intact rabbit lens by proton NMR spectroscopy. *B.B.R.C.* **138**, 1068-1073 (1986).

22. P. Kingsley-Hickman, B. Ross, T. Krick. Hexose monophosphate shunt measurement in cultured cells with [1-^{13}C]glucose: correction for endogenous carbon sources using [6-^{13}C]glucose. *Anal. Bioch.* **185**, 235-237 (1990).

23. C. Malloy, A. Sherry, M. Jeffrey. Evaluation of carbon flux and substrate selection through alternate pathways involving the citric acid cycle of the heart by ^{13}C NMR spectroscopy. *J. Biol. Chem.* **263**, 6964-6971 (1988).

24. J. Katz. Determination of gluconeogenesis in vivo with ^{14}C labeled substrates. *Am. J. Physiol.* **248**, R391-R399 (1985).

25. N. Kaplan, M. Ciotti, F. Stolzenbach. Reaction of pyridine nucleotide analogues with dehydrogenases. *J. Biol. Chem.* **221**, 833-844 (1956).

26. L. S. Dietrich, I. M. Friedland, L. A. Kaplan. Pyridine nucleotide metabolism: mechanism of action of the niacin antagonist, 6-aminonicotinamide. *J. Biol. Chem.* **233**, 964-968 (1958).

27. F. C. Kauffman, E. C. Johnson. Cerebral energy reserves and glycolysis in neural tissue of 6-aminonicotinamide treated mice. *J. Neurobio.* **5**, 379-392 (1974).

28. M. K. Gaitonde, E. Evison, G. M. Evans. The rate of utilization of glucose via hexose monophosphate shunt in brain. *J. Neurochem.* **41**, 1253-1260 (1983).

29. R. Ernst, W. Anderson. Application of Fourier transform spectrocopy to magnetic resonance. *Rev. Sci. Inst.* **37**, 93-102 (1966).

30. B. Sumegi, A. Sherry, C. Malloy. Channeling of TCA intermediates in cultured Saccharomyces Cerevisiae. *Biochem.* **29**, 9106-9110 (1990).

31. R. Badar-Goffer, H. Bachelard, P. Morris. Cerebral metabolism of acetate and glucose studied by ^{13}C-NMR spectroscopy. *Biochem. J.* **266**, 133-139 (1990).

32. Hare Research Incorporated, *Felix* for SUN 4/60, Sparc station 1, Woodinville, WA, (1990)

33. G. Weiss, J. Ferretti. Accuracy and precision in the estimation of peak areas and NOE factors. *J. Mag. Res.* **55**, 397-407 (1983).

34. D. Alderman, The theory of magnetic resonance detection and sensitivity.

35. M. R. Bendall, D. T. Pegg, D. M. Doddrell, J. Field. NMR of protons coupled to ^{13}C nuclei only. *J. Am. Chem. Soc.* **103**, 934-936 (1981).

36. R. Freeman, T. Mareci, G. Morris. Weak satellite signals in high-resolution NMR spectra: separating the wheat from the chaff. *J. Mag. Res.* **42**, 341-345 (1981).

37. F. Dickens, G. Glock. Direct oxidation of glucose-6-phosphate, 6-phosphogluconate and pentose-5-phosphates by enzymes of animal origin. *Biochem. J.* **50**, 81-95 (1951).

38. A. Barrett, V. Cullum. The biological properties of the optical isomers of propanolol and their effects on cardiac arrhythmias. *Br. J. Pharmac.* **34**, 43-55 (1968).

39. G. J. Hetenyi, G. Perez, M. Vranic. Turover and precursor-product relationships of nonlipid metabolites. *Phys. Rev.* **63**, 606-667 (1983).

40. G. Brooks, S. Henderson, P. Dallman. Increased glucose dependence in resting, iron-deficient rats. *Am. J. Physiol.* **253**, E461-6 (1987).

41. Z. Chap, et al. Effects of alpha and beta adrenergic blockade on hepatic glucose balance before and after oral glucose. *J. Clin. Invest.* **77**, 1357-1369 (1986).

42. F. Orzi, et al. Local cerebral glucose utilization in controlled graded levels of hyperglycemia in the conscious rat. *J. Cereb. Blood Flow Metab.* **8**, 346-356 (1988).

43. H. McIlwain, H. Bachelard, *Biochemistry and the central nervous system* (Churchill Livingstone, London, 1985).

44. D. Rothman, et al. ^{1}H-observe/^{13}C-decouple spectroscopic measurements of lactate and glutamate in the rat brain in vivo. *Proc. Natl. Acad. Sci., USA* **82**, 1633-1637 (1985).

45. B. Horecker, et al., in *Aspects of Yeast metabolism* A. Mills, H. Krebs, Eds. (Blackwell Scientific Publications, Oxford & Edinburgh, 1968).

46. J. den Hollander, K. Behar, R. Shulman. ^{13}C NMR study of transamination during acetate utilization by Saccharomyces Cerevisiae. *Proc. Natl. Acad. Sci. USA* **78**, 2693-2697 (1981).

47. R. London. ^{13}C labeling in studies of metabolic regulation. *Prog. NMR Spec.* **20**, (1988).

48. J. den Hollander, et al. Studies of anaerobic and aerobic glycolysis in Saccaromyces Cerevisiae. *Biochemistry* **25**, 203-211 (1986).

49. F. Dickens, H. McIlwain. *Biochem J.* **32**, 1615 (1938).

50. F. Brown, I. Campbell, P. Kuchel. Human erythrocyte metabolism studies by ^{1}H spin echo NMR. *FEBS let.* **82**, 12-16 (1977).

51. M. York, G. Beilharz, P. Kuchel. Conformation of reduced glutathione in aqueous solution by ^{1}H and ^{13}C NMR. *Int. J. Peptide Protein Res.* **29**, 638-646 (1987).

52. D. Clarke, A. Lajtha, H. Maker, in *Basic Neurochemistry: Molecular, Cellular and Medical Aspects* G. Siegel, Eds. (Raven Press Ltd., New York, 1989) pp. 541-564.

53. B. D. Ross, et al. Carbohydrate metabolism of the rat C6 glioma. An *in vivo* and *in vitro* ^{1}H magnetic resonance spectroscopy study. *NMR in Biomed.* **1**, 20-26 (1988).

54. M. Utter, H. Wood, J. Reiner. Anaerobic glycolysis in nervous tissue. *J. Biol. Chem.* **161**, 197-217 (1945).

55. P. Dreyfus. The regional distribution of tranketolase in the normal and the thiamine deficient nervous system. *J. Neuropath. Exp. Neurol.* **24**, 119-129 (1965).

56. S. S. Hotta. Glucose metabolism in brain tissue: the hexosemonophosphate shunt and its role in glutathione reduction. *J. Neurochem.* **9**, 43-51 (1962).

57. C. Wang, et al. Comparative Study of glucose catabolism by the radiorespirometric method. *J. Bacteriol.* **76**, 207-216 (1958).

58. J. Gancedo, R. Lagunas. Contribution of the pentose phosphate pathway to glucose metabolism in Saccharomyces Cerevisiae: a critical analysis on the use of labeled glucose. *Plant Sci. Lett.* **1**, 193-200 (1973).

59. J. Katz, H. Wood. The use of $C^{14}O_2$ yields from glucose-1- and -6-C^{14} for the evaluation of the pathways of glucose metabolism. *J. Biol. Chem.* **238**, 517 (1963).

60. W. Sacks. Cerebral metabolism of isotopic glucose in normal human subjects. *J. Appl. Physiol.* **10**, 37-44 (1957).

61. K. Hostetler, B. Landau, R. White, M. Albin, D. Yashon. Contribution of the pentose cycle to the metabolism of glucose in the isolated perfused brain of the monkey. *J. Neurochem.* **17**, 33-39 (1970).

62. A. Hakim, G. Moss. *Anesthesiology* **40**, 261-267 (1974).

63. G. Moss. The contribution of the hexose monophosphate shunt to cerebral glucose metabolism. *Diabetes* **13**, 585-591 (1964).

64. M. Krass, F. Labella. Hexosemonophosphate shunt in endocrine tissues. Quantitative estimation of the pathway in bovine pineal body, anterior pituitary, posterior pituitary, and brain. *Biochim. Biophys. Acta* **148**, 384-391 (1967).

65. R. Guerra, E. Melgar, M. Villavicencio. Alternative pathways of glucose metabolism in fetal rat brain. *Biochim. Biophys. Acta* **148**, 356-361 (1967).

66. S. Zubairu, J. Hothersall, A. El-Hassan, P. McLean, A. Greenbaum. Alternative pathways of glucose utilization in brain: changes in the pattern of glucose utilization and of the response of the pentose phosphate pathway to 5-hydroxytryptamine during aging. *J. Neurochem.* **41**, 76-83 (1983).

67. J. S. Hothersall, N. Z. Baquer, A. L. Greenbaum, P. McLean. Alternative pathways of glucose utilization in brain. Changes in the pattern of glucose utilization in brain during development and the effects of phenazine methosulfate on the integration of metabolic routes. *Arch. Biochem. Biopys.* **198**, 478-492 (1979).

68. M. Härkönen, F. Kauffman. Metabolic alterations in the axotomized superior cervical ganglion of the rat. II. The pentose phosphate pathway. *Brain Res.* **65**, 141-157 (1974).

69. K. Hostetler, B. Landau. Estimation of the Pentose Cycle Contribution to Glucose Metabolism in Tissue *in vivo*. *Biochem.* **6**, 2961-2964 (1967).

70. M. Gaitonde, G. Evans. The effect of inhibition of hexose monophosphate shunt on the metabolism of glucose and function in rat brain in vivo. *Neurochem. Res.* **7**, 11631179 (1982).

71. M. K. Gaitonde, J. Jones, G. Evans. Metabolism of glucose into glutamate via the hexose monophosphate shunt and its inhibition by 6-aminonicotinamide in rat brain in-vivo. *Proc. R. Soc. Lond. B* **231**, 71-90 (1987).

72. R. Friede, L. Fleming, M. Knoller. A comparative mapping of enzymes involved in hexose monophosphate shunt and citric acid cycle in the brain. *J. Neurochem.* **10**, 263 (1963).

73. H. Zimmer, H. Ibel, U. Suchner. Beta-adrenergic agonists stimulate the oxidative pentose phosphate pathway in the rat heart. *Circ. Res.* **67**, 1525-1534 (1990).

74. N. Bolo, K. M. Brennan, R. M. Jones, T. F. Budinger. Fluorodeoxyglucose brain metabolism studied by NMR and PET. *Ann. N.Y. Acad. Sc.* **508**, 451-459 (1987).

75. G. Leda-Columnano, et al. Enhancement of cholesterol synthesis and pentose phosphate pathway activity in proliferating hepatocytes nodules. *Carcinogenesis* **6**, 1371-1373 (1985).

76. S. Dessi, et al. Hexose monophosphate shunt enzymes in lung tumors from normal and glucose-6-phosphate-dehyd:ogenase-deficient subjects. *Oncology* **45**, 287-291 (1988).

77. W. Bezwoda, D. Derman, N. See, N. Mansoor. Relative value of oestrogen receptor assay, lactoferrin content, and glucose-6-phosphate dehydrogenase activity as prognostic indicators in primary breast cancers. *Oncology* **42**, 7-12 (1985).

78. A. Evans, N. Johnson, R. Butcher. A quantitative biochemical study of the glucose-6-phosphate dehydrogenase activity in premalignant and malignant lesions of human oral mucosa. *Histochem. J.* **15**, 483-489 (1983).

79. E. Zampella, E. Bradley, T. Pretlow. Glucose-6-phosphate dehydrogenase: a possible clinical indicator for prostatic carcinoma. *Cancer* **49**, 384-387 (1982).

80. P. Chan, J. Schmidley, R. Fishman, S. Longar. Brain injury, edema, and vascular permeability changes induced by oxygen-derived free radicals. *Neurology* **34**, 315-320 (1984).

81. E. Flamm, H. Demopoulos, M. Seligman, R. Poser, J. Ransohoff. Free radicals in cerebral ischemia. *Stroke* **9**, 445-447 (1978).

82. H. Demopoulos, E. Flamm, M. Seligman, J. Mitamura, J. Ransohoff, in *Neural Trauma* A. Popp, A. Bourke, L. Nelson, H. Kimelberg, Eds. (Raven Press, New York, 1979) pp. 63-78.

83. H. Demopoulos, E. Flamm, M. Seligman, D. Pietronigro, in *Pathology of oxygen* A. Autor, Eds. (Academic Press, London, 1982) pp. 127-155.

84. S. Yoshida, et al. Influence of transient ischemia on lipid-soluble antioxidants, free fatty acids and energy metabolites in rat brain. *Brain Res.* **245**, 307-316 (1982).

85. R. Pfeifer, G. Karl, R. Scholz. *Biol. Chem. Hoppe Seyler* **367**, 1063-1068 (1986).

86. J. Chatham, J. Forder, J. Glickson, Detection of flux through the pentose phosphate pathway during ischemia in the perfused rat heart by ^{13}C NMR spectroscopy. *Meeting of the Society of Magnetic Resonance in Medicine* (San Francisco, CA, 1991), vol. 1, pp. 286.

87. A. Meijer. The pentose phosphate pathway in skeletal muscle under patho-physiological conditions. A combined histochemical and biochemical study. *Prog. Histochem. Cytochem.* **22**, 1-118 (1991).

88. R. Gruetter, et al., Quantitation of the Glucose concentration in the human brain by ^{13}C-NMR at normal and at high plasma glucose levels. *Meeting of the Society of Magnetic Resonance in Medicine* (San Francisco, CA, 1991), vol. 1, pp. 189.

89. R. Ordrige, A. Connelly, J. Lohman. Image-selected in vivo spectroscopy (ISIS). A new technique for spatially selective NMR spectroscopy. *J. Mag. Res.* **66**, 283-294 (1986).

90. C.-N. Chen, D. Hoult, in *Biomedical Magnetic Resonance Technology* R. Mould, Eds. (IOP Publishing Ltd., New York, 1989) pp. 117-176.

91. R. DeFronzo, J. Tobins, R. Andres. Glucose clamp technique: a method for quantifying insulin secretion and resistance. *Am. J. Physiol.* **237**, E214-E223 (1979).

92. N. Beckmann, I. Turkalj, J. Seelig, U. Keller. ^{13}C NMR for the assesment of human brain glucose metabolism in vivo. *Biochem.* **30**, 6362-6366 (1991).

93. R. DeFronzo, E. Ferrannini, R. Hendler, J. Wahren. Influence of hyperinsulinemia, hyperglycemia, and the route of glucose administration on splanchnic glucose exchange. *Proc.Natl.Acad.Sci. USA* **75**, 5173-5177 (1978).

94. G. Shulman, et al. Quantitation of muscle glycogen synthesis in normal subjects with non-insulin-dependent diabetes by ^{13}C nuclear magnetic resonance spectroscopy. *N. Engl. J. Med.* **322**, 223-228 (1990).

Appendix. ^{1}H and ^{13}C peak integrals in the cell free brain preparation experiments.

The following are plots of the NMR peak integrals *versus* time for the cell free experiments. Integrals are given in arbitrary units. Errors are estimated by using equations 3.7 to 3.9 from section 3.1.1.

1. [^{13}C-1]-glucose experiments.

1.1. Controls.

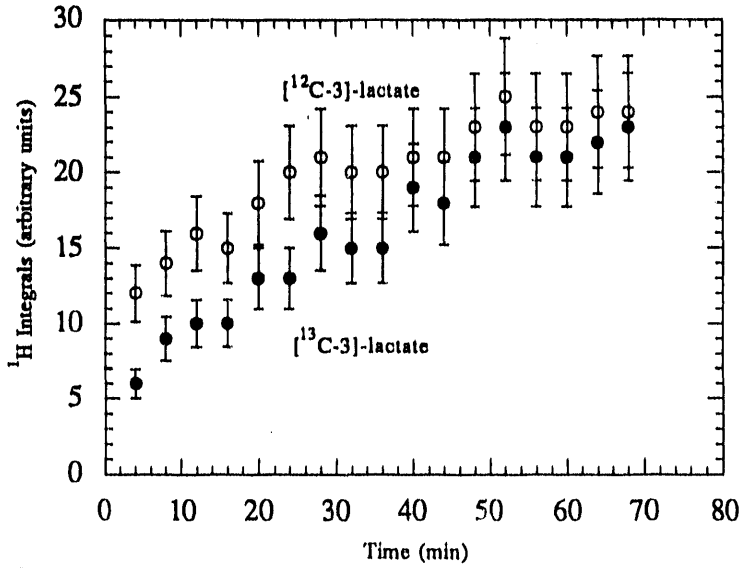

Figure A1.1. [^{13}C-1]-glucose substrate. Control cell free preparation 1. ^{1}H NMR peak integrals for [^{12}C-3]- and [^{13}C-3]-lactate.

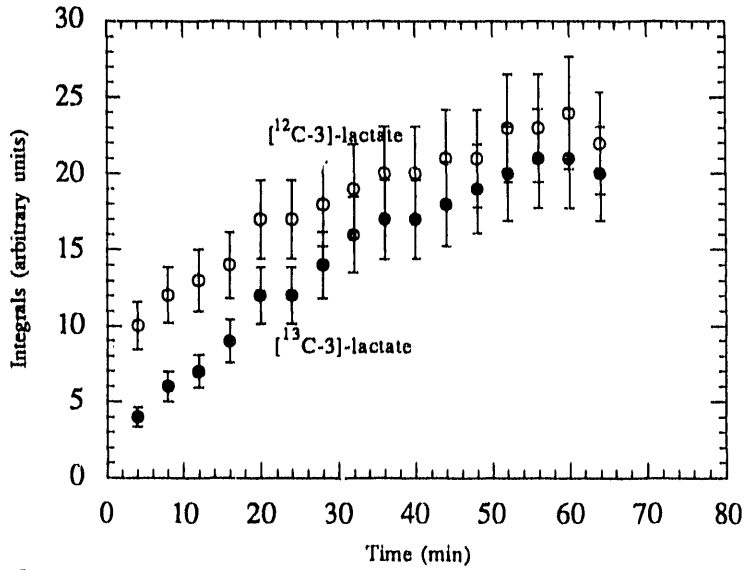

Figure A1.2. [^{13}C-1]-glucose substrate. Control cell free preparation 2. ^{1}H NMR peak integrals for [^{12}C-3]- and [^{13}C-3]-lactate.

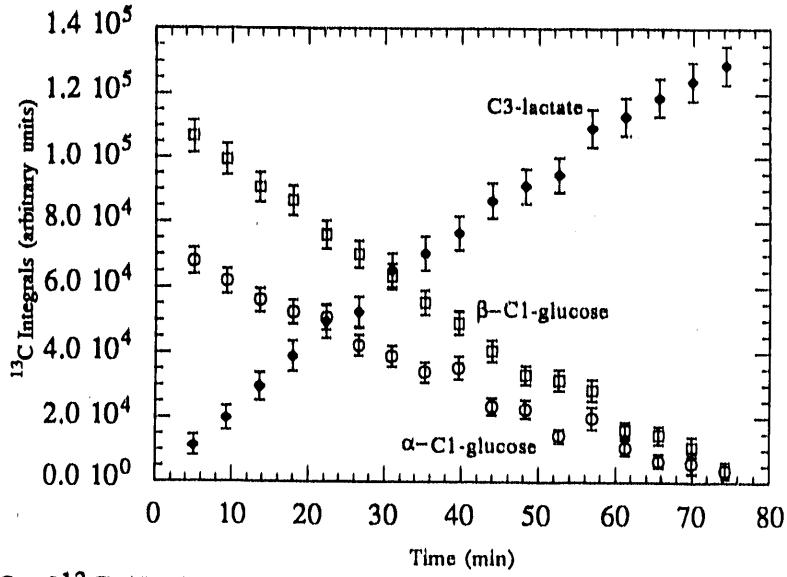

Figure A1.3. [^{13}C-1]-glucose substrate. Control cell free preparation 1. ^{13}C NMR peak integrals for α-[^{13}C-1]- and β-[^{13}C-1]-glucose and [^{13}C-3]-lactate.

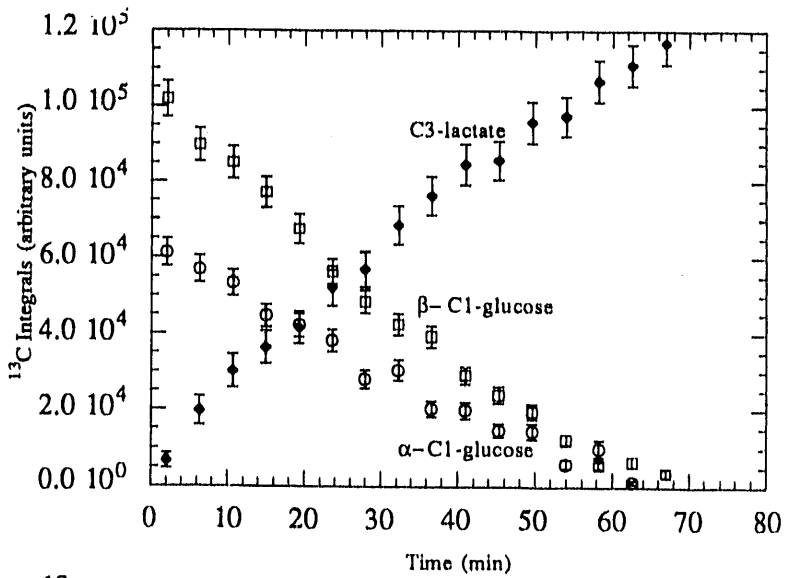

Figure A1.4. [^{13}C-1]-glucose substrate. Control cell free preparation 2. ^{13}C NMR peak integrals for α-[^{13}C-1]- and β-[^{13}C-1]-glucose and [^{13}C-3]-lactate.

1.2. GSSG stressed.

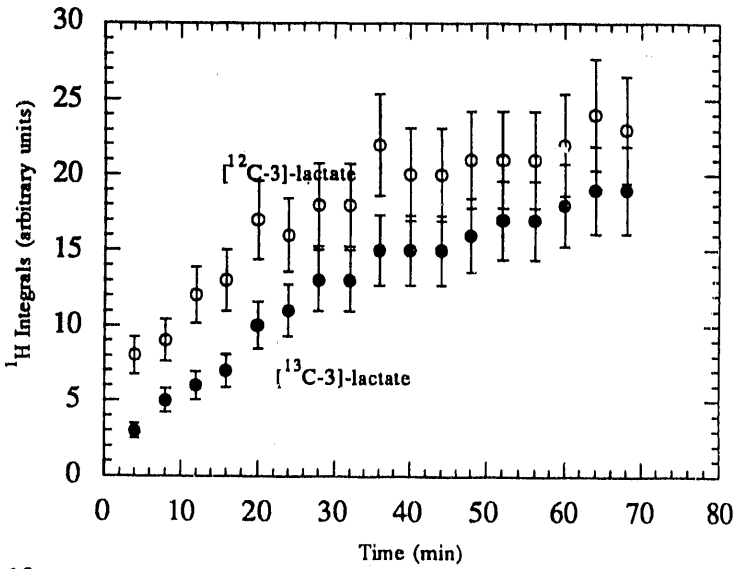

Figure A1.5. [^{13}C-1]-glucose substrate. GSSG stressed cell free preparation 1. ^{1}H NMR peak integrals for [^{12}C-3]- and [^{13}C-3]-lactate.

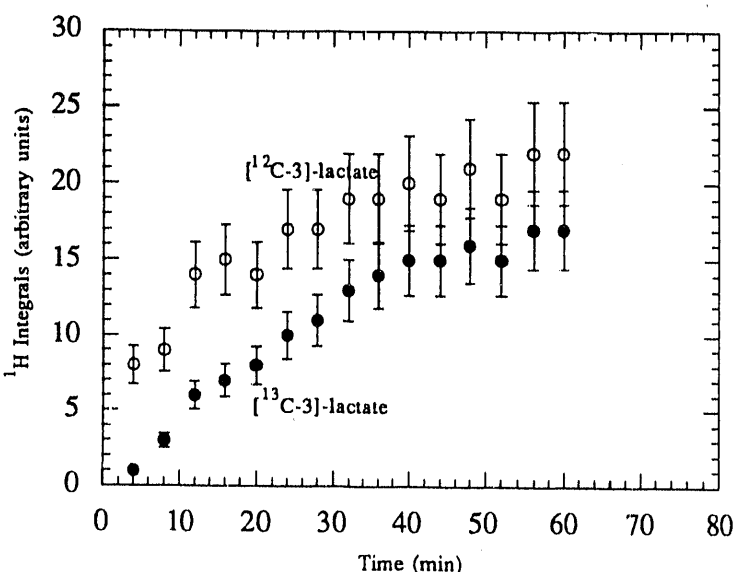

Figure A1.6. [^{13}C-1]-glucose substrate. GSSG stressed cell free preparation 2. ^{1}H NMR peak integrals for [^{12}C-3]- and [^{13}C-3]-lactate.

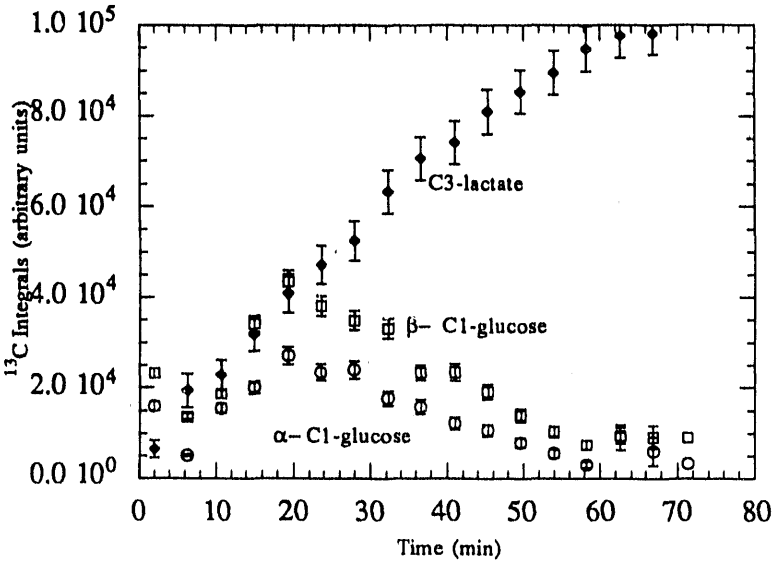

Figure A1.7. [^{13}C-1]-glucose substrate. GSSG stressed preparation 1. ^{13}C NMR peak integrals for α-[^{13}C-1]- and β-[^{13}C-1]-glucose and [^{13}C-3]-lactate.

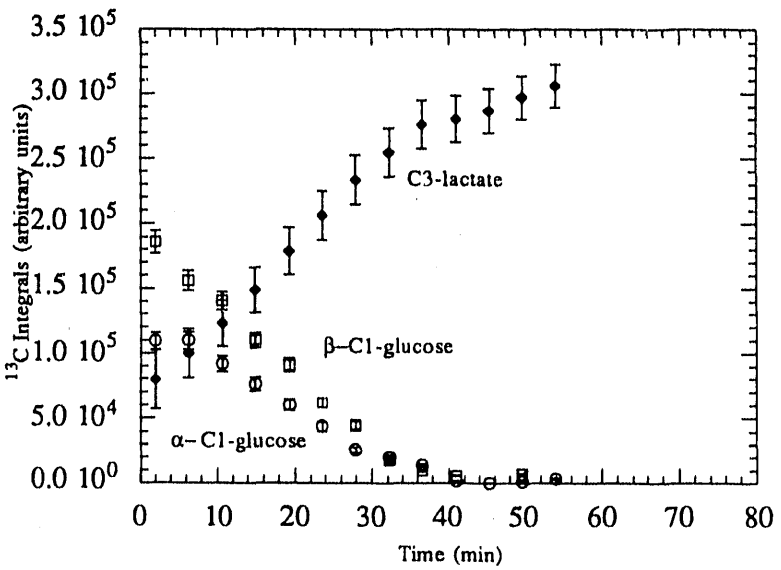

Figure A1.8. [^{13}C-1]-glucose substrate. GSSG stressed preparation 2. ^{13}C NMR peak integrals for α-[^{13}C-1]- and β-[^{13}C-1]-glucose and [^{13}C-3]-lactate.

2. [^{13}C-2]-glucose experiments.

2.1. Controls.

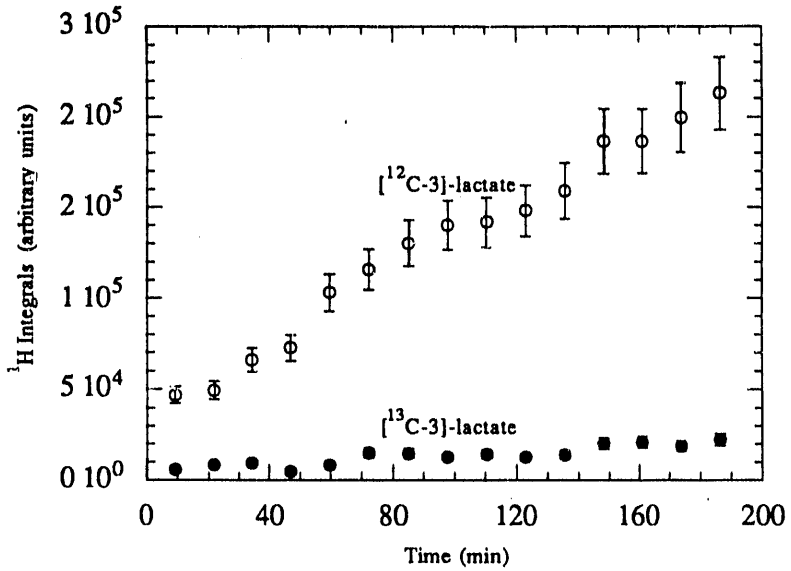

Figure A1.9. [^{13}C-2]-glucose substrate. Control cell free preparation 1. ^{1}H NMR peak integrals for [^{12}C-3]- and [^{13}C-3]-lactate.

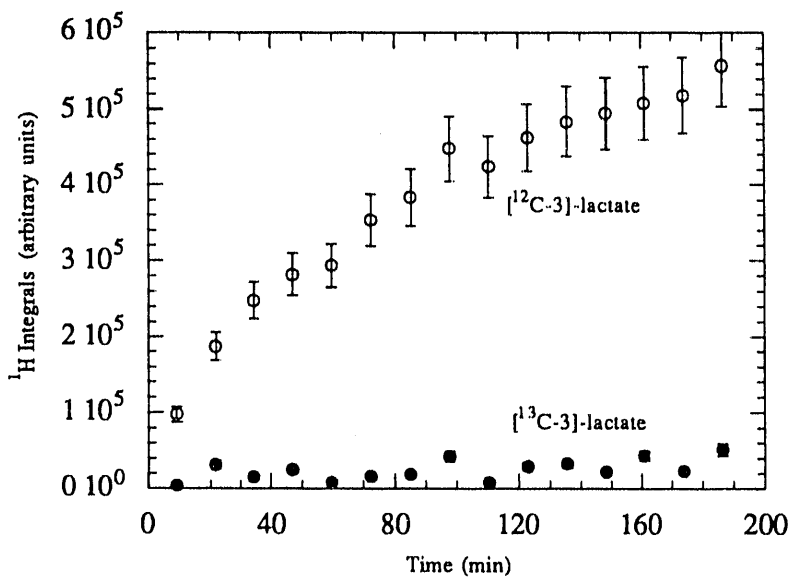

Figure A1.10. [^{13}C-2]-glucose substrate. Control cell free preparation 2. ^{1}H NMR peak integrals for [^{12}C-3]- and [^{13}C-3]-lactate.

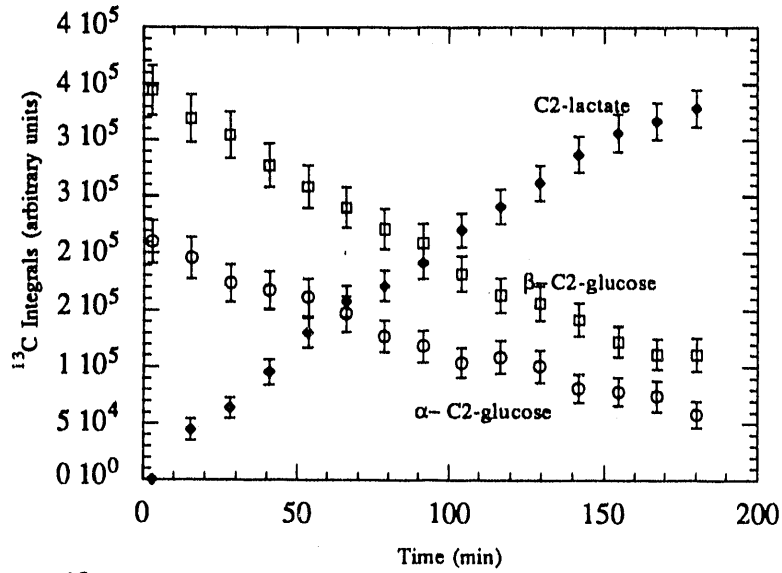

Figure A1.11. [^{13}C-2]-glucose substrate. Control cell free preparation 1. ^{13}C NMR peak integrals for α-[^{13}C-2]- and β-[^{13}C-2]-glucose and [^{13}C-2]-lactate.

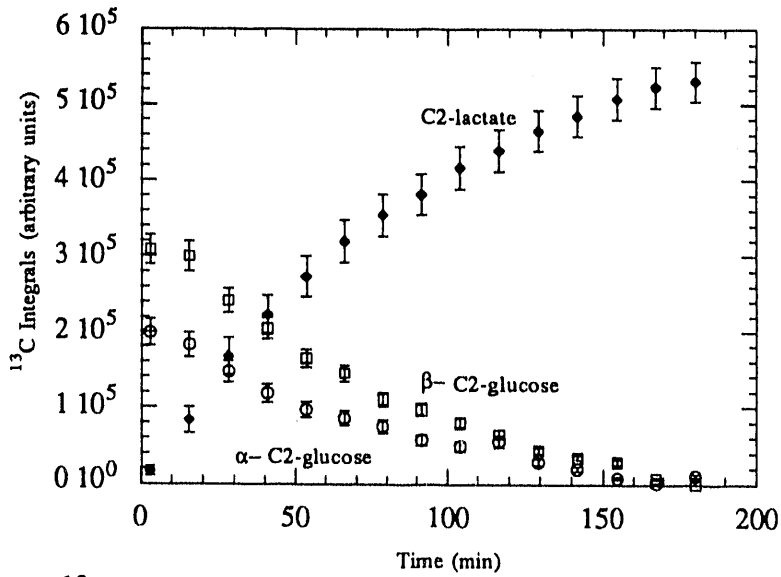

Figure A1.12. [^{13}C-2]-glucose substrate. Control cell free preparation 2. ^{13}C NMR peak integrals for α-[^{13}C-2]- and β-[^{13}C-2]-glucose and [^{13}C-2]-lactate.

2.2. GSSG stressed.

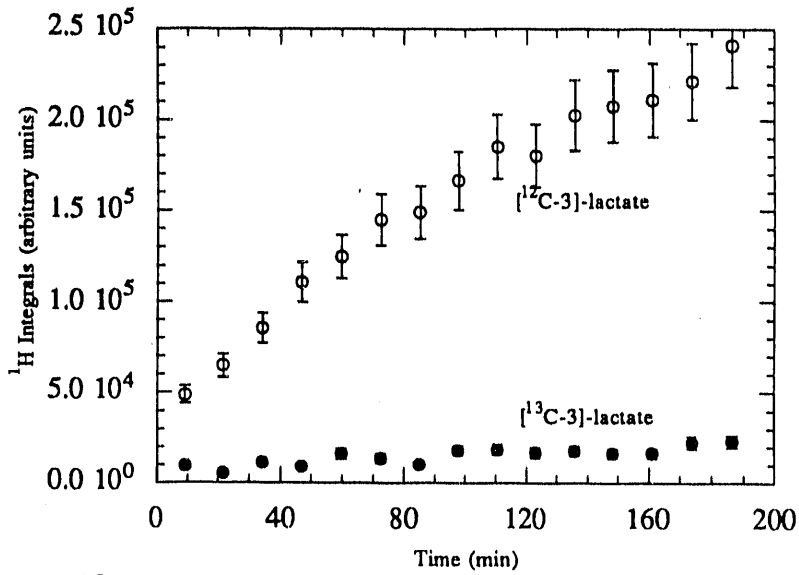

Figure A1.13. [^{13}C-2]-glucose substrate. GSSG stressed cell free preparation 1. ^{1}H NMR peak integrals for [^{12}C-3]- and [^{13}C-3]-lactate.

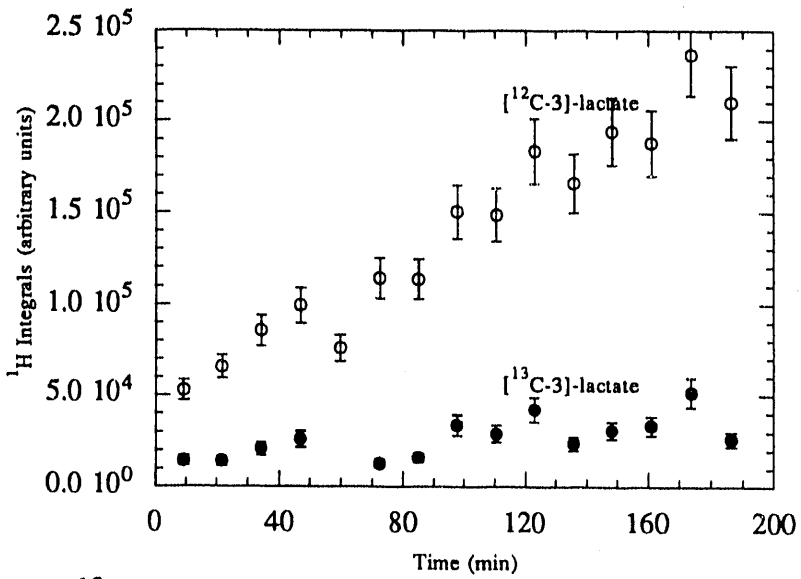

Figure A1.14. [^{13}C-2]-glucose substrate. GSSG stressed cell free preparation 2. ^{1}H NMR peak integrals for [^{12}C-3]- and [^{13}C-3]-lactate.

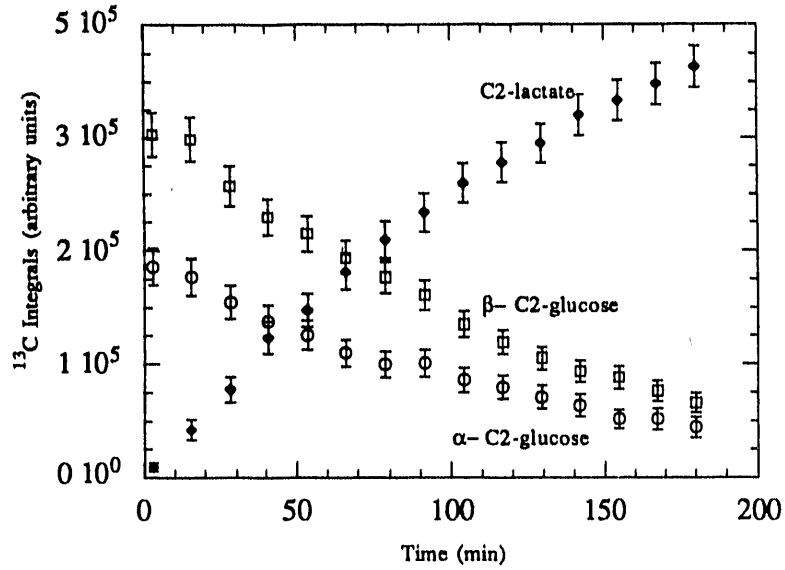

Figure A1.15. [^{13}C-2]-glucose substrate. GSSG stressed cell free preparation 1. ^{13}C NMR peak integrals for α-[^{13}C-2]- and β-[^{13}C-2]-glucose and [^{13}C-2]-lactate.

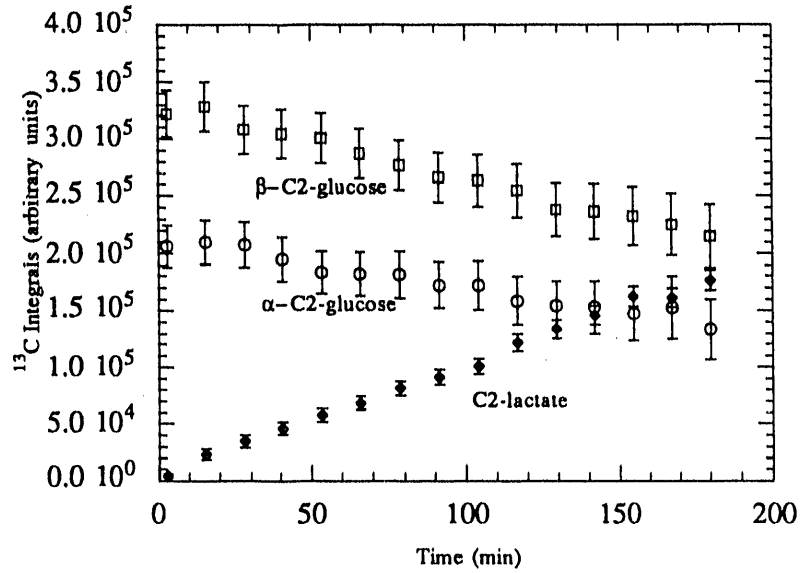

Figure A1.16. [^{13}C-2]-glucose substrate. GSSG stressed cell free preparation 2. ^{13}C NMR peak integrals for α-[^{13}C-2]- and β-[^{13}C-2]-glucose and [^{13}C-2]-lactate.

END

DATE
FILMED
5/19/92